Spectroscopic investigations on pure water and aqueous salt solutions in the mid infrared region

Thesis for the degree
doctor rerum naturalium (Dr. rer. nat.)
of the Faculty of Sciences
University of Rostock

by
Julian Riemenschneider,

Rostock, August 2011

urn:nbn:de:gbv:28-diss2012-0030-2

1st referee:	Prof. Dr. Ralf Ludwig
2nd referee:	Prof. Dr. Alfons Geiger
date of defense:	17.1.2012

Water has no taste, no color, no odor; it cannot be defined, art relished while ever mysterious. Not necessary to life, but rather life itself. It fills us with a gratification that exceeds the delight of the senses.

Antoine de Saint-Exupéry, 1939

Salt is so common, so easy to obtain, and so inexpensive that we have forgotten that from the beginning of civilization until about 100 years ago, salt was one of the most sought-after commodities in human history.

Mark Kurlansky, 2002

Contents

1 Introduction **1**

2 Theory and previous research **4**

2.1 Water 4

2.1.1 IR spectroscopy studies on pure water 4

2.1.2 Coupling and FERMI resonance 6

2.1.3 Isosbestic point 7

2.1.4 Mixture and continuum model 8

2.2 Aqueous electrolyte solutions 8

2.2.1 Hydration 9

2.2.2 The HOFMEISTER series 10

2.2.3 The concept of structure making and breaking 11

2.2.4 Long range vs. short range effect 13

2.2.5 Ion pair formation 14

2.2.6 Hydrate formation 15

3 Methods **16**

3.1 ATR FT-IR spectroscopy 16

3.1.1 Infrared spectroscopy 16

3.1.2 FOURIER transformation 17

3.1.3 Attenuated Total Reflection 19

The procedure 19

Advantages of ATR 21

Disadvantages of ATR 21

3.1.4 Isotopic substitution 24

3.1.5 Comparability of transmission and ATR spectroscopy 24

3.2 Experiment 25

3.2.1 Technical setup for ATR spectroscopy 25

3.2.2 Technical setup for transmission spectroscopy 26

3.2.3 Experimental data . . . 26
3.3 Data processing and analysis . . . 27
3.3.1 Decomposition of spectra . . . 27
3.3.2 Difference spectra . . . 28

4 Results and Discussion **29**
4.1 Mid IR spectra of H_2O and D_2O . . . 29
4.2 Identifying ν_1 and ν_3 of the H_2O molecule . . . 32
4.2.1 Theoretical calculations . . . 36
4.3 The overtone of the bending vibration of the H_2O molecule . . . 38
4.4 Free OH groups . . . 41
4.4.1 Investigations on alkali chloride salts . . . 42
Additional molecular dynamics simulations . . . 46
4.4.2 Investigations on alkali fluoride salts . . . 50
4.5 Ionic dependencies . . . 53
4.5.1 Shifts in the difference spectra of monovalent ion solutions . . . 56
Anion dependency . . . 56
Cation dependency . . . 57
4.5.2 Shifts in the difference spectra of bivalent cation solutions . . . 59
Anion dependency . . . 61
Cation dependency . . . 62
4.6 The Hofmeister series . . . 64
4.6.1 Cation dependent behaviour of the alkaline halides . . . 64
4.6.2 The sodium series and hydrophobicity . . . 68
4.7 Hydrate formation . . . 72
4.7.1 The freezing process . . . 73
4.7.2 Frozen sodium halide solutions . . . 76
4.7.3 Frozen alkali chloride solutions . . . 78
Supercooled lithium chloride solution . . . 79

5 Conclusion **81**
5.1 Summary . . . 81
5.2 Outlook . . . 84

Bibliography **87**

Appendix **100**

1 Spectroscopical setup 100
2 Physical data of salts 101
3 The overtone of the bending vibration of the H_2O molecule 102
4 Ionic Dependencies 103
4.1 Peak positions 103
One molar solutions 103
Two molar solutions 104
4.2 Anionic dependency 105
One molar solutions 105
Two molar solutions 105
4.3 Cationic dependency 106
One molar solutions 106
Two molar solutions 107
4.4 Anionic dependent behaviour of Ca and Mg halides 108
One molar solutions 108
Half molar solutions 108
5 Hofmeister series 109
5.1 Cation dependent peak heights of the hydrogen bonded network peak 109
One molar solutions 109
Two molar solutions 110
5.2 The sodium series 111

Acknowledgements **112**

Abbreviations and symbols

ATR	attenuated total reflection
IRE	internal reflecting element
IR	infrared
FT	FOURIER transformation
THz	terahertz
NMR	nuclear magnetic resonance
DTGS	deuterated triglycine sulfate

ν_1	symmetric stretch
ν_3	asymmetric stretch
ν_2	bending vibration
$2\nu_2$	first overtone of the bending vibration
$\tilde{\nu}$	wavenumber
λ	wavelength
ν	frequency
c	speed of light in vacuum ($2.99793 \times 10^{10}\,\mathrm{cm\,s^{-1}}$) (Chapter 3)
E	energy
h	PLANCK constant ($6.626 \times 10^{-34}\,\mathrm{J\,s}$)
d_p	penetration depth of the IR beam
n_1	refractive index of ATR crystal
n_{21}	ratio of refractive indices of sample and probe
θ	angle of incidence
μ	reduced mass
$g(r)$	radial distribution function
C_i	molar solubility of the hydrophobe in salt solution
$C_i(0)$	molar solubility of the hydrophobe in water
C_s	molar concentration of the salt
k_s	SETCHÉNOW salting-out coefficient
η	viscosity of an electrolyte solution
η_0	viscosity of pure water
c	ionic concentration (Chapter 2)
B	JONES-DOLE viscosity B coefficient

vs.	versus
e.g.	for example
i.e.	that is

List of Figures

2.1 Hydration of anions and cations. 9
2.2 The Hofmeister series based on the Jones-Dole viscosity B coefficient. 10

3.1 Schematic diagram of a Fourier transform spectrometer. 18
3.2 Comparison of reference and spectral interferogram. 18
3.3 Drop on top of ATR crystal. 19
3.4 The optical path of the IR beam through the ATR unit. 20
3.5 Beam path for ATR single reflection within the crystal. 20
3.6 FT-IR spectrometer with mounted ATR unit. 22
3.7 Anomalous dispersion. 23
3.8 Transmission and ATR spectra in comparison. 25
3.9 Comparison of Lorentz-, Gaussian-, and Voigt-profiles. 27

4.1 Temperature dependent spectra of the mid infrared region of H_2O. 30
4.2 Temperature dependent spectra of the mid infrared region of D_2O. 30
4.3 Temperature dependence of the intensity of the OH/OD stretch band. . . . 31
4.5 Simultaneous fit of the OD stretch band of D_2O. 33
4.4 Simultaneous fit of the OH stretch band of H_2O. 33
4.6 Intensities of contributions of the simultaneous fit of H_2O and D_2O. 34
4.7 Spectra of H_2O and D_2O in comparison to a mixture of 95 mol% D_2O/5 mol% H_2O. 35
4.8 Spectra of H_2O and D_2O in comparison to a mixture of 5 mol% D_2O/95 mol% H_2O. 35
4.9 Spectra of H_2O and D_2O in comparison to a mixture of 50 mol% D_2O/50 mol% H_2O. 38
4.10 Fit of ν_2 and $2\nu_2$ in an HDO spectrum. 39
4.11 Inclusion of $2\nu_2$ into the pure water spectrum. 40
4.12 Spectra of H_2O and a salt solution including the difference spectra. 43
4.13 Difference spectra of NaCl, KCl, RbCl and CsCl salt solutions. 44

4.14 Difference spectra of 2 and 4 M NaCl, KCl, RbCl and CsCl salt solutions for the quasi free OH group contribution. 45
4.15 Peak heights and intensities of the VOIGT functions fitting the band of the quasi free OH found in the difference spectra. 46
4.16 Oxygen-oxygen radial distribution functions for a) aqueous NaCl solutions at various concentrations and b) aqueous NaCl, KCl, RbCl and CsCl solutions at a concentration of 4.76 mol%. 47
4.17 Water-water site-site difference radial distribution functions $\Delta g_{OH}(r) = g_{OH}(r)$[salt-solution] $- g_{OH}(r)$[water] for aqueous TIP4P-Ew salt solutions for different concentrations of NaCl, KCl, RbCl and CsCl. 49
4.18 Water-water site-site difference radial distribution functions $\Delta g_{OO}(r) = g_{OO}(r)$[salt-solution] $- g_{OO}(r)$[water] for aqueous TIP4P-Ew salt solutions for different concentrations of NaCl, KCl, RbCl and CsCl. 49
4.19 Water-water site-site difference radial distribution functions $\Delta g_{HH}(r) = g_{HH}(r)$[salt-solution] $- g_{HH}(r)$[water] for aqueous TIP4P-Ew salt solutions for different concentrations of NaCl, KCl, RbCl and CsCl. 49
4.20 Difference spectra of CsF, CsCl and CsBr solutions for the OH stretch region and a spectrum of the OH stretch of water with a red contribution indicating the position of the quasi free OH group. 50
4.21 Real and difference spectra of KF solutions in comparison. 51
4.22 Difference spectra of KF, RbF and CsF solutions. 52
4.23 Anion dependent difference spectra of 4 M solutions of Li, Na, K, Rb and Cs halides. 54
4.24 Peak positions of the anionic and the network peak respectively for 4 M solutions. 55
4.25 Cation dependent difference spectra of 4 M solutions of Li, Na, K, Rb and Cs halides. 58
4.26 Anion dependent difference spectra of Mg and Ca halides. 60
4.27 Anion dependent difference spectra of 2 M Mg and Ca halide solutions. . . 62
4.28 Ions in solution in exact proportion to the water diameter. 63
4.29 Cation dependent difference spectra of 4 M solutions for the monovalent and 2 M solutions for the bivalent cations. 65
4.30 The JONES DOLE viscosity B coefficient of selected cations in comparison to the height of the network peak in the difference spectra taken from table 4.19 67
4.31 Anion dependent difference spectra of selected sodium salts. 69

4.32 Apolar particle surrounded by hydrating water. 70
4.33 Real and difference spectra of a 0.5 M NaCl solution below the freezing point. 73
4.34 Spectra of freezing 0.5 M KCl, RbCl, CsCl and NaF solutions. 74
4.35 Spectra of freezing 0.5 M NaCl, NaBr and NaI solutions. 75
4.36 Frozen 0.5 M sodium halide solutions in H_2O and D_2O. 76
4.37 OH stretch region of freezing 0.5 M NaCl solutions in 95mol% D_2O with 5mol% H_2O and in pure H_2O. 77
4.38 OH stretch region of frozen 0.5 M alkali chloride solutions in H_2O. 78
4.39 OH stretch region of a) a frozen 0.5 M lithium chloride solution in H_2O and b) LiCl solutions at several concentrations at ambient conditions. 79

1 Development of $2\nu_2$ at several mol% ratios of H_2O and D_2O. 102
2 Anion dependent difference spectra of 1 M solutions of Li, Na, K, Rb and Cs halides. 103
3 Anion dependent difference spectra of 2 M solutions of Li, Na, K, Rb and Cs halides. 104
4 Cation dependent difference spectra of 1 M solutions of Li, Na, K, Rb and Cs halides. 106
5 Cation dependent difference spectra of 2 M solutions of Li, Na, K, Rb and Cs halides. 107
6 Anion dependent difference spectra of 1 M Mg and Ca halide solutions. . . 108
7 Anion dependent difference spectra of 0.5 M Mg and Ca halide solutions. . 108
8 Cation dependent difference spectra of 1 M solutions for the monovalent and 0.5 M solutions for the bivalent cations. 109
9 Cation dependent difference spectra of 2 M solutions for the monovalent and 1 M solutions for the bivalent cations. 110
10 Anion dependent original spectra of selected sodium salts. 111

List of Tables

2.1 Positions of the peak maxima of H_2O and D_2O in the mid-IR region. . . . 4
2.2 Positions of the peak maxima of contributions to represent the OH stretch band. . . . 5
2.3 Jones-Dole viscosity B coefficient of several Hofmeister ions. . . . 13
2.4 Solubilities of alkaline and selected earth alkaline halides at 293 K. . . . 14
2.5 Heats of solutions for alkaline and selected earth alkaline halides. . . . 15

3.1 Division of the infrared region. . . . 17

4.1 Wavenumber positions of the peaks of the six contributions which fit the spectra at maximum intensity for H_2O and D_2O. . . . 34
4.2 Gaps between the six contributions which fit the spectra at maximum intensity for H_2O and D_2O. . . . 37
4.3 B3LYP/6-311++G** calculated frequencies and intensities of the hydrogen bonded and free OH vibrational modes of a cyclic water hexamer. . . . 53
4.4 Maxima of the positive peak of 4 M alkali halide solutions. . . . 55
4.5 Minima of the network peak of 4 M alkali halide solutions. . . . 55
4.6 Anion dependent shifts of the maxima of the positive peak of 4 M alkali halide solutions. . . . 56
4.7 Anion dependent average shifts for the maxima of the positive peak of 4 M alkali halide solutions. . . . 56
4.8 Anion dependent shifts of the minima of the network peak of 4 M alkali halide solutions. . . . 57
4.9 Anion dependent average shifts for the minima of the network peak of 4 M alkali halide solutions. . . . 57
4.10 Cation dependent shifts of the maxima of the positive peak of 4 M alkali halide solutions. . . . 58
4.11 Cation dependent average shifts of the maxima of the positive peak of alkali halide solutions. . . . 58

4.12 Cation dependent shifts of the minima of the network peak of 4 M alkali halide solutions. 59
4.13 Cation dependent average shifts of the minima of the network peak of alkali halide solutions. 59
4.14 Ionic radii of several HOFMEISTER ions in solution. 60
4.15 Maxima of the positive peak at $\sim$3400 cm^{-1} of 4 M solutions of Li halides and 2 M solutions of Ca and Mg halides. 61
4.16 Maxima and minima of the network peak of 4 M solutions of Li halides and 2 M solutions of Ca and Mg halides. 61
4.17 Anion dependent shifts of the maxima of the positive peak of 4 M solutions of Li halides and 2 M solutions of Ca and Mg halides. 62
4.18 Cation dependent shifts of the maxima of the positive peak of 4 M Li halide and 2 M Ca and Mg halide solutions. 63
4.19 Peak heights of the network peak for 2 and 4 M solutions of bivalent and monovalent ions respectively. 66
4.20 Ions arranged according to their effects on the structure of water represented by the parameter ΔG_{HB}. 67

1 Functional settings of the Vector 22 spectrometer. 100
2 Physical data of investigated salts. 101
3 Maxima of the positive peak of 1 M alkali halide solutions. 103
4 Minima of the negative peak of 1 M alkali halide solutions. 103
5 Maxima of the positive peak of 2 M alkali halide solutions. 104
6 Minima of the negative peak of 2 M alkali halide solutions. 104
7 Anion dependent shifts of the maxima of the positive peak of 1 M alkali halide solutions. 105
8 Anion dependent shifts of the minima of the negative peak of 1 M alkali halide solutions. 105
9 Anion dependent shifts of the maxima of the positive peak of 2 M alkali halide solutions. 105
10 Anion dependent shifts of the minima of the negative peak of 2 M alkali halide solutions. 105
11 Cation dependent shifts of the maxima of the positive peak of 1 M alkali halide solutions. 106
12 Cation dependent shifts of the minima of the negative peak of 1 M alkali halide solutions. 106

13 Cation dependent shifts of the maxima of the positive peak of 2 M alkali halide solutions. 107
14 Cation dependent shifts of the minima of the negative peak of 2 M alkali halide solutions. 107
15 Peak heights of the hydrogen bonded network peak for aqueous 1 M alkaline and 0.5 M earth alkaline halide solutions. 109
16 Peak heights of the hydrogen bonded network peak for aqueous 2 M alkaline and 1 M earth alkaline halide solutions. 110

1 Introduction

Water and its extraordinary meaning for life on earth has been accounted for by many scientists. [1–4] Saltwater is the most abundant liquid on our planet, makes up a whole ecosystem for itself and still houses the biggest creatures to have ever lived on earth. At the same time it is essential for the smallest unit of life, the cell, and as a solvent within a bare necessity for biomolecules. Ball states that from experience of life on earth, it can be concluded that life as we know it cannot sustain in a waterless environment. [1]

Despite all the research that has been done on pure water and aqueous salt solutions with so many different approaches, we know a lot but understand surprisingly little about its structure, dynamics and countless anomalies. [5] A fact that is due to hydrogen bonding which gives water its unique features. Many models have been put up to explain the structure of water. Results of research on the influence which hydrated ions have on its structure have been and are still being published and controversially discussed among the water research community. [6] In this thesis the focus was put on the structure of water as well as effects regarding the Hofmeister series, such as the structure making and breaking ability of ions. Topics which have been issues for many decades and still provide the community with more than enough substance for fruitful discussions.

Several research groups around the world work in the area of determining properties of pure water and aqueous solutions. A lot of effort is put into this research with a lot of different approaches and techniques. Only to name a few, there is the group around James Skinner in Madison, Wisconsin who by combining IR- and Raman spectroscopy with the theoretical method of molecular dynamics simulations try to reveal new aspects regarding the dynamic behaviour of water around ions [7] as well as more details regarding the hydrogen bond and its network to gain more structural information about pure H_2O. [8] Another question which is puzzling the ultrafast spectroscopists in the Netherlands in the group of Huib Bakker in Amsterdam is the question of the range of the effect which hydrated ions exert on the structure of water, is it short or long range? [9] They also analyse the dynamics of protons in water using THz Time-Domain spectroscopy. [10] Another group which applies THz spectroscopy successfully, resides at the Ruhr-University Bochum and is lead by Martina Havenith. In terms of water research they examine solute-induced

dynamical properties in solvation shells. [11] Regarding the research on the structure of water Alan Soper from England may not be forgotten. Using neutron diffraction he has made significant contributions to understanding the microscopic structure of water and aqueous solutions and investigated the way water molecules organise themselves around the ions and molecules which dissolve in or mix with water. [12] Schmidt et al. for example addressed the seemingly simple problem of locating the stretch vibrations underneath the OH stretch band in the mid IR spectrum [13], a problem which will also be discussed in this work.

Fundamental research has been provided by Kim Collins in Maryland, Baltimore over the last years on the Hofmeister series in a biochemical context. This series plays an important role for answering the question of how ions interact with biomolecules in aqueous solution and even influence their function. [14] Paul Cremer in College Station, Texas is also involved in investigations on the Hofmeister series applying vibrational sum frequency spectroscopy, trying to explain the mechanism of the Hofmeister effect and bring clarity to the definition of kosmotropic and chaotropic behaviour of ions. [15]

The process of freezing aqueous salt solution, which will also be of interest in this work, is thoroughly investigated with the help of molecular dynamics simulations in the research group of Pavel Jungwirth in Prague. A physical process which is of great interest for the marine chemist. [16]

In this work vibrational spectroscopy in general and attenuated total reflection spectroscopy in particular was used for investigations on aqueous electrolyte solutions and pure water. Especially for the investigations of the freezing process of salt solutions and brine rejection this technique can contribute very effectively. With ATR spectroscopy a small probe volume can easily be frozen and spectroscopically recorded, compared to transmission spectroscopy using vacuum sealed cells. The vibrational frequencies, foremost the OH stretch vibrations, are very sensitive to changes in their environment on a molecular level giving good information about the structure of the liquid.

A single water molecule by itself is very well understood from experiments and quantum-mechanical calculations. But if a large number of water molecules form a liquid, our understanding of its structure and dynamics is limited. [7] With ATR spectroscopy a cross section of all possible molecular arrangements in a large volume of water can be analysed to contribute to the description of the structure of water and the influence which ions have on it.

Although no differentiation between bulk, surface and hydration water can take place, effects depending on certain ions can be examined by keeping ions constant in a series of several salts. This is supported by the use of difference spectra which make it easier

to concentrate on and emphasise certain aspects which would go unnoticed in the normal spectra. This technique has been used before and proven to be very helpful. [17, 18] To support the results and interpretation of the spectroscopical findings quantum mechanical calculations as well as molecular dynamic simulations were carried out.

2 Theory and previous research

2.1 Water

2.1.1 IR spectroscopy studies on pure water

The broad OH stretch band of liquid water and its lack of well defined peaks make a decomposition into contributions and an assignment of those a challenging and controversial task. [19]

		symmetric stretch (ν_1)	asymmetric stretch (ν_3)	bending (ν_2)
gas [20]	H_2O	3657	3756	1595
	D_2O	2669	2788	1178
liquid [21]	H_2O	3400		1637
	D_2O	2500		1215
ice	H_2O	3172		1648
	D_2O	2358		1226

Table 2.1: Positions of the peak maxima in the spectra of gaseous, liquid and solid H_2O and D_2O in the mid-infrared region in wavenumbers (cm^{-1}).

In table 2.1 a general attribution of the OH modes is presented. Many attempts have been made over the last decades to decompose and explain the OH stretch band, which ranges from 2800 to 3700 cm^{-1}, and its features. Spectroscopical methods applied, are ATR FT-IR [22, 23], Raman [21, 24, 25] or vibrational sum-frequency generation which investigates water at interfaces. [26]

The substantial breadth of the OH stretch band demonstrates the sensitivity of the stretching frequency of an OH bond to its environment. It can be presumed that this is due to manyfold environments of hydrogen bonding in the liquid state of water. [19] In ice the average number of hydrogen bonds is four and they are linear. Each molecule participates in two donor and two acceptor hydrogen bonds. [19] The water molecule has a sp^3 orbital which leads to a tetrahedral structure with four potential binding sites for four neighbouring water molecules. These four spots do not necessarily need to be fully occupied. They are though in ice and the fully four coordinated water molecules are referred to as the "ice-like" structure. [27] The ideal tetrahedral angle would be 109.5°. In

reality an angle a little smaller at 104.5° is measured. That is, the hydrogen bonds are not exactly linear, but slightly distorted. The average energy of a hydrogen bond lies between the weak VAN DER WAALS interaction and that of a covalent bond at ∼5.5 kcal/mole. [28]

For the liquid state values between 3.2 and 3.7 [1, 19, 29] hydrogen bonds per molecule are reported in literature, depending on the model used for defining a hydrogen bond as shown by molecular dynamics simulations. [30] Nevertheless, AUER and SKINNER have shown in 2009 that the qualitative interpretation of spectroscopic data is not sensitive to the hydrogen bond definition. [19] They did so by comparing the interpretation of spectroscopic data using five different definitions and came to the conclusion that differences between the outcome are negligible.

The hydrogen bonds in liquid water are naturally distorted compared to those in ice and are breaking and reforming on a picosecond time scale. [6, 31] By far the bigger part of the water molecules must therefore be double donors and only a small fraction has broken bonds, i.e. in the bulk threefold and fourfold coordinated water molecules contribute most to the IR or RAMAN spectra. [19, 32] Table 2.2 gives an overview of several approaches to decompose the OH stretch band. For these contributions many different assignments are available but not entirely agreed upon. [26]

ref	peak maxima in $\tilde{\nu}$ [cm^{-1}]					
[31]	-	-	3295	3460	-	3590
[24]	-	-	3215	3450	-	3571
[33]	-	-	3250	3400	-	3600
[34]	-	-	3250	3450	-	3600
[35]	-	-	3240	3435	3540	3622
[36]	-	-	3230	3420	3540	3620
[37]	-	-	3220	3405	3520	3630
[38]	ν_{bonded}	-	3260	3364	3524	3633
[13]	3045	3134	3246	3390	3535	3629
[39]	2978	3111	3226	3362	3495	3611

Table 2.2: Positions of the peak maxima of contributions to represent the OH stretch band.

BRUBACH et al. in ref [31] call their bands network water (3295 cm^{-1}) related to the ice-structure, intermediate water (3460 cm^{-1}) and multimer water (3590 cm^{-1}) which is close to wavenumber positions found in multimers such as dimers. GOPALAKRISHNAN et al. in ref [24] assign their bands to the OH groups of four-coordinated, symmetric oscillating water molecules (3215 cm^{-1}), to the OH groups of four-coordinated, asymmetric oscillating water molecules (3450 cm^{-1}) and to the OH groups of three-coordinated, asymmetric oscillating water molecules (3571 cm^{-1}) where one OH is strong and the other weakly hydrogen bonded. SCHIFFER et al. in ref [33] and citations therein describe that the three

components are attributed to monomer, dimer or trimer species to zero-, two- and four-coordinated water molecules to non-bonded, one-bonded and two-bonded molecules. They are also attributed to the stretch vibrations ν_1, ν_3 and the bending overtone $2\nu_2$ in differing orders. $3250\,\mathrm{cm}^{-1}$ is assigned to $2\nu_2$ as well as ν_1. $3400\,\mathrm{cm}^{-1}$ is assigned to ν_1 and ν_3. Only the contribution at the highest wavenumber seems to be rather agreed upon to be ν_3.

Venyaminov et al. in ref [34] also postulate a three component model and attribute the contributions to the stretching vibrations. $3250\,\mathrm{cm}^{-1}$ being $2\nu_2$ enhanced by Fermi resonance, $3450\,\mathrm{cm}^{-1}$ as ν_1 and $3600\,\mathrm{cm}^{-1}$ as ν_3. Walrafen et al. support their decomposition into four Gaussian bands by Raman measurements but do not come up with a definition of these bands. [35] In ref [36] Wei et al. identify four bands in the OH stretch band. An icelike component at $3230\,\mathrm{cm}^{-1}$, an icelike liquid component at $3420\,\mathrm{cm}^{-1}$, a liquidlike amorphous phase at $3540\,\mathrm{cm}^{-1}$ and monomeric water molecules at $3620\,\mathrm{cm}^{-1}$. Four contributions in the liquid phase are discovered by Millo et al. in ref [37]. They analyse the second derivative of the spectrum and explain those contributions in terms of several species of water molecules each vibrating at a slightly different frequency in the same spectral region. [37] Fischer et al. come up with a five component model in ref [38]. At the low frequency end of the OH stretch band they name a ν_{bonded}, as counterpart to ν_{free} but do not attribute it to any wavenumber. They interpret $3260\,\mathrm{cm}^{-1}$ as $2\nu_2$, $3364\,\mathrm{cm}^{-1}$ as ν_1, $3524\,\mathrm{cm}^{-1}$ as ν_3 and $3633\,\mathrm{cm}^{-1}$ as ν_{free}. The bond ordering parameter by Ohno [40] parameterises the effect of the cooperativity of hydrogen bonding. This concept is used by Schmidt et al. to attribute six contributions with decreasing cooperativity from the contribution with the lowest to the one with the highest wavenumber, the contribution at $3629\,\mathrm{cm}^{-1}$ is defined as free (monomer-like). [13] In 2009 publication we attributed ν_1 to $3362\,\mathrm{cm}^{-1}$ and ν_3 to $3495\,\mathrm{cm}^{-1}$. The contribution at $3611\,\mathrm{cm}^{-1}$ was called the quasi free OH group. An attribution of the first three is pending. [39]

In general the area in the low wavenumber range of the OH stretch band is referred to as the "ice-like" region, since it is similar in position to the very dominant peak in the ice spectrum (see figure 4.1). [41, 42]

2.1.2 Coupling and Fermi resonance

Problems which add to the challenge of decomposing the OH stretch band are coupling and Fermi resonance. [19, 21] Coupling causes changes in the frequency and occurs when two oscillating bonds with the same characteristic frequency and energy are weakly connected. This is the case for two adjacent OH groups from different water molecules in liquid water or ice. If two oscillators additionally are physically connected, in the case of water via the

oxygen, coupling is even stronger since intramolecular coupling also occurs between ν_1 and ν_3.

The effect of coupling can be eliminated. If two oscillators of different bond length and frequency are connected the frequency changes produced are very small, the two bonds are thus uncoupled. Uncoupling in water is achieved by substituting hydrogens for deuterons. The OD bond has a much lower frequency than the OH bond, therefore inter- and intramolecular coupling is largely eliminated. [8] The large shift of approximately $1000\,\mathrm{cm}^{-1}$ is due to the doubling of the mass of a hydrogen compared to a deuteron. Practical are solutions of small amounts of HDO in H_2O or D_2O. [21]

The main vibrations of liquid water are the symmetric ν_1, asymmetric ν_3 and bending ν_2 vibration, where ν_1 and ν_3 are coupled. [21] The overtone of the bending vibration $2\nu_2$ is theoretically expected at around $3290\,\mathrm{cm}^{-1}$ and is therefore situated right underneath the broad band of the normal modes of water. The intensity of $2\nu_2$ is only a fraction of its origin ν_2 and therefore very minute. Compared to the intensity of the OH stretch band it should be negligible.

It is known from literature that in apolar solvents such as CCl_4 the overtone in fact is negligible. [42] In polar environments, such as water, overtones tend to be of significant intensities. [43] Overlapping vibrational modes can 'borrow' intensity from each other and the overtone could contribute significantly to the OH stretch band in this region around $3290\,\mathrm{cm}^{-1}$. Intensity and position could vary from theoretical presumptions. This phenomenon is called Fermi resonance and can also be reduced by isotopic substitution, i.e. the partial exchange of hydrogens for deuterons. [21]

2.1.3 Isosbestic point

Isosbestic, derived from the greek words isos:equal and sbestos:extinguishable, describes a point, i.e. wavenumber, wavelength or frequency, in a spectrum where absorbance stays the same during a chemical reaction or the physical change of a sample. [44] In 2005 Smith et al. have shown that an isosbestic point not necessarily needs to be a point caused by two interconverting species, but can also be caused by simple thermal variations of a single species lineshape. [29] Geissler contributes to this topic analysing that an isosbestic point can be caused by inhomogeneous broadening. [45] This is also pointed out by the IUPAC. [44]

2.1.4 Mixture and continuum model

Two types of models have been in open scientific competition over the last years to explain the structure of water from data obtained by IR spectroscopy. First the *mixture* or *multicomponent model*, which suggests that the structure of water can be explained by a number of discrete species. [13,21,35,40,46,47] This image was first proposed by RÖNTGEN in 1892. [48] Several of these mixture models are described in section 2.1.1 and table 2.2. In general two main local structures are identified, one distorted tetrahedral arrangement and some amount of interstitial water molecules being only weakly bonded or non bonded. [49] A modern mixture model was proposed by STANLEY et al. in 1980 describing the degree of connectivity observed in a lattice of four coordinate sites, distinguishing two groups by an energy criterion. [50, 51] In recent years models with more than just two states have emerged (see table 2.2). WALRAFEN, as avid supporter of the mixture model, wrote that each identified class encompasses broad GAUSSIAN components and each component refers to structures which involve a range of bond angles and distances around the components peak position. [52]

The second, the *continuum model*, claims that the hydrogen bond geometries and energies of water can be explained as a continuum of several states with distorted but not broken hydrogen bonds of varying strength which cannot be separated sharply but display rather stageless transitions. [29, 33, 53–55]

It has also been stated and criticised that the decomposition of the OH stretch band into GAUSSIAN components is most likely fortuitous. [29] Recent studies of LAROUCHE et al. have called the continuum model into question, since they find distinct hydrogen bond regimes that lead to distinct OH stretch vibrations. [56]

Some research groups try to find some common ground between the extremes of the mixture and the continuum model. [17, 50, 51, 53, 55]

2.2 Aqueous electrolyte solutions

The importance of ions dissolved in water throughout biology and chemistry cannot be dismissed. Ions in solution affect the conformation and activities of proteins and nucleic acids. Ion complexation in cells is crucial for the activities of biomolecules such as enzymes and drugs. Ions regulate the conductance and permeability of cell membranes. In chemistry ions can affect the rate of chemical reactions. They are widely used in food applications and ion exchange mechanisms for chemical separation. [57]

Dissolving salts in water leads to a change of the OH stretch band. [36] New contributions

can be observed which are caused by the hydrogen bonded ions. Thus three OH species are present: water molecules hydrogen bonded to another water molecule, water molecules hydrogen bonded to anions via a hydrogen atom and water molecules interacting with the cation via the oxygen atom. The interaction with the cation is generally considered to be of minor influence. Ion bonded OH groups absorb at different frequencies, because the OH stretch frequency depends on the strength of the hydrogen bond. [58] For the studies during the course of this work this influence is of major importance.

There are many physical properties of pure water which change significantly when salts are dissolved, for example the viscosity or conductivity. [59] Changes naturally depend on size and ionic charge of the dissolved salt. But what is of greatest interest is how the structure of water is influenced by the hydrated ions and how changes of macroscopic properties are reflected in the molecular structure.

A problem is the quantification of these effects because the structure of water itself is a great and only partially solved puzzle. [60] In this work a backward approach is employed: by studying changes of a system, additional information can hopefully be gained for the unchanged system which is not entirely unravelled.

2.2.1 Hydration

When a salt is dissolved in water it dissociates into the ions it consists of. Ions are either positively or negatively charged particles. Water is a polar solvent, the hydrogen atom carries a positive partial charge whereas the oxygen atom is partially negatively charged. Due to the charged nature of all participants, some reorientation takes place. A hydration shell forms around the ions.

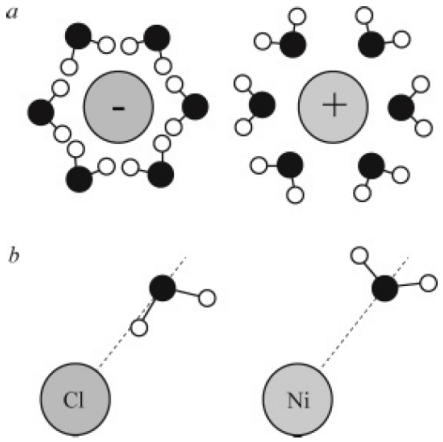

Figure 2.1: Hydration of anions and cations. a) The conventional view. b) Water orientations revealed by neutron scattering. [1]

The common and old fashioned text book picture of a hydration shell is shown in figure 2.1a. This simple picture does not match the present state of research on hydration shells. But what it basically shows is still valid. The hydrogen atom with its positive charge points towards the anion and the negatively charged oxygen is directed towards the cation. In figure 2.1b it can easily be seen, that the actual picture is more complex. Neutron scattering experiments have revealed a more asymmetric arrangement of the molecules around ions. [61] For anions the OH group is pointing almost perpendicular towards the ion and for the cation the HOH angle is not in perfect symmetry but is slightly tilted. What is not included in these pictures is that for some ions even a second hydration shell is well defined and can be described. [62]

In general anions are more strongly hydrated than cations with similar charge densities. Collins mentions two arguments. First, anions which interact with the hydrogen of the water allow hydrogen bonding to take place inside the hydration shell, whereas cations, interacting with the oxygen do not. Another characterisation for strong hydration is the charge transfer to the solvent. It is easier for the hydrogen to accept the negative charge from the anion, than for the oxygen to accept the positive charge from the cation. [63] This is also the reason why the cation effect described above is considered to be of minor influence.

2.2.2 The Hofmeister series

Always mentioned in the context of aqueous salt solutions is the notorious Hofmeister series which was put up during an empirical study that was conducted by Franz Hofmeister in Prague at the end of the 19^{th} century. This series orders salts according to their ability to precipitate (salt out) proteins from an aqueous solution, i.e. decrease their solubility. [64] It can be explained more generally by the hydrophobic or Hofmeister effect. That means that dissolved salts cause hydrophobic effects not only for proteins but for other molecules too, such as benzene. [65] Salting out is thus an increase and salting in a decrease of hydrophobicity.

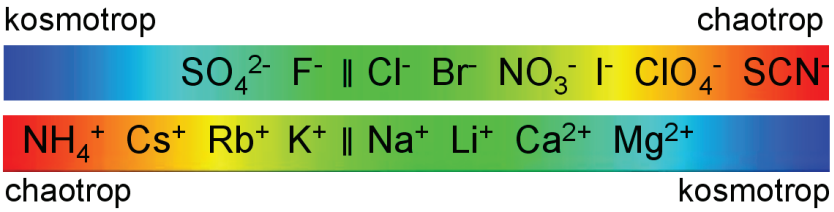

Figure 2.2: The Hofmeister series based on the Jones-Dole viscosity B coefficient. [66] The anion series is also based on the sequence in which they elute from a Sephadex® G10 column. [67] The || marks the border between kosmo- and chaotropes.

The HOFMEISTER effect is directly proportional to the salt concentration and it can be expressed by the SETCHÉNOW equation. It was developed by SETCHÉNOW in 1892 when he was carrying out experiments on the solubility of CO_2 in blood and found it to be directly proportional to the salt concentration. [65]

$$ln[C_i/C_i(0)] = -k_s C_s \tag{2.1}$$

C_i and $C_i(0)$ are the molar solubilities of the hydrophobe in a salt solution and in water respectively. C_s is the molar concentration of the salt, and k_s is the salt's SETCHÉNOW salting-out coefficient.

The appearance of this rank-ordering of ions has been observed on a wide range of phenomena [67, 68] especially regarding macromolecules. From this fact arises the curiosity of the series, since it is not quite clear and difficult to explain why this sequence is so common for so many different properties such as solubility of salts, electrolyte activities, pH-measurements, buffers, bacterial growth, protein and polymer folding or enzyme activity. [15, 68]

A description of the effect on a molecular level is far from complete and the question of how the effect is mediated remains unanswered. Is it mediated through direct interactions between the ions and the macromolecule or do the ions alter the physical and chemical properties of water in such a way that these changed properties cause the effect through the water? It is widely accepted that the HOFMEISTER effect is more pronounced for the anions than for the cations. [69]

The series has experienced a renaissance over the last decade and has moved back into the focus of researchers. The ROYAL SOCIETY OF CHEMISTRY will even hold a Faraday Discussion titled "Ion specific Hofmeister effects" in Oxford, 2012.

2.2.3 The concept of structure making and breaking

Small highly charged ions (F^-, Li^+, Na^+, Ca^{2+}, Mg^{2+}), the structure makers or kosmotropes, bind stronger to a water molecule than a water molecule to another water molecule in the pure liquid. On the other side large monovalent ions (I^-, Br^-, Cl^-, Rb^+, Cs^+), the structure breakers or chaotropes, exhibit weaker interactions to the next water molecule than a water molecule to another water molecule again in the pure liquid. [63] Kosmotropes are therefore strongly and chaotropes weakly hydrated. Around kosmotropes more and stronger hydrogen bonds per water molecule can be found compared to pure water. In the surrounding of chaotropes less and weaker hydrogen bonds can be observed. [3, 70]. The polyatomic ions SO_4^{2-} and PO_4^{3-} are structure makers,

whereas NO_3^-, ClO_4^- and SCN^- are structure breakers. [71]

Regarding the Hofmeister series one has to be careful with the terms kosmotropic and chaotropic since they refer to the ions influence on water [63], whereas the Hofmeister series itself originally deals with protein stability. As one can see in figure 2.2 kosmotropic anions and chaotropic cations cause stabilising of the protein, i.e. salting out, a decrease of solubility and denaturation causing aggregation. On the other side of the series chaotropic anions and kosmotropic cations cause a destabilising of the protein, i.e. salting in, an increase in solubility and denaturation.

In some publications the term "stabilising proteins" and kosmotropic are used synonymous, just like "destabilising proteins" and chaotropic. [72] But this only holds true for the anions. This misconception may occur, because the cationic Hofmeister series is only scarcely investigated and discussed in literature. [3]

It was not before the works of Cox and Wolfenden in 1934 and the work of Gurney in 1953 that the terms structure making and structure breaking were brought into the context of the structure of water, based on works on the viscosity of electrolyte solutions. [3] The viscosity of electrolyte solutions is expressed by the Jones-Dole viscosity B coefficient represented in the following formula. [2, 66, 73]

$$\frac{\eta - \eta_0}{\eta_0} \cong A\sqrt{c} + Bc \tag{2.2}$$

η is the viscosity of the electrolyte solution, η_0 is the viscosity of pure water, A and B are constants and c the ionic concentration. The equation holds true for concentrations up to $\sim$1M. Coefficient A is independent of c and related to the electrostatic interactions between the ions and can easily be calculated. [74] B on the other hand represents the influence of the ion on the hydrogen bond network and is also a measure for the structuredness of water. [75] A positive B coefficient can be found for ions with high charge density (strongly hydrated), a negative value often occurs with ions of lower charge density (weakly hydrated). The former are the structure makers the latter the structure breakers. [2, 66] The change from negative to positive sign indicates ideal behaviour, that is water-ion interaction is approaching behaviour of water-water interaction (see table 2.3).

In 1962 Hamaguchi et al. came up with the term chaotropic and Collins et al. introduced the term kosmotropic in 1985. [67, 76] Franks denotes that it is not the structure of pure water, i.e. the tetrahedral network which is made or broken, it is a structure which is imposed on the water by strong ion-dipole forces. [77] Mancinelli and Wright also stress this point. [71, 78]

Cation	B ($dm^3\ mol^{-1}$)	Anion	B ($dm^3\ mol^{-1}$)
Mg^{2+}	0.385	PO_4^{3-}	0.590
Ca^{2+}	0.285	CH_3COO^-	0.250
Ba^{2+}	0.220	SO_4^{2-}	0.208
Li^+	0.150	F^-	0.100
Na^+	0.086	$HCOO^-$	0.052
K^+	−0.007	Cl^-	−0.007
NH_4^+	−0.007	Br^-	−0.032
Rb^+	−0.030	NO_3^-	−0.046
Cs^+	−0.045	ClO_4^-	−0.061
		I^-	−0.068
		SCN^-	−0.103

Table 2.3: JONES-DOLE viscosity B coefficient of several HOFMEISTER ions. [63]

Over the last decade this concept of kosmotropic and chaotropic behaviour of ions has been challenged by computer simulations [1], diffraction measurements [78, 79], terahertz spectroscopy [6] and ultrafast spectroscopy. [9,80] This moved the HOFMEISTER series back into the focus of research. [69] These experiments do not falsify the concept of structure making and breaking, but they demonstrate its weaknesses and show that the concept has to be refined.

In this work the terms kosmo- and chaotropic are used only in the sense of making or breaking the structure of water. In this respect not the structure of pure water is meant, but an imposed structure due to electrostatic forces. [71] When discussing the stability of proteins the terms stabilising or destabilising shall be applied.

2.2.4 Long range vs. short range effect

Well defined first and second hydration shells have been recorded for most ions, but how far the electric field influences the beyond is undetermined or controversially discussed. [2, 3] The question of long or short range influence of the hydrated ions on the structure of water goes hand in hand with the question of structure making and breaking.

Researchers are divided into two parties. Those who show in their research that the influence of the ions on the water structure goes beyond the second hydration shell [62, 79, 81], and those who find that the influence is restricted to first and second hydration shells [82, 83] or may even be insignificant. [9]

The ultrafast spectroscopists around HUIB BAKKER measure the orientational-correlation times of water molecules near and far from the ion. They find that the orientational-correlation time outside the first hydration shell is the same as in pure water.They also

find that water molecules hydrating a cation show almost the same dynamical behaviour as the bulk water, whereas the hydration shells of the anions demonstrate slow dynamics compared to bulk water. [83] They conclude that the water structure outside the first hydration shell cannot be strongly influenced and is similar to pure water.

Holzmann, Mancinelli and Leberman observe major changes with the pair correlation function $g_{OO}(r)$ from molecular dynamics simulations and neutron scattering in the bulk water of salt solutions and compare the effect of the salt on the water structure with the effect of pressure put onto the liquid. [62, 79, 81] Dougherty comes to similar conclusions from Raman experiments and studies of the "apparent density" of electrolyte solutions [84, 85]. He finds a strong influence on the hydrogen bonded network, namely an increase in the strength of hydrogen bonds in the bulk phase.

2.2.5 Ion pair formation

The molar solubilities presented in table 2.4 of simple inorganic salts in water show a striking pattern. Small anions in combination with a small cation have a very low molar solubility, large anions and cations in combination behave very similar. On the other hand small anions with large cations or vice versa, have very high molar solubilities. This is due to the lattice enthalpies, but Collins notes that solubilities are also influenced by the formation of solvent-separated ion pairs. He argues that for some ion combinations the formation of ion pairs can be energetically more favourable than the hydrated state. [63] This is the case for small anions and cations (kosmotropes) as well as for large anions and cations (chaotropes), the same combinations which tend to be of very low molar solubility. [86]

	F^-	Cl^-	Br^-	I^-
Li^+	2.7 (0.0501)[1]	830 (19.5782)	1770 (20.3811)	1650 (12.3276)
Na^+	40 (0.9526)	360 (6.1599)	910 (8.8441)	1790 (11.9418)
K^+	950 (16.3520)	347 (4.6545)	670 (5.6301)	1440 (8.6746)
Rb^+	1310 (12.5399)	910 (7.5256)	1100 (6.6517)	1520 (7.1572)
Cs^+	3700 (24.3575	1860(11.0479)	1080 (5.0750)	790 (3.0407)
Mg^{2+}	0.08 (0.0013)	542 (5.6926)	1020 (5.5401)	1480 (5.3216)
Ca^{2+}	0.016 (0.0002)	745 (6.7127)	1420 (7.1040)	2090 (7.1116)

[1] at 299 K

Table 2.4: Solubilities in g/l of alkaline and selected earth alkaline halides at 293 K unless otherwise indicated. Values in brackets are molar solubility. See appendix 2 for references.

Large/small combinations tend to stay apart from each other and are therefore highly soluble. The less soluble a salt, the more likely it is to form ion pairs. Since the ion pair

itself remains hydrated it is commonly called an inner sphere ion pair. Ion pair formation occurs also at higher concentrations [78], but is negligible for concentrations below three mol/l. [85]

The behaviour of the solubility is also represented by the values of the heats of solutions. A similar pattern as in table 2.4 is found. For kosmotrope/chaotrope combinations the heat of solution is negative (exothermic). An endothermic standard heat of solution (positive) can be found for kosmotrope/kosmotrope and chaotrope/chaotrope combinations. [63] This is shown in table 2.5.

	F^-	Cl^-	Br^-	I^-
Li^+	4.73	−37.053	−48.86	−63.346
Na^+	1.9	3.9	−0.6	−7.5
K^+	−17.744	17.228	19.887	20.348
Rb^+	−26.126	17.291	21.897	25.121
Cs^+	−36.886	17.7939	26	33.369
Mg^{2+}	−7.9	−160	−185.6	−213.2
Ca^{2+}	11.5	−81.3	−103.1	−119.7

Table 2.5: Heats of solutions in kJ/mole. Li^+, K^+, Rb^+, Cs^+ values taken from ref [59]. Na^+, Mg^{2+} and Ca^{2+} values taken from ref [87].

2.2.6 Hydrate formation

The formation of hydrates is something well known from pocket sized heat pads preferably used in the colder seasons of the year. But hydrates and their formation are also a vast research area for themselves. Especially in marine chemistry they play a great role in the formation of sea ice.

Upon freezing of sea water brine pockets are formed in the ice in which highly concentrated salt solutions are trapped and change the thermodynamic behaviour of the ice. Their radius can vary from 1 mm to 2 cm. [88] Over the duration of several month these pockets are rinsed out by melting water which drains from the top to the bottom of the ice through connected cavities into the sea. [89] Inside these pockets salt can be found in solution, precipitated or as hydrates, depending on the condition of the ice. [88, 90] In hydrates water molecules are firmly bonded to the salt. These bonded OH groups can be distinguished very well in an IR spectrum.

3 Methods

Pure water and aqueous salt solutions have been studied by many techniques to obtain static or dynamic structural information. Using neutron diffraction and applying isotopic substitution good information about the positions of the hydrogen and oxygen can be gained. [61,78,79] Another method is X-ray diffraction or scattering, which is not sensitive to the hydrogen but sensitive to the oxygen position and provides the oxygen-oxygen radial distribution function. It also reveals the distances between the oxygen and the ions. [91,92]

Plenty of spectroscopic methods have also been applied, for example terahertz (THz) spectroscopy [6,93], dielectric relaxation [94] or nuclear magnetic resonance (NMR) spectroscopy [95,96] which is very useful for measuring correlation times for the rotation of molecule-fixed-axes. X-ray absorption and RAMAN are sensitive to the electronic excited states in the liquid. They are difficult to calculate and therefore not easy to interpret. [49,97] RAYLEIGH, BRILLOUIN and MÖSSBAUER spectroscopy have been used too. [2,96] Of course IR spectroscopy is a major player for investigating pure water and aqueous solutions. [13,21,35,37]

For most of these spectroscopic methods occurs the problem that one can only observe long time effects on a nano to microsecond time scale. Changes in the hydrogen bond network occur on the picosecond time scale, as well as the exchange between hydration shell and bulk water. [2] What can be observed is an average of all possible states of a molecule during the measurement. It is also hard to differentiate between water in the hydration shells and the bulk water. Most information on the dynamics of water, especially the ionic hydration shell, are coming at the moment from femtosecond pump-probe spectroscopy [9,80] or molecular dynamics simulations. [62,98]

3.1 ATR FT-IR spectroscopy

3.1.1 Infrared spectroscopy

Spectroscopy, derived from the latin words spectrum:*appearance, image* and scopus:*aim, target*, is the technique by which the interaction between radiation and matter as a function of wavelength (λ) is studied. Infrared spectroscopy has its focus on the infrared (IR)

region, which can be found below (lat:infra) the red region of the visible light and was discovered by Sir William Herschel in 1800. The first IR spectrometer was developed in Ludwigshafen (BASF) in 1937 by Erwin Lehrer still using the dispersive technique. Once Albert Michelson had introduced the interferometer named after him, IR spectroscopy rapidly became a standard technique in modern laboratories. [99] Main uses of IR spectroscopy are analytical methods for preparative and analytical chemists.

Among spectroscopists the IR region is divided into the near, mid and far infrared with relation to the visible light spectrum. The limits between these regions are not strictly defined and therefore vary in different publications. [99]

	wavenumber (cm^{-1})	wavelength (μm)	frequency (Hz)
Near	14000 to 4000	0.714 to 2.5	4.19×10^{14} to 1.19×10^{14}
Mid	4000 to 400	2.5 to 25	1.19×10^{14} to 1.19×10^{13}
Far	400 to 10	25 to 1000	1.19×10^{13} to 2.99×10^{11}

Table 3.1: Division of the infrared region.

Wavenumber ($\tilde{\nu}$), wavelength (λ) and frequency (ν) are defined as follows, where c is the speed of light in vacuum ($2.997 \times 10^{10}\,\mathrm{cm\,s^{-1}}$), E is energy in Joule and h is the Planck constant ($6.626 \times 10^{-34}\,\mathrm{J\,s}$).

$$\tilde{\nu} = \frac{\nu}{c} = \frac{1}{\lambda} = \frac{E}{hc} \tag{3.1}$$

The far-infrared, embraced by the mid infrared and terahertz region, can be used for detecting rotational vibrations and vibration of hydrogen bonds themselves due to the low energy levels needed. The mid-infrared, which was mainly investigated in this work, is used to study fundamental vibrations, such as the OH stretching vibrations. The high energy of near-infrared radiation, can excite overtone and harmonic vibrations. Applying infrared spectroscopy on aqueous solutions, as done in this work, is most adequate to detect variations in bond oscillations due to the large transition dipole moment of water. [31]

3.1.2 Fourier transformation

FT-IR has great advantages in comparison to the scanning monochromator (or dispersive) technique which is more commonly used in UV-Vis spectroscopy. Using the monochromator technique the wavelength is varied using a monochromator and the amount of energy absorbed at each wavelength is recorded one at a time. FT-IR makes use of an interferometer, in general a Michelson interferometer (see figure 3.1), to vary the wavelength of the infrared light which is passed through the sample. [100]

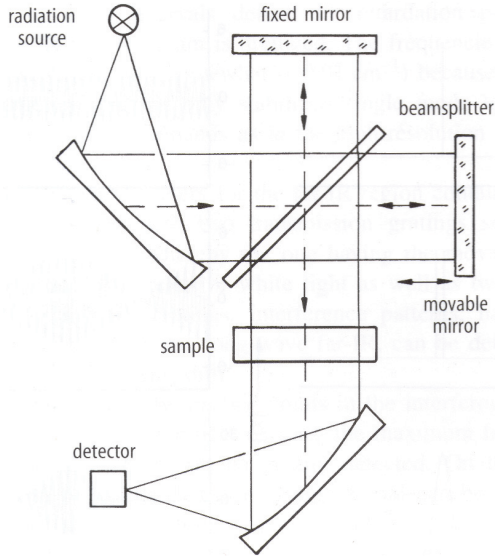

Figure 3.1: Schematic diagram of a FOURIER transform spectrometer with a standard MICHELSON interferometer. [99]

The signal recorded is an interferogram. The FOURIER transformation, named after the french physicist JEAN FOURIER (1768 - 1830), is a mathematical procedure which is of very widespread appliance and often unconsciously used, because a FOURIER transformation nowadays comes with the mouseclick.

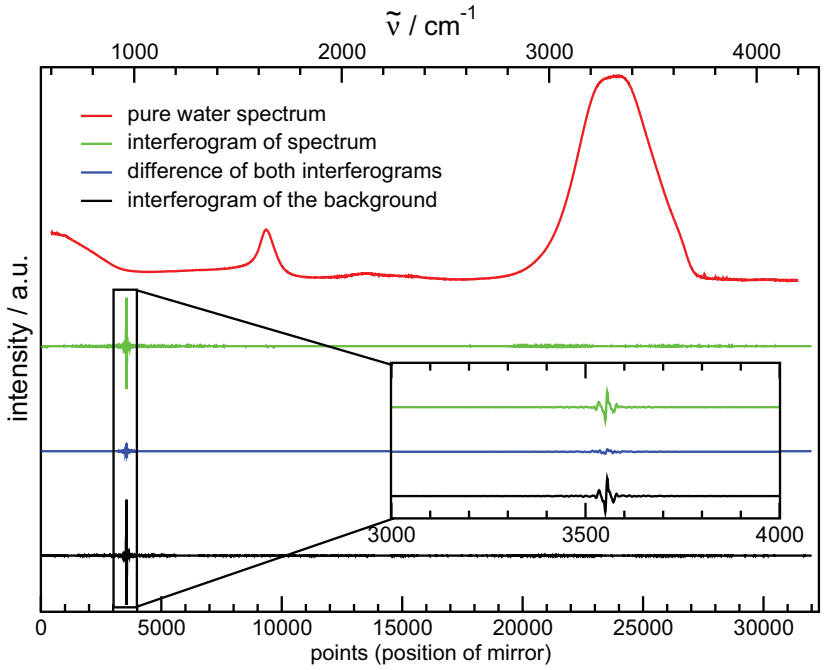

Figure 3.2: Comparison of reference and spectral interferogram. Including the resulting ATR spectra after FOURIER transforming the interferogram. The upper x-axis stands for the spectrum, while the lower x-axis is affiliated with the interferograms.

Performing a FOURIER transformation on this interferogram results in a spectrum identical to that obtained using dispersive infrared spectroscopy (see figure 3.2). The analysis of a signal for its spectral content is therefore easily done by a FOURIER transformation. [101] In figure 3.2 the effect of the FOURIER transformation on the interferogram can be apprehended. The portentousness of this procedure becomes clear, when one realises that the red spectrum results from a FOURIER transformation of the blue line. The great advantage of the FT-IR over the monochromator technique is that the information at all frequencies is collected simultaneously (FELLGET'S advantage) and sensitivity is greatly enhanced, because no light is absorbed by the monochromator (JACQUINOT'S advantage). [100]

3.1.3 Attenuated Total Reflection

In FT-IR ATR experiments the basic parts of the spectroscopic setup remain the same (see figure 3.1). The only difference being an ATR unit (see figure 3.4) put into the system instead of a cell.

The procedure

Internal reflection, which is the basis for ATR spectroscopy, was first described by ISAAC NEWTON (1643 - 1727). He also observed and described the evanescent wave that occurs during internal reflection which today is used to analyse samples via ATR spectroscopy. Like many inventions and discoveries ATR spectroscopy was a matter of independent development in the late fifties of the last century. N. J. HARRICK was researching on semiconductors at Philips Laboratories in Irvington-on-Hudson, New York and JACQUES FAHRENFORT was conducting similar studies in Amsterdam, Netherlands. They came to akin ideas and conclusions with two different approaches. FAHRENFORT introduced the phrase *attenuated total reflection*. [102] Once FT-IR spectroscopy became widely accepted ATR also had its breakthrough. Nowadays it is mainly used for analytical purposes, e.g. for quality control purposes in the wine industry. [103] And for substances which are impossible to measure in transmission, such as pastes or fabrics.

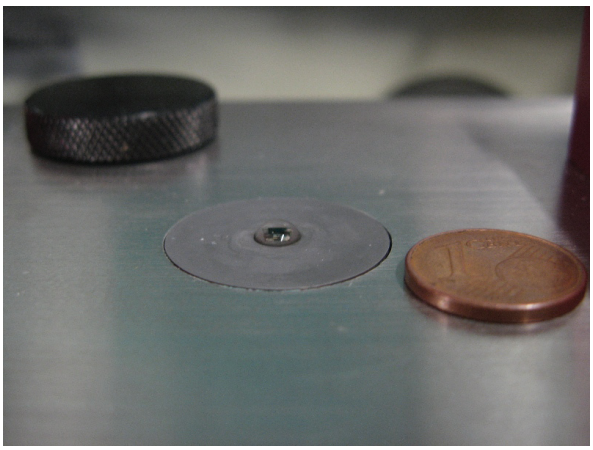

Figure 3.3: Drop on top of ATR crystal.

The procedure described here is for single reflection ATR (see figure 3.5). Using a standard FT-IR spectrometer the infrared beam travels, instead of being transmitted through cell and sample, through an ATR unit which is mounted inside the sample compartment (see figure 3.6). The beam is coming from the interferometer and passed into the mirror and lens system of the ATR unit (see figure 3.4). It travels through a non-absorbing crystal to suffer internal reflection at the back of the crystal. This is at the same time the interface between crystal and probe (see figure 3.3). Unlike the name suggests, the internal reflection is not total after all. The reflection is attenuated. A small part of the wave, the evanescent wave, penetrates the interface and interacts with the probe (see figure 3.5). This evanescent electric field can be observed for every wavelength. For the evanescent wave to occur one of the two touching media has to be of low the other of high refractive index. The IR beam lost a bit of its energy which was absorbed by the probe and now contains structural information. The detector finally takes up the signal.

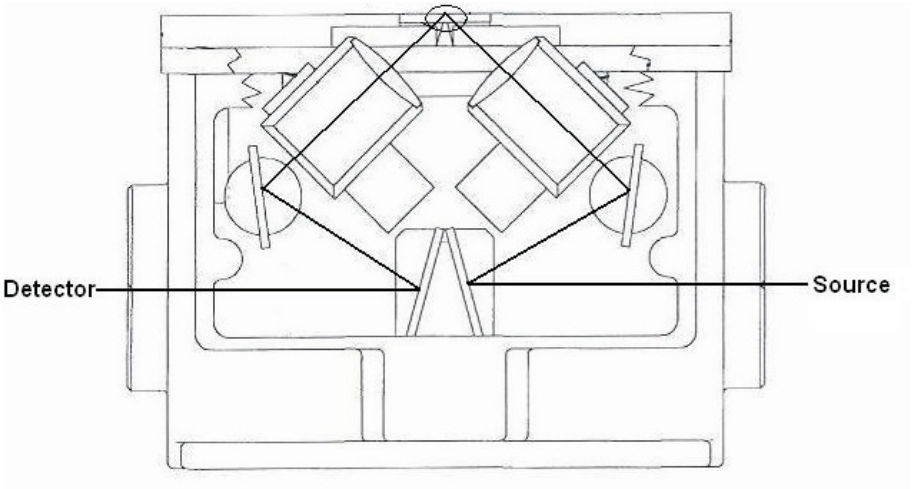

Figure 3.4: Optical path of IR beam through ATR unit. [104]

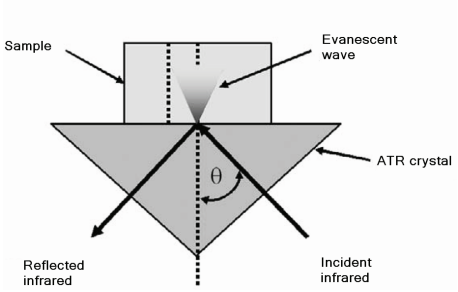

Figure 3.5: Beam path for ATR single reflection within the crystal. [105]

Advantages of ATR

Water is the compound mainly used in this work. The specific physical properties of water make the use of ATR inevitable. From the BEER-LAMBERT law it is well-established that each species will absorb light in proportion to its concentration. [56] Due to a very high molar concentration (55.5 mol/dm^3) of water and therefore an extremely large molar absorptivity (see equation 3.2) of the fundamental OH stretch band at 3400 cm^{-1} (ϵ_{solv} = 104.4 M^{-1}cm^{-1} [22, 106], 99.9 M^{-1}cm$^{-1}\pm$0.8 [34]) IR transmission measurements are difficult to obtain for this region. [47,106] The molar absorptivity E at the peaks wavelength λ is dependent on the absorbance A, the path length l and the concentration C.

$$E^{\lambda} = A^{\lambda}/lC \tag{3.2}$$

Technical feasible is a cell with a spacer as thin as 6 μm which produces an intensity level with very little information to be gained from the spectrum due to signal saturation. [22, 36, 107] This is also the main reason why the literature is almost devoid of IR studies using standard transmission technique. [17] In figure 3.8a the signal saturation of water measured in transmission with a 6 μm spacer is compared to the smooth curve of the same measurement with ATR spectroscopy. Calculations from VENYAMINOV et al. based on the molar absorptivity call for an optimal path length of 0.8 μm for the region of the OH stretch band. [34] In a cell with a very small path length influences from the surface cannot be ruled out. It is also very difficult to fill the small cells without the inclusion of air.

With ATR it is an easy task to obtain a penetration depth of 2 μm. By obtaining only a very small penetration depth it is possible to overcome the large absorption coefficient of water in the mid-infrared region. [37] It has to be considered that only the OH stretch band at around 3400 cm^{-1} is causing maximum absorbance. Other features of the spectrum such as the bending motion at 1637 cm^{-1} for example do not experience signal saturation in transmission. [34] Transmission experiments in regions far from the largest water absorption band can be applied without technical difficulties. [107] ATR provides a technique which is capable of producing consistent, reliable and easily reproduced results in the mid IR region especially for the intense OH stretch band. [22, 108]

Disadvantages of ATR

Two features of ATR spectroscopy shall be mentioned which affect the spectra adversely. First the so called *wavelength dependency* of the spectra and secondly the *anomalous dispersion* (AD).

Figure 3.6: FT-IR spectrometer with mounted ATR unit.

The first distortion occurring with ATR is very obvious when looking at equation 3.3. The penetration depth d_p is depending on the wavelength λ of the beam, thus with increasing wavelength the penetration depth and therefore intensity increases. [107, 109] Other important dimensions are n_1 which is the refractive index of the crystal, n_{21} is the ratio of refractive indices of sample and probe, and θ the angle of incidence.

$$d_p = \frac{\lambda}{2\pi n_1 \left(\sin^2\theta - n_{21}^2\right)} \tag{3.3}$$

The wavelength dependency or the $1/\nu$ effect is considered by the commercial OPUS software. [110] This distortion is rather small, very well taken care of and does not alter the band shapes significantly. [22] If direct comparison of ATR spectra to transmission spectra is required this correction has to be carried out. It is done by dividing the intensity of the ATR- spectra with λ [100, 111]. In fact the dependence of the penetration depth provides the opportunity to choose, whether one wants to investigate the surface or the bulk phase of the sample. The larger the incident angle and the higher the refractive index of the internal reflecting element is, the lower the penetration depth, thus only the surface is investigated (e.g. germanium at an angle of 60°). If one is more interested in the bulk phase an angle of 45° and a material of a smaller refractive index is chosen. These materials would be diamond, like in this work, or ZnSe. [100]

Secondly, anomalous dispersion is a strongly discussed feature in literature and amongst researchers using ATR spectroscopy. Dispersion means the dependency of any dimension on the wavelength. In optics this is generally the refractive index. Normal dispersion occurs when the refractive index n increases with decreasing wavelength λ (see relation 3.4). Most common example of normal dispersion is the dispersion of visible light by a

prism.

$$\frac{dn}{d\lambda} < 0 \tag{3.4}$$

Anomalous dispersion can be observed when the refractive index increases with increasing wavelength. It describes the effect which the changing refractive index along the wavelength has, on the shape and position of the OH stretch band in the mid-infrared region. In general the refractive index of water is given as $n = 1.33$ recorded at the sodium-d line (589 nm or 16977 cm^{-1}). But the refractive index of water changes significantly exactly in the spectral region of the OH stretch band (see figure 3.7).

Anomalous dispersion can change band positioning and intensity [22, 107] but does not create new bands or peaks although it makes quantitative analysis difficult. Max et al. have shown that anomalous dispersion does not influence the results of the solution analysis.

In general ATR spectra are very similar to transmission spectra. Differences can be observed due to the wavelength dependency and of course anomalous dispersion. It is important to note that anomalous dispersion can cause a shift of 70 cm^{-1} to lower frequencies (red shift). [22] If ATR spectroscopy is used for analytical purposes and unknown substances need to be identified anomalous dispersion is a drawback and needs to be clarified. In this work, where only water and aqueous solutions are investigated it is of minor significance. [100] [112]

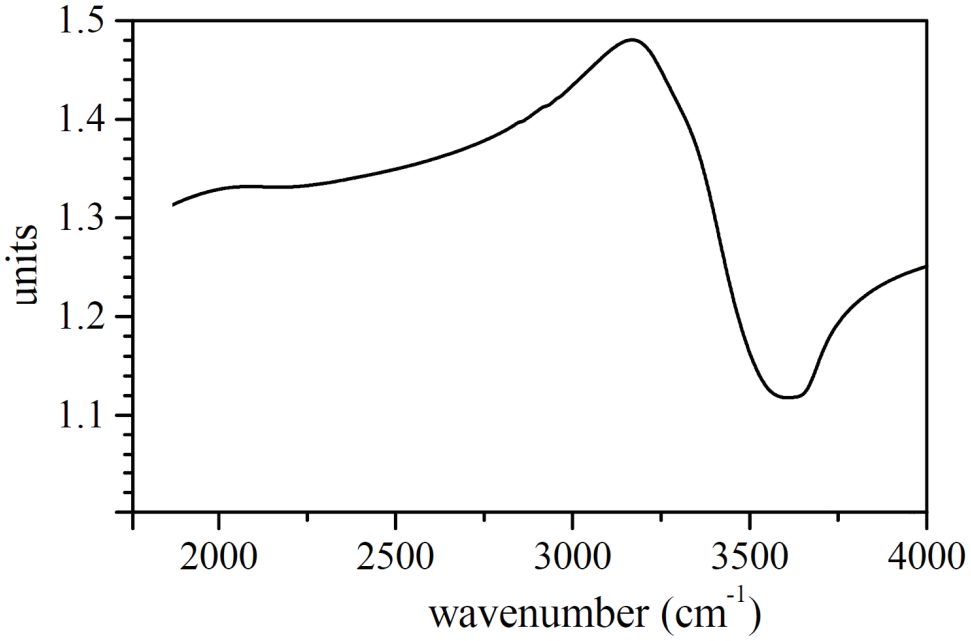

Figure 3.7: Anomalous dispersion, behaviour of n. [22]

Although anomalous dispersion can affect the position and shape of the bands ATR can

be employed with no concerns. Requirements are only that the refractive index of the crystal is far above that of the solution[1], the angle of incidence is appropriate and the length of the ATR crystal is sufficient. [36] Like Schmidt et al., Wei et al., and Max et al., the author does not believe that the conclusions drawn from the solutions spectra are significantly affected by anomalous dispersion. [36, 108, 112]

3.1.4 Isotopic substitution

HDO studies can help to interpret pure water studies. In the H_2O molecule two oscillators are present, a symmetric and an asymmetric one. They are coupled and influence each other, since they are very close to each other in their frequencies. [47, 113] This leads to a difficult interpretation of the spectra. To avoid coupling, deuterium, an isotopic substitute of hydrogen is used. In HDO the ν_{OH} and ν_{OD} are far apart from each other and are decoupled. The principles of coupling are explained in detail in section 2.1.2. OD and OH bands show similar features and can be compared. [17]

3.1.5 Comparability of transmission and ATR spectroscopy

Max et al. have shown that spectra obtained by transmission spectroscopy and ATR spectroscopy can be compared and that anomalous dispersion does not change the outcome of the solutions analysis. [112] In section 4.2 in table 4.1 the assigned contributions of D_2O measured in transmission and using ATR are listed and compared. A shift of about $20\,\mathrm{cm}^{-1}$ can be observed for each contribution from ATR to transmission, this is due to anomalous dispersion. [22] The course of intensities is the same for all contributions as shown in figure 4.6.

In figure 3.8b the varying outlook between D_2O in transmission and ATR becomes obvious. This is mainly due to a much smaller sample volume and therefore less molecules to vibrate and to add to the intensity. The molar absorptivity of D_2O is not as high as that of H_2O and D_2O can therefore be examined by transmission with an appropriate thin spacer of $6\,\mu$m.

[1] Diamond has a refractive index of 2.417

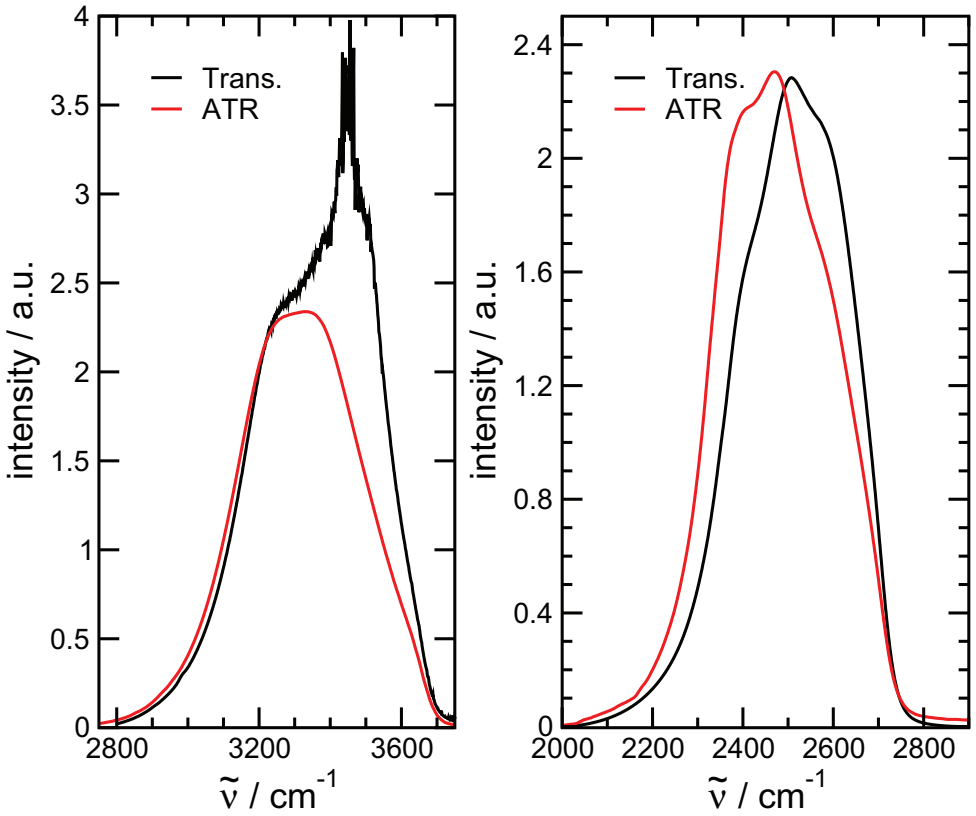

Figure 3.8: Transmission and ATR spectroscopy in comparison. a) Signals obtained by transmission and ATR spectroscopy for H_2O and b) D_2O measured with transmission and ATR spectroscopy. The ATR spectra are maximised to the intensity of the transmission spectra. The transmission spectra are obtained using vacuum sealed cells with a spacer of 6 μm.

3.2 Experiment

3.2.1 Technical setup for ATR spectroscopy

IR spectra were recorded using the very reliable Vector 22 FT-IR spectrometer supplied from Bruker with a standard DTGS detector. Beam source is a globar made of silicon carbide (SiC). ATR experiments were carried out with equipment mainly allocated by Specac. The MK II Golden Gate^{TM} Single Reflection ATR System with a heatable top-plate was applied for the measurements of this work. Low temperature measurements were achieved by applying the Low Temperature Golden Gate^{TM} Diamond ATR System cooled by liquid nitrogen. With the available equipment a temperature range of almost 200 K (173 K to 363 K) was accessible. To avoid evaporation at high temperatures a small lid with a rubber spacer was placed over the liquid sample. The top-plate was equipped with a 45° horizontal diamond as internal reflecting element (IRE) fitted in a tungsten carbide plate. The lattice vibrations of a diamond are situated at around 2000 cm^{-1} in the

mid-infrared region. A very short path length through the diamond provided good quality spectra nevertheless.

The temperature of the plate was controlled electrically using the 4000 Series^{TM} Stability Temperature Controller. The temperature could be changed at steps no less than 1 K. The optical compartment of the spectrometer was separated from the sample box by KBr windows. Both sections are purged with dry air processed by a Zander^{TM} ecodry KMA5 to avoid interference with high concentrations of water vapour coming from the atmosphere.

Sample measurements were taken against the reference of the dry and uncovered diamond surface. 50 scans were recorded for each spectrum at a spectral resolution of 1 cm^{-1}. Exact technical details of the spectroscopic setup are accounted for in appendix 1. Measurements were very sensitive to changes in the reference. Spectra of the background were therefore taken before each recording of a concentration dependent series of measurements. For temperature dependent measurements background spectra were recorded at every investigated temperature.

3.2.2 Technical setup for transmission spectroscopy

For the transmission experiments carried out during the course of this work sealed cells with CaF_2 windows provided by L.O.T-Oriel GmbH came into use with the same Vector 22 FT-IR spectrometer. Spacers with a thickness of 6 μm were most appropriate for the investigated samples. With these cells it was possible to cover a temperature range for water and especially D_2O from around 278 K to up to 353 K. The temperature was controlled by a cryostat (Thermo Haake C25P), allowing temperature changes of 0.1 K steps, the cooling agent was ethylene glycol. Purging of the spectrometer with dry air was achieved as described in section 3.2.1.

3.2.3 Experimental data

Sigma-Aldrich was the supplier for the salts used. They were used without further purification but drying in a drying cabinet at 523 K before preparing the solutions. Aqueous solutions were prepared using water from an ion exchanger which was additionally distilled twice. Fresh water was prepared in regular periods. D_2O was also supplied by Sigma-Aldrich with an isotopic purity of 99.9% and used without any further treatment. Physical and chemical properties of chemicals used can be found in appendix 2.

3.3 Data processing and analysis

The Opus software (Version 6.5) which comes with any Bruker spectrometer records and saves the spectra as Opus-files. Several processes have to be run before these data can be analysed and decomposed. First of all the region of interest is cut out, the spectra are then smoothed using the algorithm of Savitzky and Golay to reduce the noise significantly. [110] One has to be aware that smoothing can also have a large influence on the intensity of small bands. It has to be handled with care and not to many points may be taken for smoothing. Afterwards a base line correction is carried out. The Opus-file is then transformed into a simple xy-file and saved in the *.csv* format.

3.3.1 Decomposition of spectra

The simple xy-style is necessary since many more information besides the actual spectrum are saved in an Opus-file. With the help of home-programmed [114] software the spectra can be decomposed into several contributions described as Voigt-profiles. Every Voigt-profile is a convolution of a Gaussian- and a Lorentzian-shaped curve (see figure 3.9) and is determined by four values (intensity, wavenumber at the maximum, Gaussian and Lorentzian halfwidth), which can be fitted variable using the Levenberg-Marquardt algorithm. [115–117]

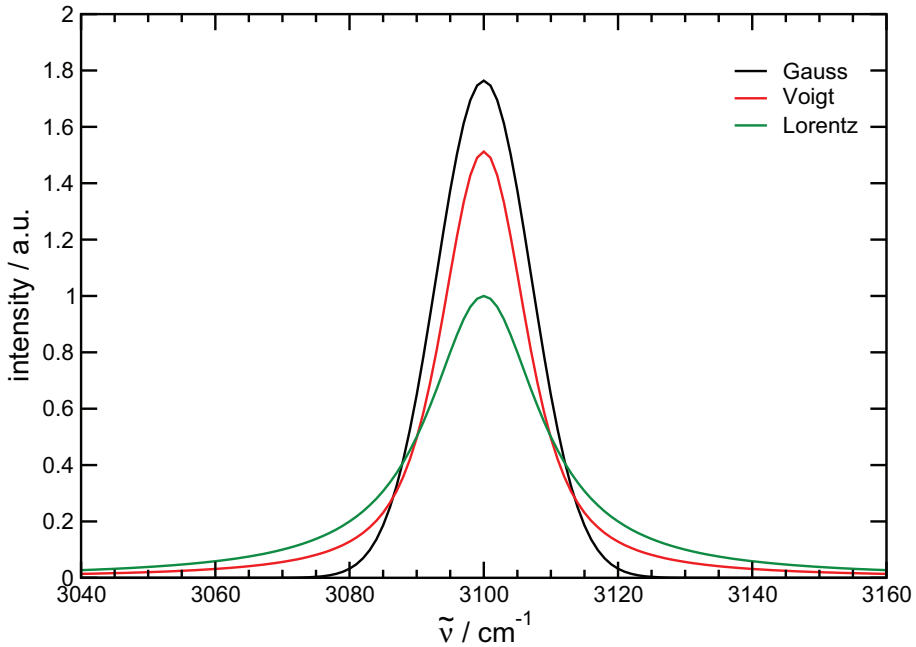

Figure 3.9: Comparison of Lorentz-, Gaussian-, and Voigt-profiles at equal areas under the curve. The halfwidth of the Lorentz and the Gaussian profile is 10 cm^{-1} The Voigt profile has a Lorentz and Gaussian halfwidth of 5 cm^{-1}. [114]

One major point of criticism on this procedure is the fact that the number of contributions is not calculated, by factor analysis for example [106], but predetermined by the scientist. [100] The choice of how many contributions are used for the fitting is based on chemical and physical knowledge and of course experience. It is possible to indirectly falsify or verify the choice made, by running a simultaneous decomposition of a couple of spectra of which only the wavenumber is fixed while the other three features are variable. This is a necessary simplification, as a simultaneous fit would not work otherwise. In general the programme should not be able to properly fit the spectra when the number of contributions is not appropriate. [118]

The software works with a convergence criterion which is a useful tool to define the end of a fitting procedure. In the end these processes are all "only" done by the computer and do not necessarily need to make any physical sense. It is inevitable that the final decision about the correctness of the decomposition obviously has to be made by the scientist. [100]

3.3.2 Difference spectra

Another very useful tool for the analysis and interpretation of the IR spectra are difference spectra. Difference spectra have been used on aqueous salt solutions as early as 1973 by Low. [119] When there are only small changes in the spectrum upon adding a salt it can be helpful to subtract the pure water spectrum from the spectrum of the aqueous salt solution at equal experimental conditions and only look at the specific differences and changes in particular areas. [17] This technique is widely used in scientific research on aqueous systems. [34, 36–38, 108, 120, 121]

The usage of difference spectra permits the separate analysis of the influence of anions and cations on the OH stretch band of water. Disadvantage of this technique is the fact, that only a cross section of the whole solution can be observed. A differentiation between hydration water or bulk water is impossible. Nevertheless, features specific to certain ions can easily be studied.

4 Results and Discussion

4.1 Mid IR spectra of H_2O and D_2O

For H_2O and D_2O the same behaviour upon changing the temperature was observed, as depicted in the figures 4.1 and 4.2. Beginning at 233 K, water being in its frozen state, an overall decrease of intensity upon heating as well as a blue shift (i.e. to higher wavenumbers) of the centre of gravity occurs.

Interesting to observe is that D_2O is still frozen at a temperature of 277 K, while H_2O has already melted at that point. In figure 4.3 it becomes obvious that the decrease of intensity[1] is slower in the solid phase than in the liquid phase. The slope of the intensity is steeper for the liquid phase. An isosbestic point can be seen in the spectrum at the upper end of the OH stretch band. Overall the intensity is decreasing, but the spectrum can be distinguished into two parts. The intensity of the part below the isosbestic point is decreasing with temperature, while the upper parts' intensity is increasing. The formation of a shoulder can be observed in similar experiments on water using RAMAN spectroscopy. [35] Another differentiation can be made for the part below the isosbestic point. The decrease of intensity of the spectrum is more significant at the bottom end of the spectrum, where the ice-like structures are expected. Close to the isosbestic point the decrease is less pronounced.

The bending vibration ν_2 at 1637 cm^{-1} for H_2O and 1215 cm^{-1} for D_2O also show temperature dependent behaviour, but not as significant as the stretching vibration. ν_2 is increasing with increasing temperature and its centre of gravity is red shifted (i.e. to lower wavenumbers). The intensity of the bending vibration loses a lot of its intensity upon freezing. The band becomes more narrow with increasing temperature.

[1] In this context, the area under the curve is meant.

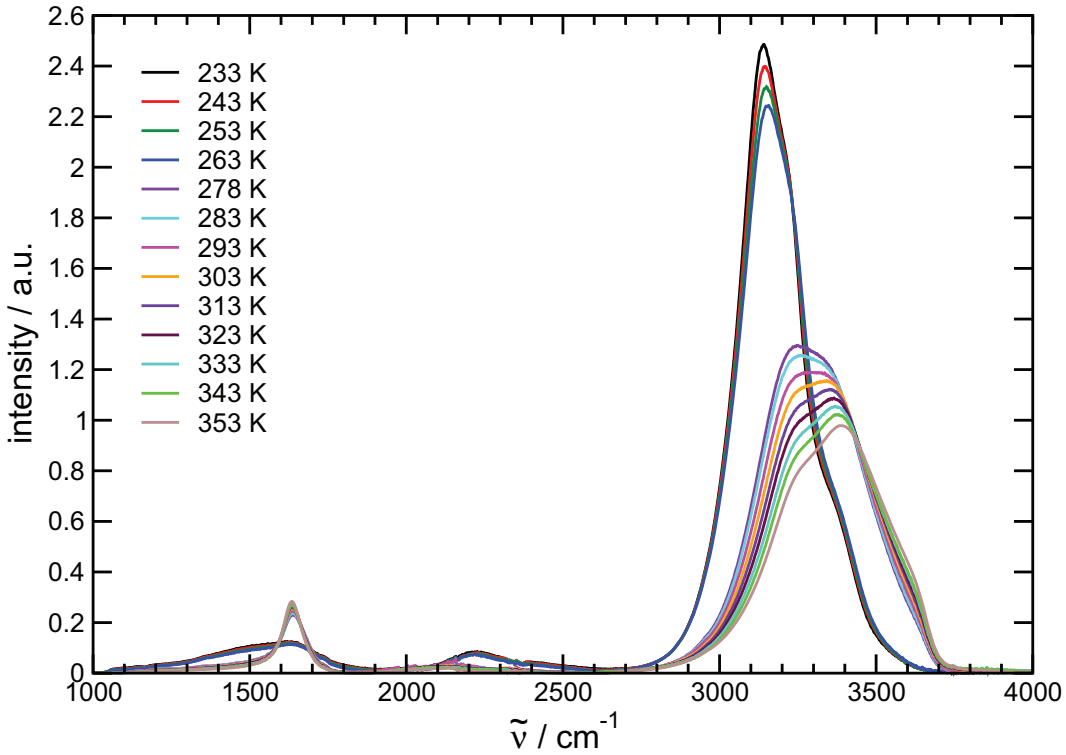

Figure 4.1: Temperature dependent spectra of the mid infrared region of pure H_2O from 233 K to 353 K.

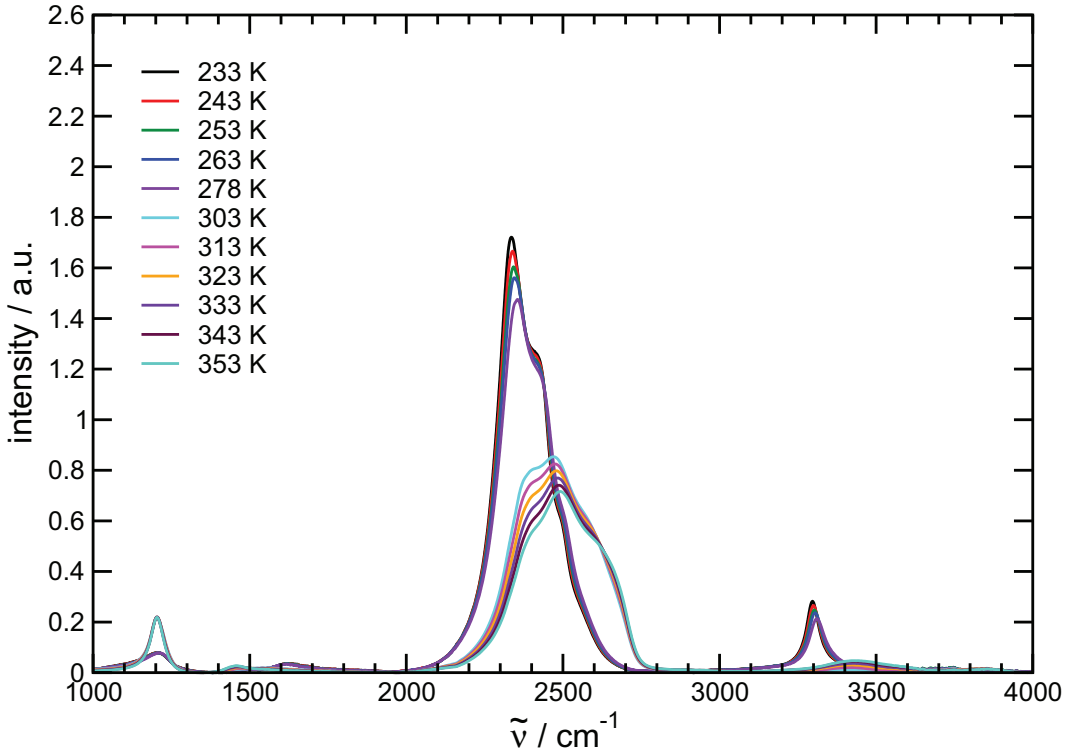

Figure 4.2: Temperature dependent spectra of the mid infrared region of pure D_2O from 233 K to 353 K. The OH peaks at 3400 cm^{-1} are a result of atmospheric diffusion.

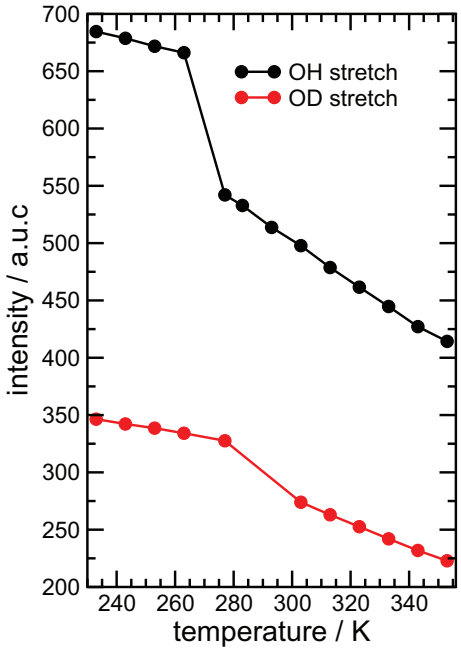

Figure 4.3: Temperature dependence of the intensity of the OH/OD stretch band from 233 K to 353 K.

The frequency of the OH stretching mode is very sensitive to its molecular surrounding. [8] Changes induced onto the system like pressure, hydrated salts or temperature gradients can change the intensity and position of the band within the spectrum significantly. The bending vibration ν_2 of water is not as sensitive as his bigger brother, does not interact as much with its molecular surrounding as the stretching vibration and is hence less affected by changes in the system. [20]

When the temperature of pure water is increased the molecules vibrate more vigorously and at increasing frequencies. This is why the OH stretch band is shifted to higher wavenumbers (see equation 3.1). The stronger the molecules vibrate the more decreases the strength of a hydrogen bond, in turn strengthening the covalent OH bond. [21] The H_2O molecules are more loosely bonded via hydrogen bonding at higher temperatures than at room temperature.

The bending vibrations' divergent behaviour, i.e. its red shift and increase of intensity with rising temperature is the consequence of the importance of hydrogen bonding at lower temperatures. At lower temperatures hydrogen bonding is much stronger and tends to reduce bending vibrations and enhance stretching vibrations. [20] Upon heating hydrogen bonding becomes weaker overall and the hydrogen bonded network can no longer suppress the bending vibration.

In the spectra of ice the main band can be found at the lowest wavenumbers compared to the spectra of the liquid or gas state, because hydrogen bonding is strongest and the

covalent OH bond weakest. The intensity of the OH stretch band being much higher compared to the liquid is due to the increased transition dipole moment. Intensity, hydrogen bonding and the transition dipole moment go hand in hand. The stronger the hydrogen bonding the greater the magnitude of the transition dipole moment. The greater the transition dipole moment the greater the intensity of the infrared band. [122] This is the reason for the decrease of intensity overall and especially for the dip from solid to liquid water, where transition dipole moments differ greatly (see figure 4.3). The difference in density contributes to the decrease in intensity as well. [122]

4.2 Identifying ν_1 and ν_3[2]

Temperature dependent spectra of H_2O and D_2O, figures 4.4 and 4.5, are decomposed and simultaneously fitted. A couple of interpretations are already available and presented in section 2.1.1. Regarding the effect of coupling, a new interpretation of the position of the symmetric and asymmetric stretch vibration is presented in this section. Only four temperatures are used for a simultaneous fitting procedure. Looking at figures 4.1 and 4.2 the deviations for this small temperature range are considered small enough and taking these four spectra is believed to be sufficient. For the relatively small temperature range of 30 K the assumption can be made that the shifts are not too big in order to disturb the qualitative analysis.

The intensities of the contributions simulated by the fit are shown in figure 4.6. Five of the six contributions are decreasing while one is increasing with rising temperature. This behaviour is consistent for the OH and for the OD stretch band.

H_2O and D_2O can be interpreted in an equal manner, although intensities and resolution of the bands are different. These differences are also due to anomalous dispersion described in section 3.1.3 which can change the intensity of a band. But the differences in this case are mainly due to the different physical nature of the deuterium as it is heavier and induces stronger "hydrogen" bonds. [123]

[2]This section is mainly based on the publication in *Zeitschrift für physikalische Chemie* 2008. [39]

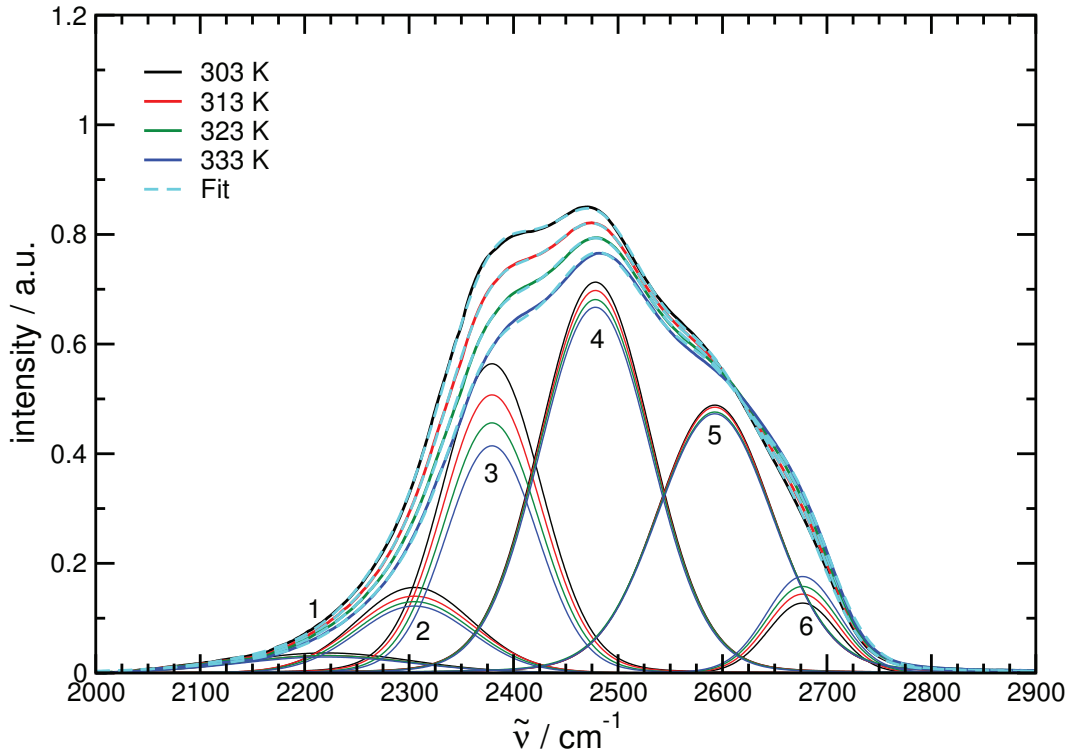

Figure 4.5: Simultaneous fit of the OD stretch band of pure D_2O from 303 K to 333 K.

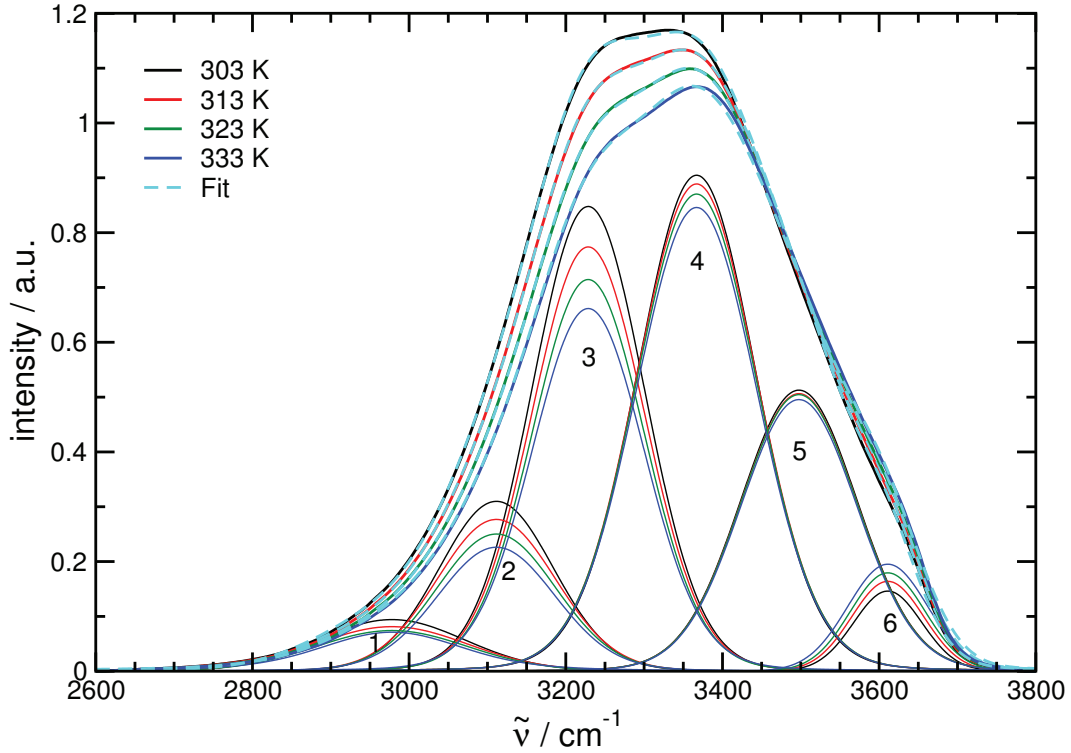

Figure 4.4: Simultaneous fit of the OH stretch band of pure H_2O from 303 K to 333 K.

sample	1	2	3	4	5	6
H_2O (ATR)	2978	3111	3226	3362	3495	3611
D_2O (calc.)	2167	2263	2347	2446	2542	2627
D_2O (ATR)	2220	2305	2372	2473	2594	2677
D_2O (Trans)	2240	2325	2396	2500	2611	2683

Table 4.1: Wavenumber positions of the peaks of the six contributions at maximum intensity for H_2O and D_2O measured with ATR spectroscopy, D_2O measured with transmission spectroscopy and calculated for D_2O from the ATR values obtained for H_2O. [39]

The contour of the OH/OD stretch band is fitted with six contributions similar to the approaches taken by Schmidt et al. and Fischer et al.. [13, 38] The peak positions of these contributions are listed in table 4.1. Considering coupling effects the question is which contributions can be assigned to ν_1 and ν_3.

To identify the symmetric and asymmetric stretch vibration ν_1 and ν_3, additional information are gained by applying isotopic substitution (for details on this technique see section 3.1.4). Two mixtures are used: 5 mol% H_2O/95 mol% D_2O (figure 4.7) and 5 mol% D_2O/95 mol% H_2O (figure 4.8). In these mixtures, besides H_2O and D_2O, the next major component will be HDO molecules. The OH vibration will be decoupled in its OD dominated environment and the OD vibration will be decoupled in its OH dominated environment. Decoupling results in two single band shaped peaks observed in the two mixtures at 3410 cm^{-1} for the OH group in D_2O and at 2504 cm^{-1} for the OD group in H_2O.

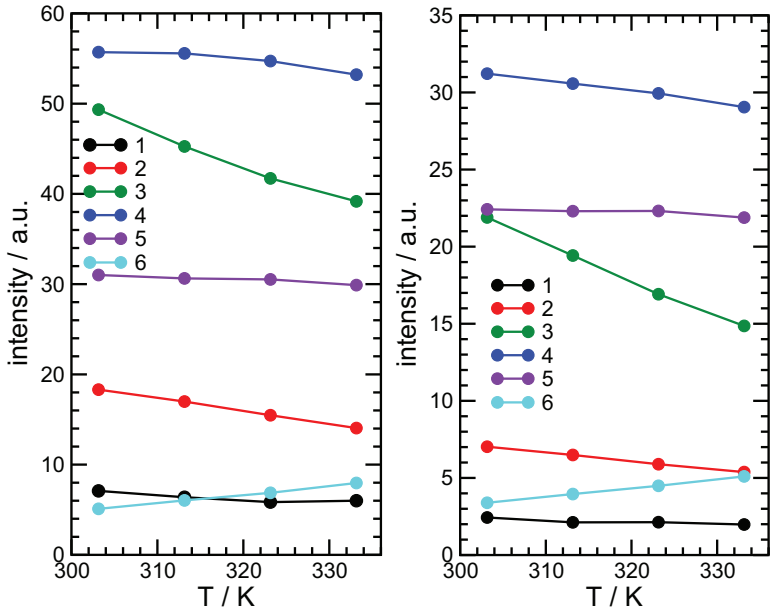

Figure 4.6: Intensities of the contributions of the simultaneous fit of H_2O and D_2O as a function of temperature.

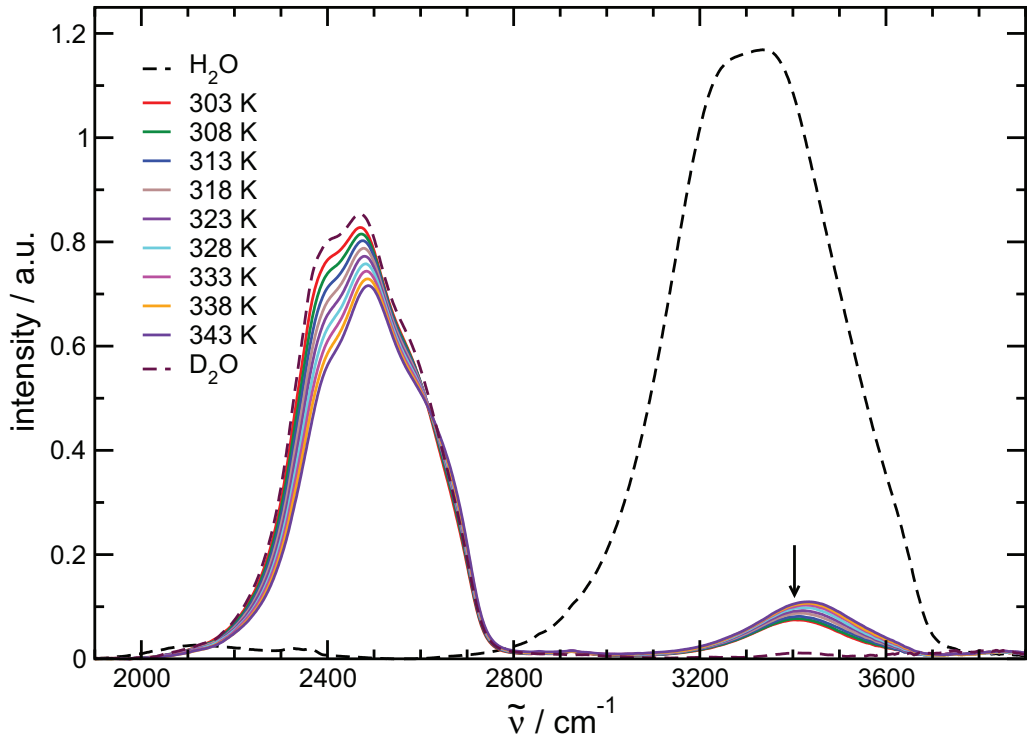

Figure 4.7: The stretching bands of pure H_2O and pure D_2O (dashed lines) at 303 K in comparison to an isotopic mixture of 5 mol% H_2O/95 mol% D_2O as a function of temperature.

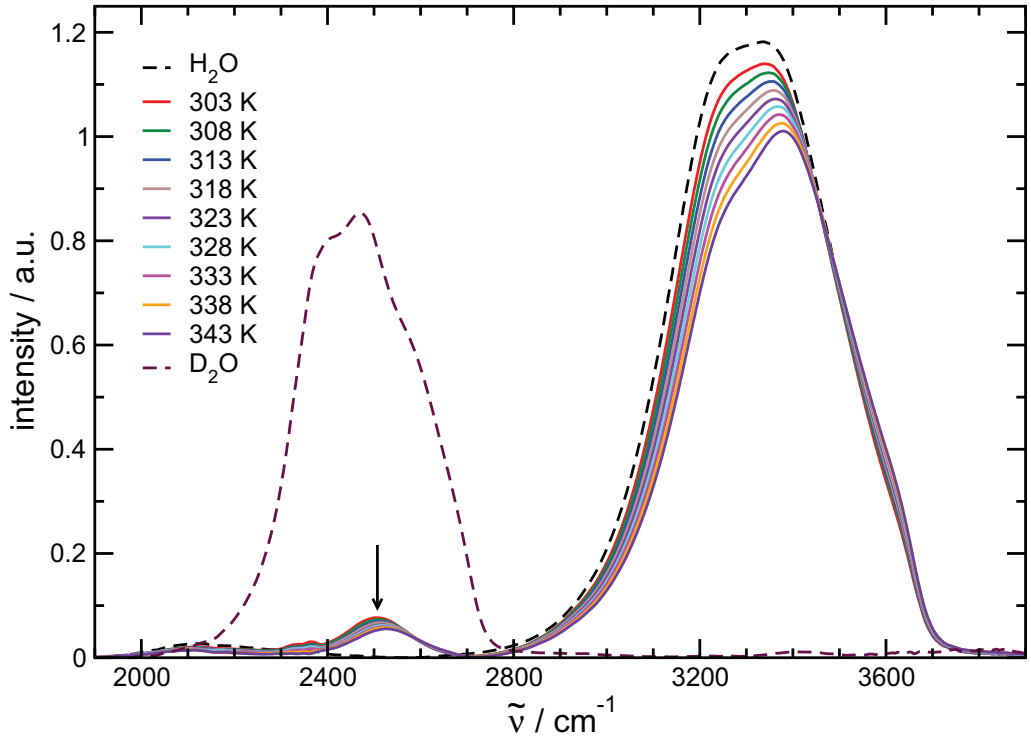

Figure 4.8: The stretching bands of pure H_2O and pure D_2O (dashed lines) at 303 K in comparison to an isotopic mixture of 5 mol% D_2O/95 mol% H_2O as a function of temperature.

At a closer examination of the decoupled peaks indicated by the arrows in figures 4.7 and 4.8 it can be noticed that the decoupled OH vibration in D_2O is increasing with rising temperature, rather than decreasing as it should and as the OD vibration in H_2O does. This is due to diffusion of atmospheric water vapour. The employed experimental setup does not allow working under a controlled argon atmosphere to avoid atmospheric water intrude into the system and cause isotopic exchange.

The symmetric and asymmetric vibration of the OH oscillator are coupled in pure water. By decoupling these vibrations the position of the peak wavenumber of the decoupled oscillator should be found in-between the coupled vibrations. A much larger gap between the two coupled vibration is expected in H_2O than in D_2O. [124] A look into table 4.1 shows that contributions four and five embrace the decoupled OH and OD band at $3410\,cm^{-1}$ and $2504\,cm^{-1}$ respectively. The exact and calculated middle in-between contributions four and five would be $3428\,cm^{-1}$ and $2533\,cm^{-1}$.

The actual measured values are somewhat shifted to lower wavenumbers. This can be explained by the different physical surrounding of the oscillators which are still surrounded and part of the hydrogen bonded network which in its strength is different in D_2O compared to H_2O. D_2O makes stronger "hydrogen" bonds and therefore has a larger effect on the decoupled OH, this is indicated by a difference of $29\,cm^{-1}$ between calculated and measured values compared to a difference of only $18\,cm^{-1}$ for the decoupled OD in H_2O.

4.2.1 Theoretical calculations

It is possible to calculate the positions of the contributions in D_2O from the contributions found in H_2O. After isotopic substitution the force constant stays the same and only the reduced mass changes. The following equation holds true.

$$\frac{\tilde{\nu}_{OH}}{\tilde{\nu}_{OD}} = \sqrt{\frac{\mu_{OD}}{\mu_{OH}}} \tag{4.1}$$

μ_{OH} being $16 \times 1/(16+1) = 0.9412$ and μ_{OD} being $16 \times 2/(16+2) = 1.7778$ [99] the following ratio of $\tilde{\nu}_{OH}$ to $\tilde{\nu}_{OD}$ is found.

$$\tilde{\nu}_{OD} = \frac{\tilde{\nu}_{OH}}{1.3744} \tag{4.2}$$

Theoretical calculations of the peak positions are done by dividing the H_2O values by a factor of 1.3744[3]. [39] These values are presented in table 4.1. The calculated values

[3] This represents a correction of the publication [39] in which values were divided by the factor $\sqrt{2}$, i.e. 1.4142. This leads to values on average $67\,cm^{-1}$ higher compared to the data obtained with 1.3744. The old D_2O values thus produced an overall difference between calculated peak positions and measured peak positions of around

are located at lower wavenumbers than the actual measured positions. From literature a difference between calculated and measured values of $43\,cm^{-1}$ is reported when positions are calculated that way. [99] In this investigation a difference of $41\pm15\,cm^{-1}$ is observed.

From spectroscopical studies on the behaviour of water dissolved in ionic liquids it was found that the gap between ν_1 and ν_3 increases going from H_2O to D_2O, while the wavenumber gaps of the other contributions are closing in. [124] Drawing conclusions from the H_2O data a gap of $96\,cm^{-1}$ is expected between ν_1 and ν_3 in D_2O from the theoretically calculated values. It is found to be be $25\,cm^{-1}$ higher (see table 4.2) than expected and shows similar behaviour to that observed in ionic liquids. All other gaps are getting smaller or remain almost unchanged, just like reported in the literature. [124]

Contributions four and five are coupled and show strong similarities, for example the behaviour of their intensities (see figure 4.6). It is hence logical to presume that they represent the symmetrical and asymmetrical bands ν_1 and ν_3.

	Δ1-2	Δ2-3	Δ3-4	Δ4-5	Δ5-6
H_2O (ATR)	133	115	136	133	116
D_2O (calc.)	96	84	99	96	85
D_2O (ATR)	85 (-11)	68 (-16)	100 (+1)	121 (+25)	83 (-2)

Table 4.2: Gaps between the six contributions which fit the spectra at maximum intensity for H_2O and D_2O measured with ATR spectroscopy and calculated for D_2O. [39]

Schiffer states that an assignment of ν_1 and ν_3 is inappropriate for the broad OH stretch band, saying that this would imply that there is but one type of water molecule in the liquid that has the fundamental vibrations ν_1 and ν_3. He also suggests that this type of water would retain many of its gaseous characteristics. [33] A sole contribution is acknowledged to have a FWHH of $\sim35\,cm^{-1}$. [23] The bands identified as ν_1 and ν_3 have a FWHH of $\sim170\,cm^{-1}$ for H_2O and of $\sim130\,cm^{-1}$ for D_2O. Regarding the FWHH of the bands it seems unreasonable to presume that bands with a half width of around $170\,cm^{-1}$ could be made up of only one type of molecule arrangement, but rather of a couple of states which add up to one big contribution. To explain the structure and properties of water the picture of tetrahedrally coordinated molecules is of great importance. [32] Schiffer's statement would also contradict recent research which has identified more than one discrete species in liquid water. [62]

$100\,cm^{-1}$, which is not accurate enough.

4.3 The overtone of the bending vibration of the H_2O molecule

The bending vibration of the water molecule and especially its overtone contribute to the question of how or how not to interpret the OH stretch band of liquid H_2O. [26, 33] The bending vibration of water can be found at 1637 cm^{-1} at 303 K.

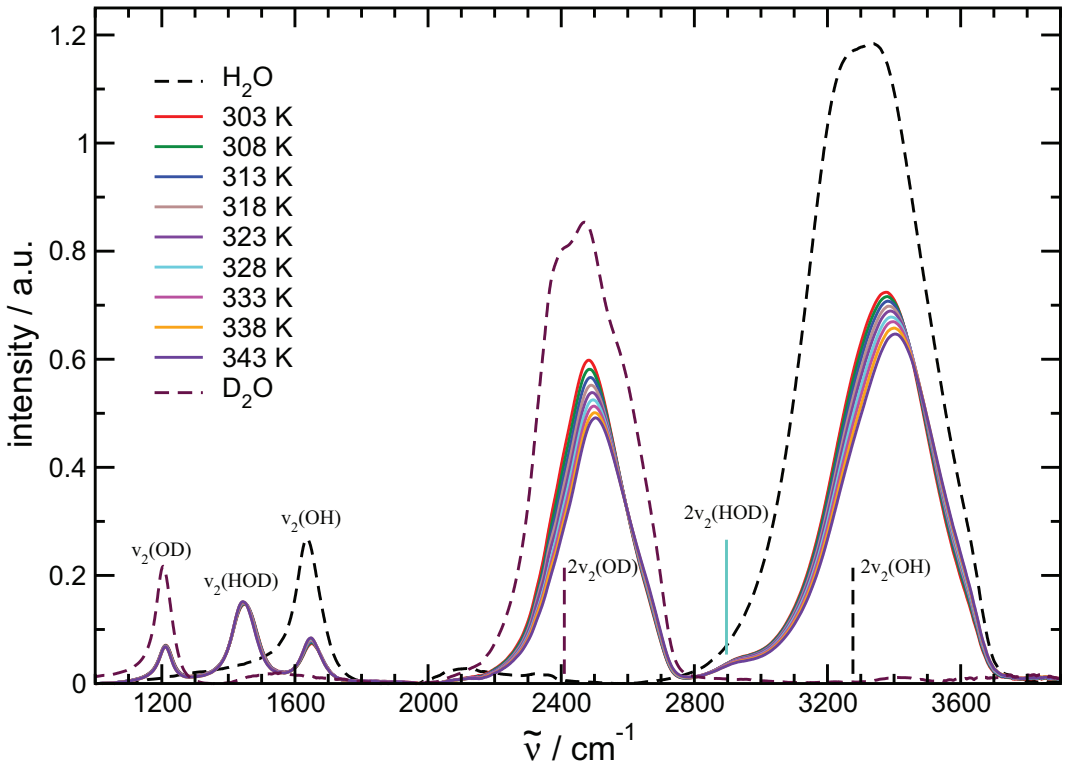

Figure 4.9: The stretching bands of pure H_2O and pure D_2O (dashed lines) at 303 K in comparison to an isotopic mixture of 50 mol% H_2O/50 mol% D_2O as a function of temperature. The fundamental bending vibrations and the respective first overtones are indicated.

Overtones are expected at whole number multiples of the fundamental vibration. The first overtone $2\nu_2$ is therefore expected in the proximity of 3274 cm^{-1}. The expected position lies underneath the broad OH stretch band and it is difficult to identify it from experiments with pure H_2O only. An assignment is not trivial because water is a very polar solvent and overtones tend to be more intense in such surroundings. An exact positioning by just multiplying is not appropriate, since the position may also be altered by FERMI resonance (see section 2.1.2). [26, 120, 122]

The overtone has been attributed to several values in literature, e.g. 3220 cm^{-1} [120], 3225 cm^{-1} [125] and 3250 cm^{-1} [34]. It has also been published that the overtone of the bending vibration probably contributes to the OH stretch band by FERMI resonance but that its contribution is expected to be small. [26] Most interpretations of infrared spec-

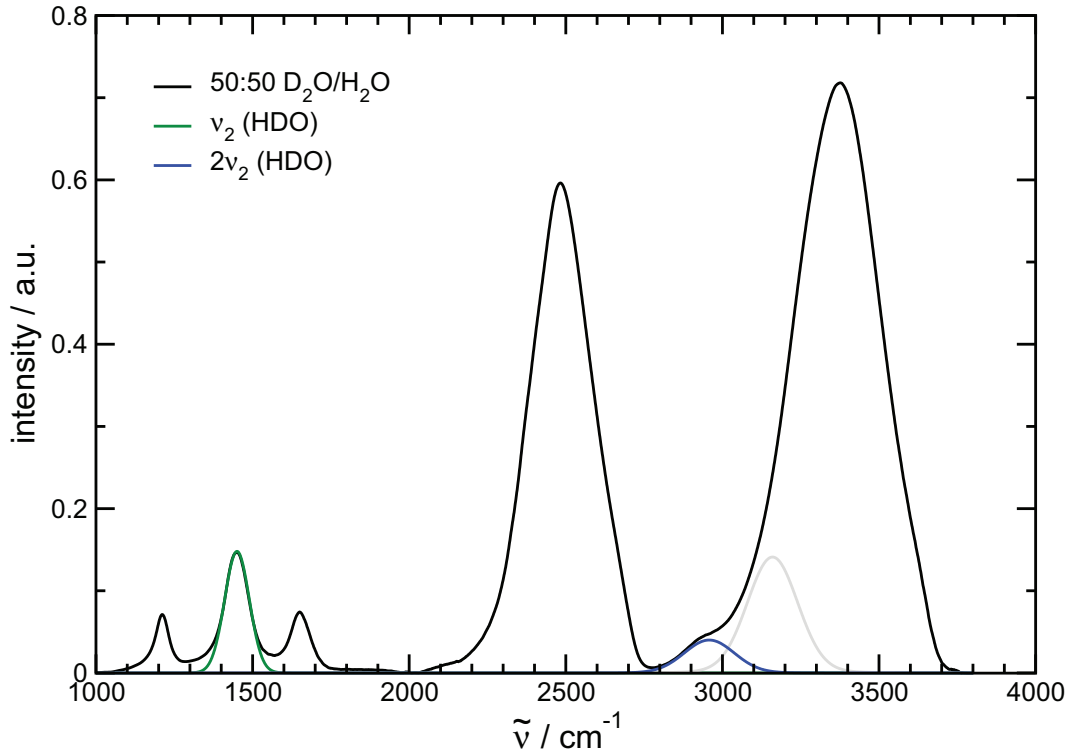

Figure 4.10: Fit of ν_2 (green) and $2\nu_2$ (blue) in an HDO spectrum at 303 K. The grey contribution is added for a more realistic fit.

tra, trying to explain the water structure, hence work without the overtone. [55] In this work, especially in section 4.2, the overtone is not included into the analysis. Its inclusion can make an interpretation regarding all other spectral aspects almost impossible. Buch and Devlin pointed out in 1999 that features from IR- and Raman spectra could be reproduced numerical without the inclusion of the overtone or the effect of Fermi resonance. [126] Nevertheless, another attempt shall be made in this work to pinpoint the location of the overtone in pure liquid H_2O with the help of isotopic substitution. In figure 4.9 temperature dependent spectra of a mixture of 50 mol% H_2O and 50 mol% D_2O are shown. This generates a ratio of 25% D_2O to 25% H_2O and 50% HDO molecules. The ratio can be apprehended by the intensities of the three fundamental bending vibrations which represent this ratio nicely. An overtone is not necessarily found at the exact whole number multiple of the fundamental vibration. The HDO's bending vibration is found at 1450 cm^{-1} with an intensity of 14.64, hence it is safe to attribute the shoulder observed at the marked position (2900 cm^{-1}) to the first overtone of ν_2(HDO). This shoulder was observed before by Maréchal [47] and Max et al. [127], the former explains its formation by Fermi resonance without attributing it to the overtone of the HDO's bending vibration, while the latter also identify this shoulder as the overtone of the bending vibration of

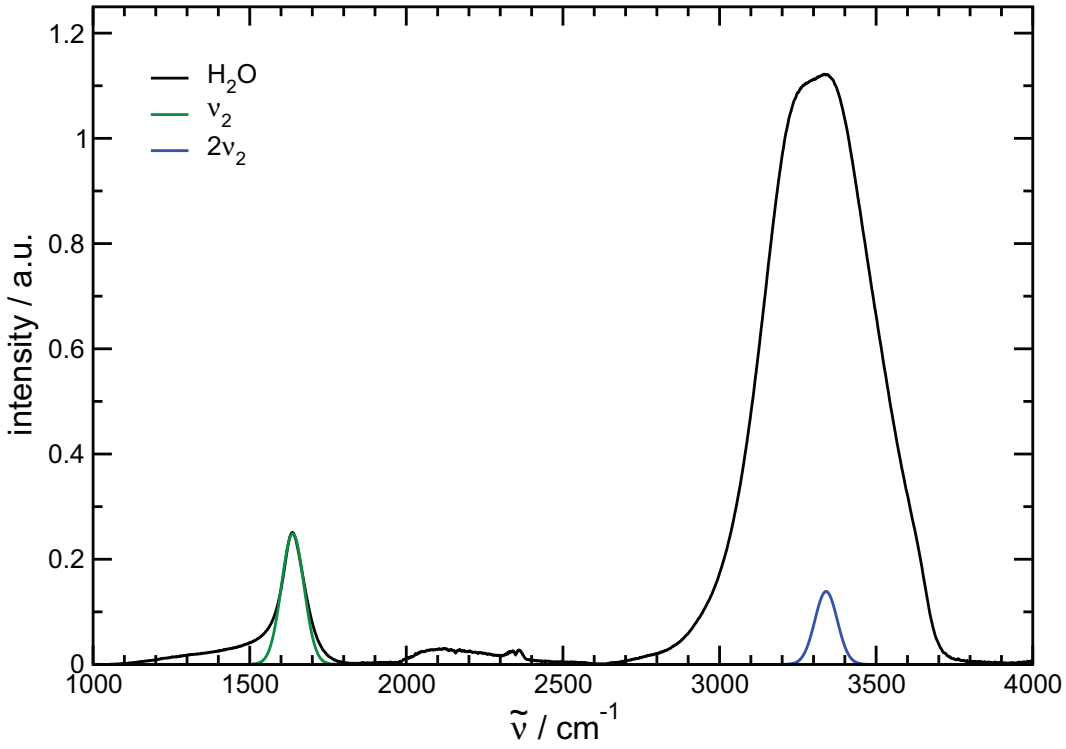

Figure 4.11: Inclusion of the overtone of ν_2 (blue) into the pure H_2O spectrum at 303 K.

the HDO molecule using factor analysis. Max et al. mark it at a position of 2965 cm^{-1}. In this work a decomposition is carried out and produces a contribution at 2959 cm^{-1} with an intensity of 8.151 for the first overtone (see figure 4.10). The determined position of the overtone is in good agreement with Max' data. The formation of the overtone in different mixtures of D_2O and H_2O can already be observed at a very low molar percentage of H_2O with an overwhelming percentage of D_2O (see appendix figure 1). Already at a level of 5 mol% H_2O the overtone can be observed separated from the main OH band. Upon increasing the mol% of H_2O the overtone and the OH band fuse to produce the shape as seen in figures 4.9 and 4.10. The proportion of the wavenumber position of the fundamental bending vibration to the position of the first overtone produces a ratio of 1:2.0401, comparing the intensities leads to a ratio of 1:0.56. That is, the overtone is found at a position 2.0401 times higher and with an intensity of 56% of its fundamental vibration. The ratio found for Max data is 2.0505 for the wavenumber and 23% for the intensity. As already established the difference in the wavenumber position is only 6 cm^{-1} and therefore in good accordance. The great difference of more than a factor of two for the intensities may be due to the different technical approaches and demonstrates the controversies and the necessity of the overtone discussion. [127] In another publication Max et al. claim that the $2\nu_2$ is not easily identified under the broad OH stretch band. [128] They observe the overtone

of H_2O in aqueous acetone and acetonitrile and state very reasonable that intensities may not be extrapolated from these solutions. But the pure H_2O system and the isotopic substituted system are comparable and it can be presumed that similar proportions as found in the substituted system may be applied to the pure H_2O system. Taking these facts into account, conclusions can be drawn for pure water.

4.4 Free OH groups

The question of whether or not free OH groups exist is among other things a question in terms of the ongoing mixture model vs. continuum model discussion as stated in section 2.1.4. The isosbestic point in the OH stretch region which can be observed at around $3300\,\mathrm{cm}^{-1}$ has been described extensively in the literature for temperature dependent studies [34] and so far supported the proposition of a mixture model, suggesting two interconverting species upon the change in temperature or pressure. The increasing contribution being generally acknowledged to be attributable to weakly bonded or even free OH groups. [29, 35, 41, 130] This notion has been questioned in recent times as already mentioned in section 2.1.3. Geissler et al. were able to show that a temperature dependent isosbestic point could also be caused by a smooth distribution of hydrogen bond geometries lacking qualitatively distinguishable species. [45] This would falsify the attribution of an isosbestic point to the mixture model since a smooth distribution of hydrogen bond geometries is the main characteristic of the continuum model to describe the structure of water. This aspect is taken into account in this work by only focusing on spectral features which are not shifted in wavenumber and can therefore undoubtedly be attributed to a distinct vibrational band.

As Stillinger already pointed out in 1980, it is safe to presume "that the majority of the H-bonds survive the trauma of melting", in other words compared to the solid where all molecules are hydrogen bonded there is a small fraction of ruptured hydrogen bonds in the liquid. [28] Some even doubt the existence of free OH groups altogether. [23, 54, 56, 120] Eaves et al. have shown in 2005 that non hydrogen bonded OH groups are an insignificant species in liquid water. They also state that free OH or broken bonds do exist but are more of a curiosity than a key player. [131]

Support for the existence of free OH groups comes from molecular dynamics simulations, vibrational sum-frequency generation of interfaces, Raman and IR spectroscopy. [25] From interfacial studies of the surface of liquid water it is relatively easy to prove the existence of dangling OH groups protruding from the surface into the gas phase. A sharp and dominant peak located at $3700\,\mathrm{cm}^{-1}$ has been shown by Gopalakrishnan et al. and proven to be

a dangling OH group. [26] Being located at 3700 cm^{-1} it can be found above the high wavenumber end of the OH stretch band of liquid water.

In the common IR spectrum of liquid water no contributions can be found at 3700 cm^{-1} at any temperature. In bulk water no free OH group will be found like that dangling OH protruding from the surface. Still, hydrogen bonds break and reform and a small amount of broken hydrogen bonds, i.e. free OH groups, does exist. These free OH groups will not vibrate at the same frequency as a dangling OH, because they are still surrounded by water molecules and influenced by their electrical fields and dipoles. [120] They are henceforth called **quasi free OH groups**. Quasi free OH groups in the bulk water are expected to be found at the top end of the OH stretch band. The frequency (or wavenumber) of the OH bond increases while the strength of the OH bond decreases. Non hydrogen bonded OH groups have a weak OH bond.

This reflects the very similar model brought forward by Giguère in 1984, in which he described the unbalanced stoichiometry of hydrogen bonding in liquid water with the presence of bifurcated hydrogen bonds between three water molecules. [120, 132] He also emphasises that no 'free' or 'vapour like' OH groups can exist in bulk water. This concept was confirmed by Sciortino et al. with the help of molecular dynamics simulations. [133]

Aqueous salt solution are mainly examined via ATR FT-IR spectroscopy and additional molecular dynamics simulations were carried out to obtain further clues for the existence of quasi free OH groups in the bulk phase of liquid water.

4.4.1 Investigations on alkali chloride salts

Figure 4.12 shows a typical difference spectrum (green line). It is obtained by subtraction of the pure water spectrum (black line) from any spectrum of a particular salt solution (red line) at equal experimental conditions. Spectra of 2 and 4 M solutions of NaCl, KCl, RbCl and CsCl were recorded at 303 K and their difference spectra calculated (figure 4.13).

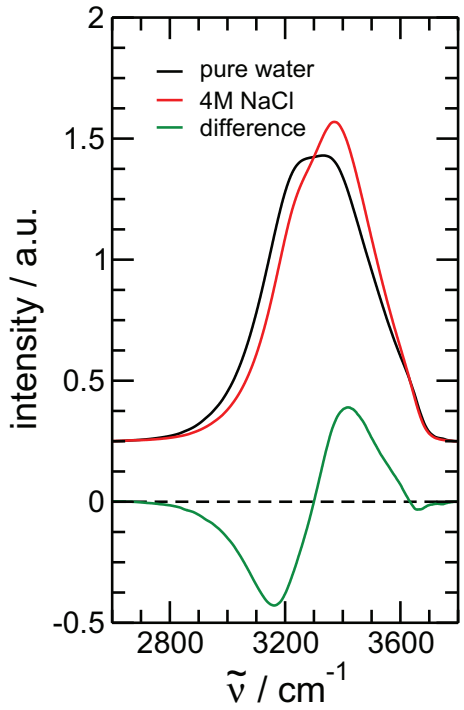

Figure 4.12: Pure water spectrum and the spectrum of an aqueous 4 M sodium chloride solution in the OH stretch region at 303 K. Additionally the difference spectrum between both spectral line shapes is shown enlarged by a factor of two.

The large positive peak which generally appears around ∼3450 cm^{-1} is attributed to anions bonded to water molecules via the hydrogen directly influencing the OH bond. [18] This shall be shown in more detail in section 4.5.1. The negative dip is attributed to the reduction of the hydrogen bonded network in pure water. [36] This peak shall henceforth be called the **network peak**. The differences in intensity of the network peak has been correlated to the different structure making or breaking behaviour of the dissolved ions. [134] This shall also be dealt with later on in section 4.6.1.

Focus is put on the very minute peak at ∼3650 cm^{-1} which has the highest wavenumber in the difference spectra. It is small but shows characteristic cation dependency. Because the same anion is present in all solutions the changes can be traced to the different cation and/or occur in the bulk phase of the water. [18] This peak can only be assigned to quasi free OH groups in the salt solution and demonstrates a characteristic behaviour depending on the salt chosen. Rossi et al. also identify this peak in aqueous salt solutions at the same wavenumber position and attribute it to non bonded free OH groups. [17]

Compared to the average value of the symmetric and asymmetric OH stretch of gaseous water (3707 cm^{-1}) and the OH stretch of a dangling OH group on a water/air interface (3700 cm^{-1}) this vibrational band is shifted 50-60 cm^{-1} to lower wavenumbers. From the comparability studies in section 3.1.5 a shift of the ATR spectra of 20 cm^{-1} to lower

wavenumbers has been determined to occur with this experimental setup in comparison to transmission experiments. This has also been shown mathematical and is the result of anomalous dispersion. [18] Hence the actual value lies around 3670 cm^{-1} which nicely fits into the series of gaseous, surface and bulk water.

Figure 4.14 shows the contribution of the quasi free OH group for the 2 and 4 M salt solutions including the fitted VOIGT functions. A negative peak, i.e. a decrease in concentration of the quasi free OH group is observed. Clearly the concentration of quasi free OH groups has to decrease with increasing salt concentration, because more anions present in the solution mean more and stronger docking sites for OH groups and therefore diminishing their number as the salt concentration rises.

An interesting behaviour is found for the fitted peak heights and the fitted intensities of the VOIGT function representing the quasi free OH group (see figure 4.15). The intensities become more and more negative with increasing size and decreasing ionic strength of the cation.

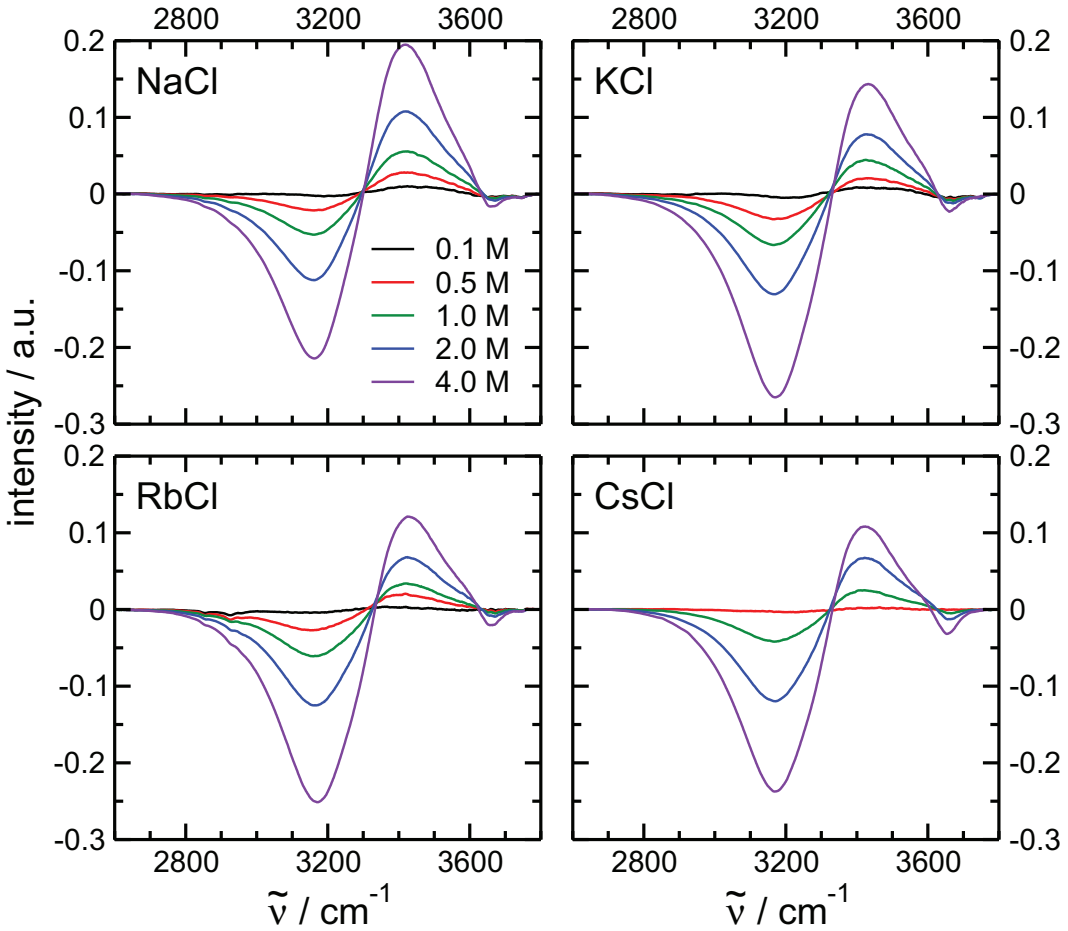

Figure 4.13: Difference spectra of NaCl, KCl, RbCl and CsCl salt solutions for the OH stretch region as a function of salt concentration at 303 K.

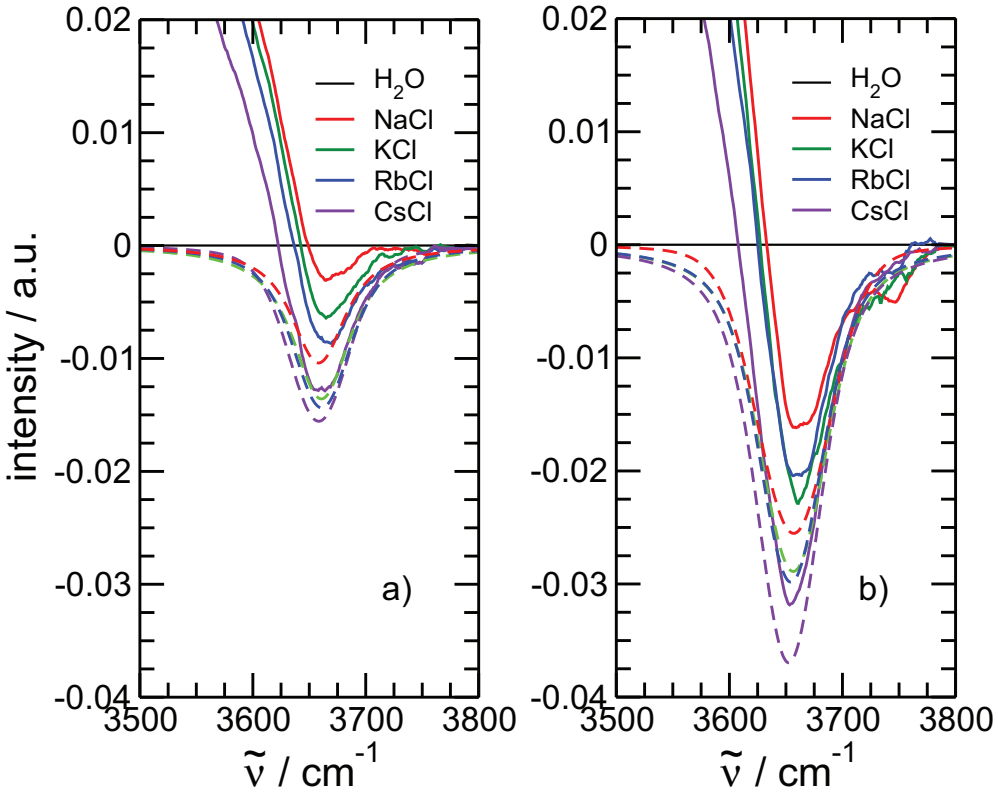

Figure 4.14: Difference spectra of NaCl, KCl, RbCl and CsCl salt solutions for the quasi free OH group in a) 2 M and b) 4 M solutions at 303 K. Additionally the fitted functions (dotted lines) are shown.

The number of quasi free OH bonds is reduced in the order Na^+, K^+, Rb^+ and Cs^+. With the experimental setup used it is not possible to resolve the arrangement of hydrogen bonds around the solvated ion directly. [18] Nevertheless there are only two related possible explanations for the vanishing quasi free OH group.

Firstly, the hydration shell of the cations is changing and there is a balance between electrostatics and hydrogen bonding. [57] Larger cations of lower charge density and therefore weaker electrostatic forces allow hydrogen bonding to occur within the hydration shell. Hribar et al. also derive from the Mercedes Benz model that the number of hydrogen bonds per water molecule in the first hydration shell increases from 1.8 for Na^+ to 2.1 for Cs^+. [57] This would cause a decrease of the quasi free OH groups of about 20% from the 4 M NaCl solution to the 4 M CsCl solution. There is a factual difference in the intensities of about 50%. This leads to the conclusion that in addition the bulk water, i.e. the water beyond the first hydration shell of the ions, has slightly changed its structure due to the presence of the ions. Fewer quasi free OH groups would be present if more water molecules are hydrogen bonded in a tetrahedral fashion. This second possibility can be checked by molecular dynamics simulations. [18]

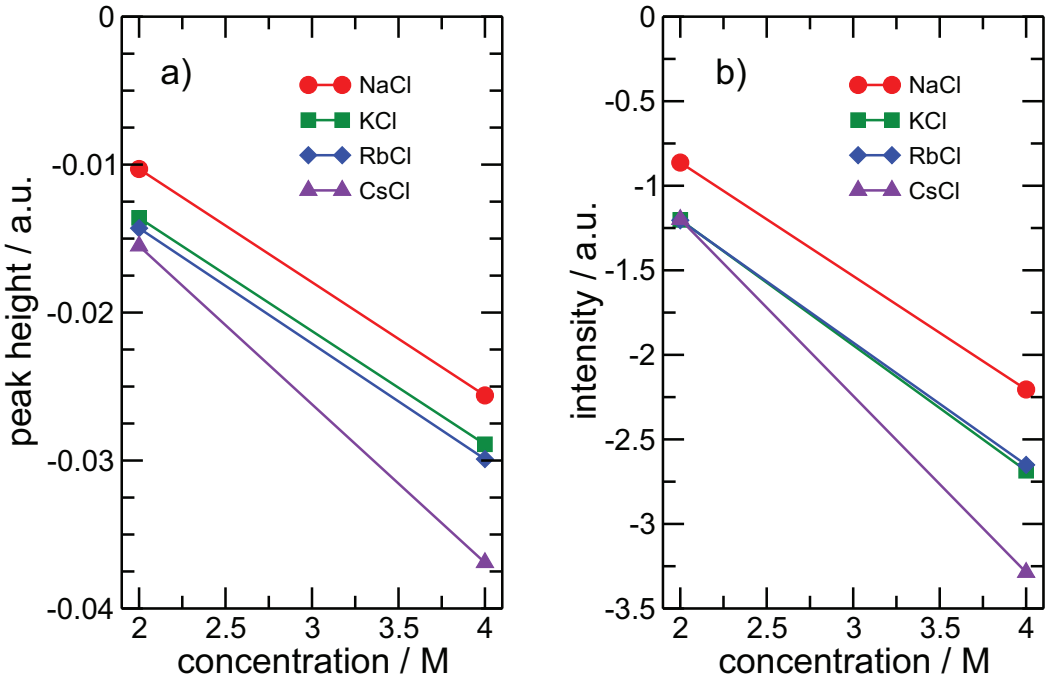

Figure 4.15: a) Peak heights and b) intensities of the VOIGT functions fitting the band of the quasi free OH found in the difference spectra of 2 and 4 M salt solutions at 303 K.

Additional molecular dynamics simulations [4]

Simulations were carried out for the same aqueous salt solutions at different concentrations however, but the simulated concentrations are in the same range as the spectroscopical measurements and show the same trends. The changes in the water structure that occur upon increasing the concentration or using a different cation can be monitored and compared to spectroscopical results.

The water-water site-site radial distribution functions $g_{OO}(r)$, $g_{OH}(r)$ and $g_{HH}(r)$ were calculated as a function of salt concentration for each salt solution. In figure 4.16a the oxygen-oxygen radial distribution functions for NaCl solutions at different concentrations are depicted. For all alkali chloride solutions the oxygen-oxygen radial distribution function at the highest simulated concentration is shown in figure 4.16b.

The oxygen-oxygen radial distribution function is most sensitive to small changes in the water structure. [78] Figure 4.16a focuses on the influence which the concentration has on the location and the height of the first and second maxima. The first maxima decreases significantly upon raising the concentration level of NaCl, while the second maxima also decreases and shifts inward.

[4] Pictures and data are presented in this section by courtesy of DR. JÖRG HOLZMANN who carried out these simulations. [18]

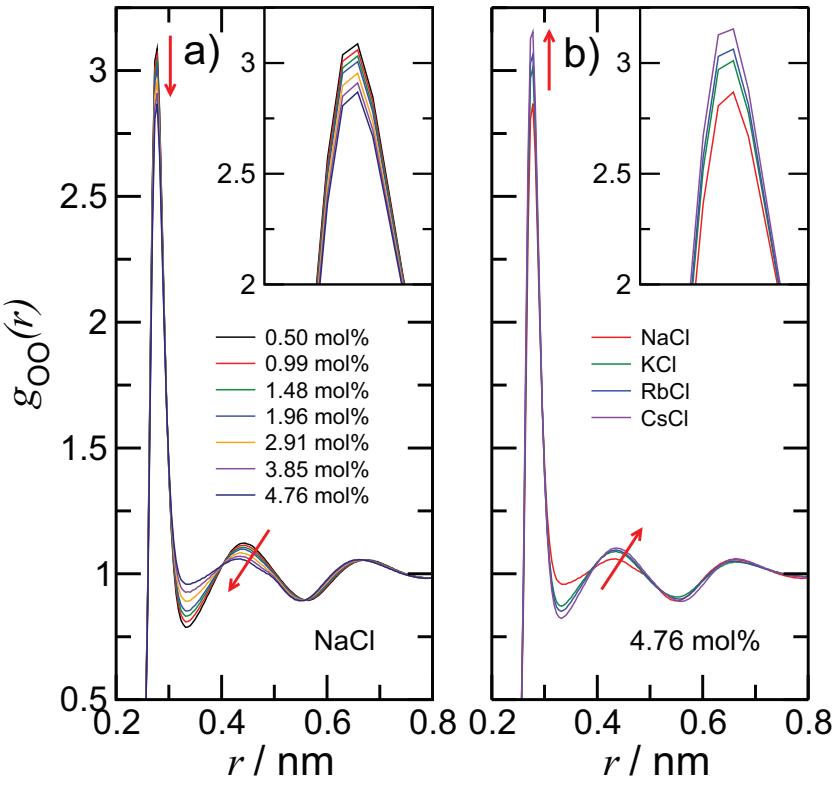

Figure 4.16: Oxygen-oxygen radial distribution functions for a) aqueous NaCl solutions at various concentrations and b) aqueous NaCl, KCl, RbCl and CsCl solutions at a concentration of 4.76 mol%. The arrows indicate the positions and shifts of the first and second maxima as a) salt concentrations increase and b) the salts change. The insets show the enlarged first maxima for both cases.

This inward shift suggests that the presence of the ions induces a change onto the water structure similar to that caused by pressure. Soper and Ricci have shown with experiments on liquid water that this could be indicative for a distorted but not necessarily broken hydrogen bonded network. The second peak is generally regarded as the signature of the tetrahedral bonding in water. [18]

In figure 4.16b where the $g_{OO}(r)$ of all the alkali chloride salts at maximum concentration are compared an increase of the first maximums' intensity, i.e. from NaCl to CsCl, and an outward shift of the second maximum is observed. The hydrogen bonded network of liquid water is strengthened with increasing size and lower charge density of the cation. More water molecules are bound in a tetrahedral fashion at the expense of quasi free OH groups. This is in agreement with the spectroscopical findings described in this section above.

Leberman and Soper used neutron diffraction to measure and compare the influence of pressure and high salt concentrations on the hydrogen bonded network of water and found that ions change the structure equivalent to the application of high pressures. [18, 81]

Botti et al. have reported analogous findings from their studies on the hydration of H^+ and OH^-. Mancinelli et al. showed in 2007 that perturbation of the water structure in KCl and NaCl solutions outside the first hydration shells are caused by the monovalent ions. [78]

Similar to the difference spectra used in section 4.4.1 the radial distribution function of liquid water can be subtracted from the radial distribution function of a salt solution as shown in equation 4.3.

$$\Delta g_{XY}(r) = g_{XY}(r)_{\text{salt solution}} - g_{XY}(r)_{\text{pure water}} \tag{4.3}$$

All $\Delta g_{XY}(r)$ for all concentrations and solutions are shown in the figures 4.17, 4.18 and 4.19. The $\Delta g_{OH}(r)$ in 4.18 mainly underlines the arguments for the $g_{OO}(r)$ radial distribution function. $\Delta g_{OO}(r)$ in figure 4.17 indicates that the addition of NaCl leads to a decrease in the hydrogen bonding peak at 0.185 nm. The broad negative peak of $\Delta g_{OH}(r)$ at about 0.5 nm can be correlated to the decrease of the second maximum of $g_{OO}(r)$ in figure 4.16, thus indicating a reduction of the tetrahedral coordination of the water molecules. This effect is less pronounced upon increasing size and decreasing charge density. Figure 4.17 also shows positive contributions for CsCl solutions which are enhanced upon increasing the salt concentration. This behaviour is in accordance with the outward shift of $g_{OO}(r)$ for water in this salt solution. This is again a prove for stronger hydrogen bonds in the CsCl solution than in pure liquid water. [18]

The calculated $g_{HH}(r)$ depicted in figure 4.19 are in good agreement with the neutron diffraction results presented by Leberman and Soper for a 4 M NaCl solution. [81] They report a negative region at a radius $r = 0.2$ nm, a positive at $r = 0.3$ nm and a broad negative region at $r = 0.45$ nm.

In this work values of 0.23 nm, 0.31 nm and 0.5 nm are found respectively. The negative $\Delta g_{HH}(r)$ at $r = 0.2$ nm also switches to positive values in the case of CsCl. The hydrogen bonded network of water seems to be strengthened in CsCl solution whereas it is significantly distorted in NaCl solutions. The tetrahedral water structure is more pronounced in the CsCl solution than in the NaCl solution. This is consistent with the findings from the spectroscopic investigations, that less quasi free OH groups are present in the salt solutions from NaCl, KCl, RbCl up to CsCl.

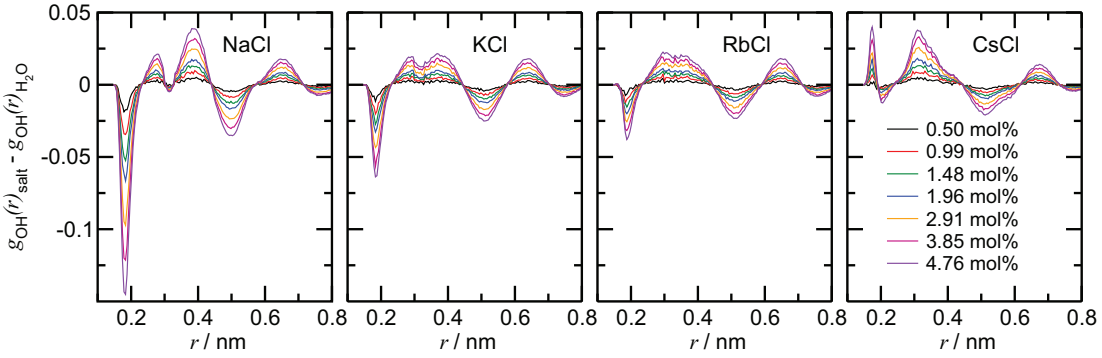

Figure 4.17: Water-water site-site difference radial distribution functions $\Delta g_{OH}(r) = g_{OH}(r)$[salt-solution] $- g_{OH}(r)$[water] for aqueous TIP4P-Ew salt solutions for different concentrations of NaCl, KCl, RbCl and CsCl at 300 K.

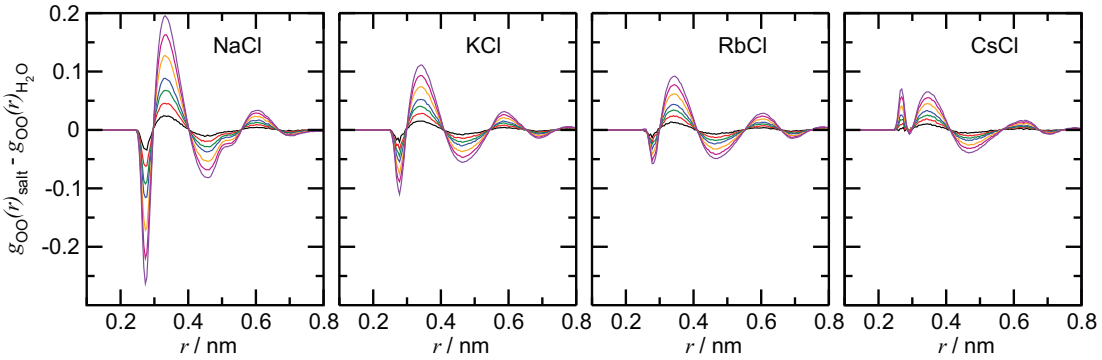

Figure 4.18: Water-water site-site difference radial distribution functions $\Delta g_{OO}(r) = g_{OO}(r)$[salt-solution] $- g_{OO}(r)$[water]] for aqueous TIP4P-Ew salt solutions for different concentrations of NaCl, KCl, RbCl and CsCl at 300 K.

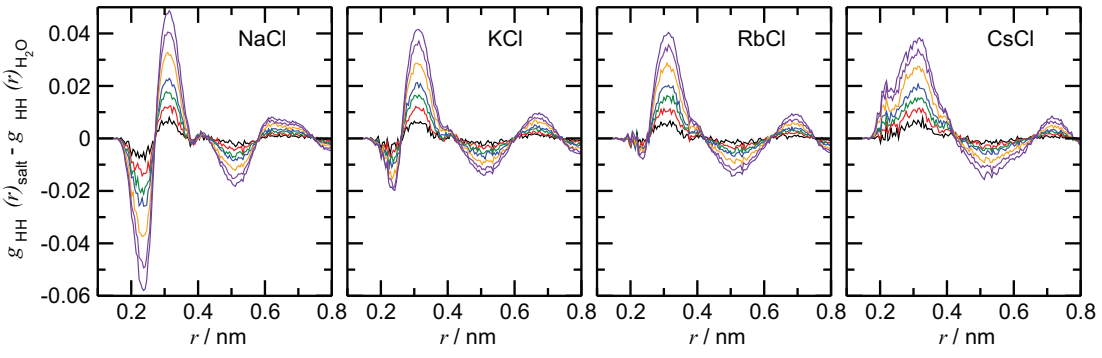

Figure 4.19: Water-water site-site difference radial distribution functions $\Delta g_{HH}(r) = g_{HH}(r)$[salt-solution] $- g_{HH}(r)$[water] for aqueous TIP4P-Ew salt solutions for different concentrations of NaCl, KCl, RbCl and CsCl at 300 K.

4.4.2 Investigations on alkali fluoride salts

In 2010 Max et al. published spectroscopic data which, according to their interpretation proved that no free OH groups exist in liquid water. [23] Max et al. claimed that from spectroscopic experiments with methanol in hexane one could expect a free OH group in liquid water around 3654 cm^{-1}. [135] They demand with respect to previous research a reasonable FWHH of 35 cm^{-1} for the free OH group. All these features can already be attributed to the quasi free OH group contribution identified at 3655 cm^{-1} in 4.4.1. However, this contribution could still be caused by inhomogeneous broadening for example, described by Geissler et al. [29, 45], further proof and certainty is needed. Additionally to the chloride measurements described in 4.4.1 all alkali fluoride salts were measured for this work in aqueous solution as well.

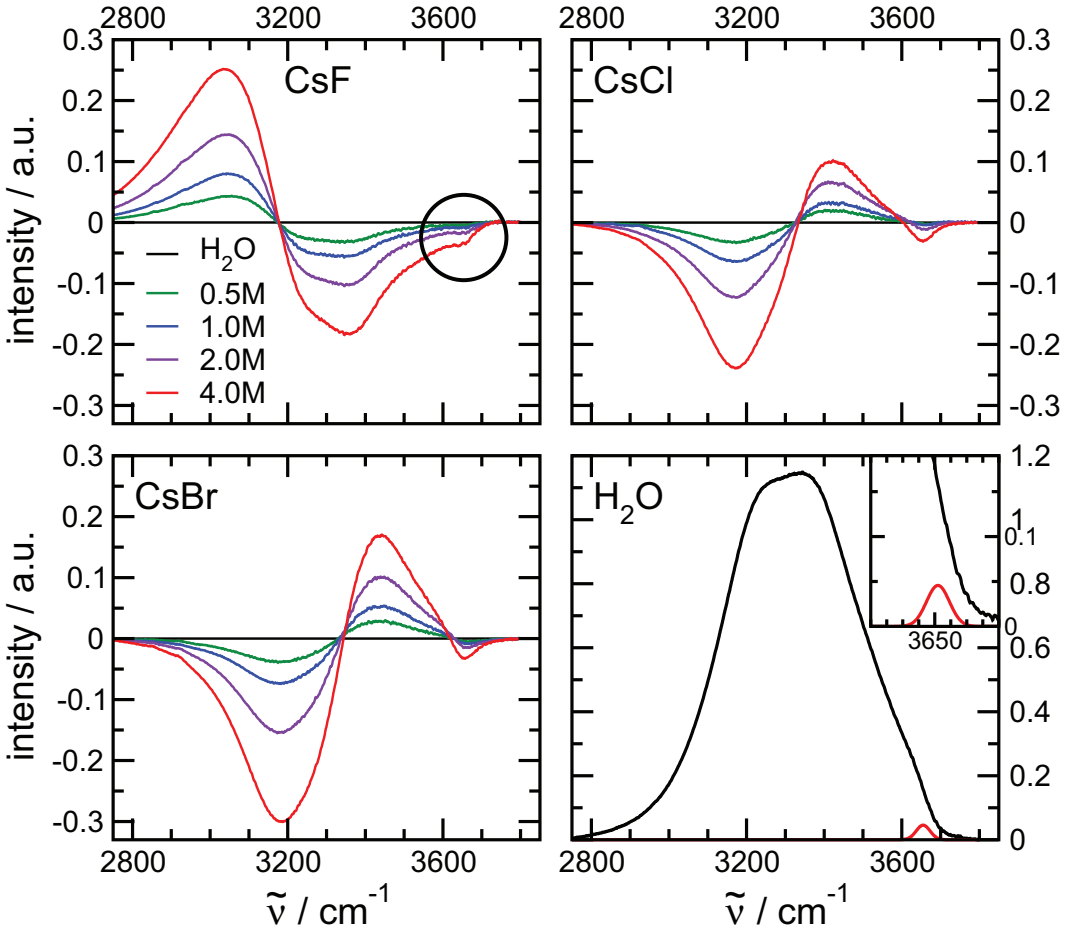

Figure 4.20: Difference spectra between spectral line shapes of pure liquid water and those of caesium halide salt solutions for the OH stretch region as a function of salt concentration at 303 K. The bottom right picture shows a pure water spectrum at 303 K with a red contribution indicating the position of the quasi free OH group in the water spectrum. At a position of 3655 cm^{-1} it possesses a FWHH of 42 cm^{-1}.

Looking at the spectra for the caesium halide series in figure 4.20 a very interesting feature can be observed in the CsF spectra, which is not caused by any of the described effects which cause misleading conclusions from isosbestic points described in section 2.1.3. A clear-cut contribution can be observed at 3655 cm^{-1}. The great advantage of the fluoride ion is that it interacts with the OH group at a much lower frequency leading to an increase of the OH stretch band at the lower wavenumber end, while Cl, Br and I salts cause an increase at higher wavenumbers.

Vice versa, a decrease of the intensity is observed at higher wavenumbers where Cl, Br and I salts would cause an increase (see figure 4.20). Only one isosbestic point can be seen. This effect has been described by Giguère already in 1986, but was interpreted in a different manner. [120]

Fortunately the large negative network peak does not coincide entirely with the small peak already observed for the alkali chloride salts. A clear cut contribution is formed at the exact same position which leaves very little doubt for quasi free OH groups not to exist and that their concentration is reduced with increasing salt concentration.

It may be argued that this peak is due to electrostriction forces, i.e. the shift of a peak due to different charge densities. If that were the case the peak would not remain at the exact same position for all investigated monovalent salts and no real isosbestic point could be observed.

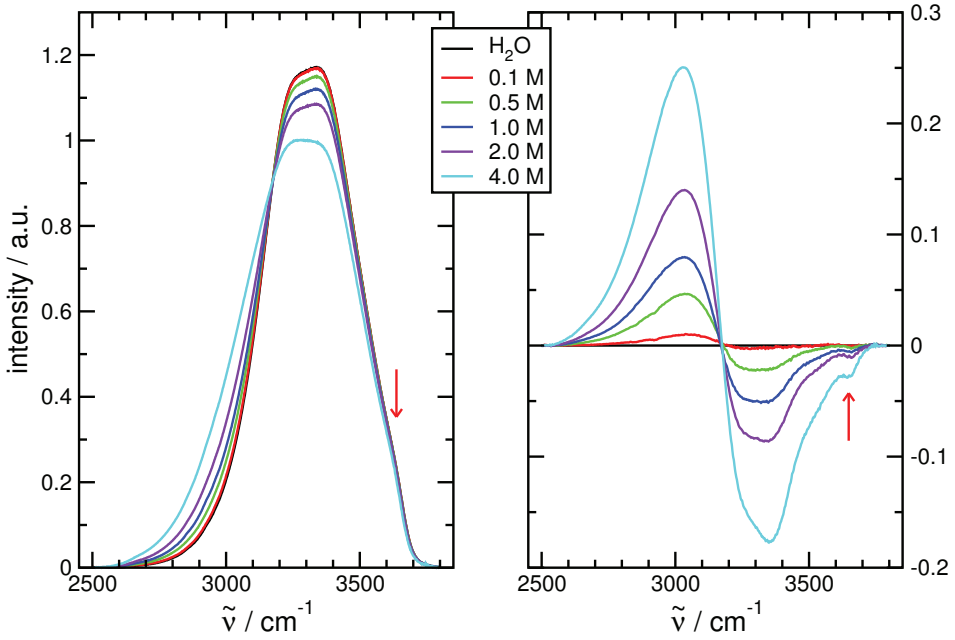

Figure 4.21: Real and difference spectra of KF solutions as a function of concentration at 303 K in comparison. The red arrows indicate the position of the quasi free OH group contribution.

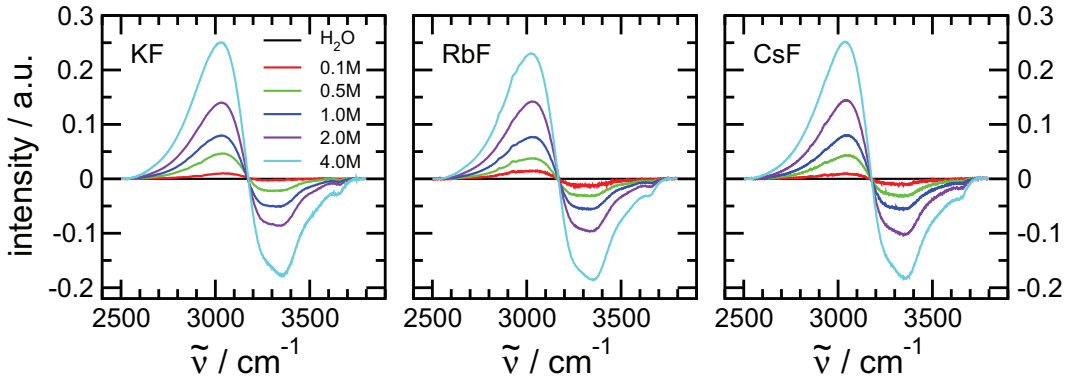

Figure 4.22: Difference spectra of KF, RbF and CsF solutions as function of concentration at 303 K.

The shoulder observed is not unique to CsF (figure 4.20) or KF (figure 4.21), but can be observed for RbF in figure 4.22 as well. LiF and NaF have very low molar solubilities of 0.01 M and 1.0 M respectively and can therefore not be investigated, as changes induced to the water spectrum regarding the quasi free OH groups are untraceable by ATR spectroscopy and difference spectra at these low concentrations.

In the pure water spectrum there is no distinct contribution observable at 3655 cm^{-1}. Max et al. state *"that free OH is not present in the bulk of liquid water from room temperature to as high as 378 K."* [23] But from the fluoride salt solutions it was shown that quasi free OH groups do exist.

The negative contribution present in the difference spectra is smaller than the actual contribution at the same position in the pure water spectrum. If such a spectral contribution is assumed for pure water (see figure 4.20) the intensities taken from the spectrum would suggest a ratio for the quasi free OH group of about 1:250, i.e. 0.4%. It was determined from ab initio and density functional theory calculations that the intensities of hydrogen bonded and free OH groups differ significantly (see table 4.3). [136]

Cooperative effects can cause the hydrogen bonded OH groups to have a 15 times stronger intensity than a free OH group. [51]

A 1:250 ratio can thus easily change into a 1:17 ratio indicating ∼5% of free OH present in liquid water. A factor of two lower than the value which has been suggested by Brubach et al.. [31] Concentration levels of quasi free OH groups is very low, but not so low as to be untraceable by ATR spectroscopy.

Emphasis has to be put on the indirect detection of the quasi free OH group. By observing the reduction of intensity at 3655 cm^{-1} in an aqueous salt solution with increasing concentration it can be deduced that there is a contribution present in neat water which disappears upon adding salt and can be attributed to quasi free OH groups.

This finding may seem to contradict our 2008 interpretation of the neat water spectrum,

hydrogen bonded OH		free OH	
wavenumber cm^{-1}	intensity km/mole	wavenumber cm^{-1}	intensity km/mole
3310.9	0.0	3884.3	189.29
3389.5	2879.8	3884.5	0.0
3389.5	2879.8	3884.5	0.0
3449.3	0.0	3885.2	104.5
3449.3	0.0	3885.2	104.5
3468.5	141.54	3885.9	0.0
	$\sum$ 5901.1		$\sum$ 398.3

Table 4.3: B3LYP/6-311++G** calculated frequencies and intensities of the hydrogen bonded and free OH vibrational modes of a cyclic water hexamer. The ratio of intensities between the free OH groups and the hydrogen bonded OH group is 1:15 in the water hexamer. [136]

where a contribution at 3611 cm^{-1} was also attributed to quasi free OH groups. [18] As already pointed out in section 2.1.4, broad components decomposing a spectrum into a couple of contributions refer to structures which involve a range of bond angles and distances distributed around the component peak position. Consequently the small peak identified at 3655 cm^{-1} is part of the broad band which can be seen in figure 4.4.

4.5 Ionic dependencies

To observe specific features of the OH stretch band depending on the ion, the ions are systematically changed. For anionic specificities the cation is kept constant while changing the anion. In order to find out more about the cationic behaviour the anion remains the same while the cation is exchanged. A strong anionic influence on the intensity and the position of the OH stretch band is prominent (see figure 4.23) while the influence of the cation is rather small (see figure 4.25). The cationic dependency on the large positive and the large negative contribution is limited to very small changes in band positioning. The lithium salts are an exception from the relatively constant intensity, this shall be discussed later.

Changing the anion produces greater shifts of both large peaks at equal concentration levels. Looking at the large positive and negative peaks a well defined shift from lower to higher wavenumbers can be observed for the positive peak with the largest gap being between F^- and Cl^-. In this series it is the fluoride salts which represent an exception, they shall also be discussed later. The spectra of the 4 M salt solutions are presented here as they depict the changes most obviously. Equivalent observations can be made from the 2 and 1 M solutions (see appendix 4). In this section the 4 M salt solutions are to be discussed representative for all concentrations.

The peak positions of the positive and the negative peak are recorded in table 4.4 and 4.5 and graphical depicted in figure 4.24. They show nicely the relatively constant peak position across (cation dependent) and the constantly changing position down (anion dependent) the table. Deviations from this behaviour, namely with the fluoride and lithium salts, are discussed in the next sections.

The peak for the quasi free OH group at 3655 cm^{-1} was discussed in section 4.4 and shall not be dealt with in this section. The large negative peak has already been labelled as the network peak in section 4.4.1 which is caused by the reduction of the hydrogen bonded network, this label shall be continued here.

LiF, NaF and CsI are not soluble at a concentration of 4 M and are therefore not depicted in the tables and figures above. The solubility of LiF is so low, that no prediction can be made about its influence. The influence of CsI and NaF at lower concentrations fits into the described and discussed patterns.

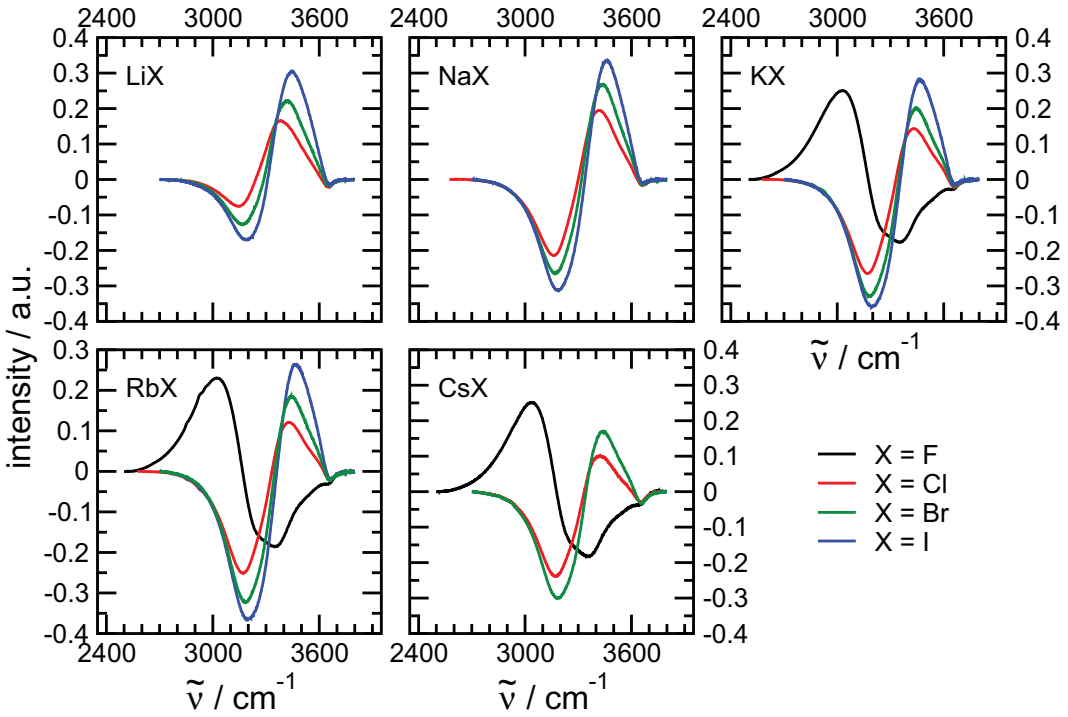

Figure 4.23: Anion dependent difference spectra of 4 M solutions of Li, Na, K, Rb and Cs halides at 303 K.

	Li^+	Na^+	K^+	Rb^+	Cs^+
F^-	-	-	3029	3026	3039
Cl^-	3381	3420	3433	3427	3422
Br^-	3422	3439	3445	3447	3442
I^-	3447	3463	3466	3467	-

Table 4.4: Maxima of the positive peak in cm^{-1} of 4 M alkali halide solutions at 303 K taken from the difference spectra in figure 4.23.

	Li^+	Na^+	K^+	Rb^+	Cs^+
F^-	-	-	3351	3354	3360
Cl^-	3146	3162	3171	3172	3172
Br^-	3169	3174	3187	3186	3185
I^-	3191	3188	3196	3200	-

Table 4.5: Minima of the network peak in cm^{-1} of 4 M alkali halide solutions at 303 K taken from the difference spectra in figure 4.23.

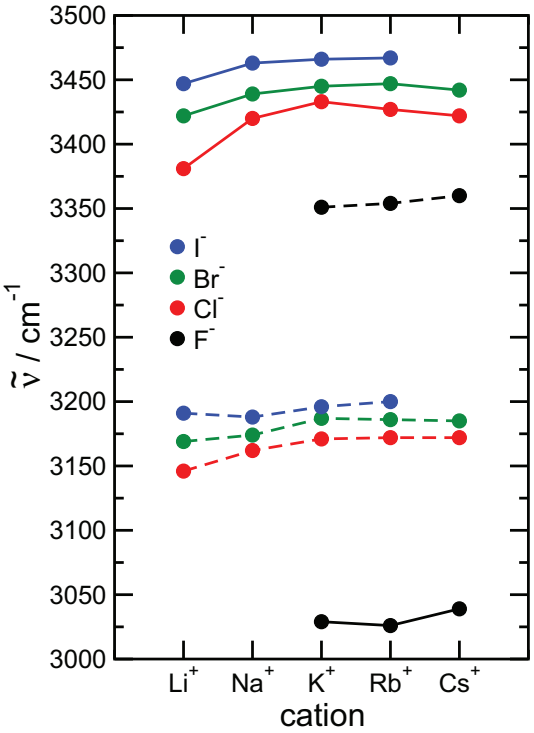

Figure 4.24: Peak positions from tables 4.4 (straight lines) and 4.5 (dashed lines) of the anionic and the network peak respectively for 4 M solutions.

4.5.1 Shifts in the difference spectra of monovalent ion solutions

Anion dependency

A closer look needs to be taken at the shifting positive peak for a fixed cation in combination with the monovalent ions F^-, Cl^-, Br^- and I^- (see figure 4.23 and table 4.4). In table 4.6 the average shifts are presented when F^- is changed to Cl^-, Cl^- to Br^- and Br^- is changed to I^-. All the values are close to the average, apart from the shift from LiCl to LiBr which is almost $20\,cm^{-1}$ higher. Calculating the average shifts for 2 and 1 M solutions (see table 4.7) produces very similar results. The increasing wavenumber with increasing size of the anion from F^- to I^- can also be apprehended from the constantly increasing shift. This is expected from simple electrostatic considerations. It is traditionally accepted that most strongly bound water OH groups vibrate at the lower end of the OH stretch band, while the weakest bound OH groups can be related to the top end of the OH stretch band. Charge density decreases from F^- to I^-, and especially from F^- to Cl^-. [67] This is the main reason why there is such a great gap when the fluoride changes to chloride.

Taking a look at the shifts of the minima of the network peak in table 4.8 it is understood that the effect of the anion on this peak is less intense and that average shifts are smaller. Like for the positive peak the average shifts are very similar for all three concentrations as displayed in table 4.9.

	Li^+	Na^+	K^+	Rb^+	Cs^+	**avg.**
F^--Cl^-	-	-	+404	+401	+383	**+396**
Cl^--Br^-	+41	+19	+12	+20	+20	**+22**
Br^--I^-	+25	+24	+21	+20	-	**+23**

Table 4.6: Anion dependent shifts of the maxima of the positive peak of 4 M alkali halide solutions at 303 K. The shift of the positive peak from RbCl to RbBr is found at the intersection of column Rb^+ and row Cl^--Br^-.

	1 M	2 M	4 M
F^--Cl^-	+382	+385	+396
Cl^--Br^-	+24	+24	+22
Br^--I^-	+24	+25	+23

Table 4.7: Anion dependent average shifts for the maxima of the positive peak of 4 M alkali halide solutions at 303 K. The average shift of any cation in combination with Cl^- to the combination with Br^- at 2 M is found at the intersection of the column 2 M with the row Cl^--Br^-.

Wei et al. concluded in 2005 that the large positive peak can be attributed to the anion influencing the OH stretch band in that particular area. [36] The findings in this work support this interpretation. The large positive peak shows a profound anionic dependent

behaviour. The network peak is less influenced by the anion. One also would not expect the anion which is hydrogen bonded to the OH group to decrease the intensity of this particular OH bond. Quite the contrary, a strong binding anion would increase the intensity of the OH bond due to the change of the transition dipole moment. Thus it is logical to assign the positive peak to the interaction of the OH group with the anion. The network peak can therefore not be attributed to the anion interaction but to the reduction of the hydrogen bond network of pure water, as already mentioned above. [136]

	Li^+	Na^+	K^+	Rb^+	Cs^+	**avg.**
F^--Cl^-	-	-	−180	−182	−188	**−183**
Cl^--Br^-	+23	+12	+16	+14	+13	**+16**
Br^--I^-	+22	+14	+9	+14	-	**+15**

Table 4.8: Anion dependent shifts of the minima of the network peak of 4 M alkali halide solutions at 303 K. The shift of the network peak from RbCl to RbBr is found at the intersection of column Rb^+ and row Cl^--Br^-.

	1 M	2 M	4 M
F^--Cl^-	−172	−174	−183
Cl^--Br^-	+15	+14	+16
Br^--I^-	+15	+15	+15

Table 4.9: Anion dependent average shifts for the minima of the network peak of 4 M alkali halide solutions at 303 K. The average shift of any cation in combination with Cl^- to the combination with Br^- at 2 M is found at the intersection of the column 2 M with the row Cl^--Br^-.

Cation dependency

The influence of cations on the OH stretch band are discussed while the anion remains the same. Looking at figure 4.25 it becomes apparent that the influence of the cation on the band position is very minor. An exception is the shift from Li^+ to Na^+. The peak height of the large positive and the network peak change very little for K^+, Rb^+ and Cs^+. Changes of peak heights can be observed for Na^+ and Li^+. Looking into the numbers of the positive peak very little deviations can be seen on average in table 4.10. Only the shifts for the lithium to the sodium salts are strikingly different.

While with anion dependency great shifts were observed for the network and the positive peak, no such behaviour is seen on average with the cation dependency in tables 4.10 and 4.12 apart from the Li^+-Na^+ transition which will be discussed in the next passage.

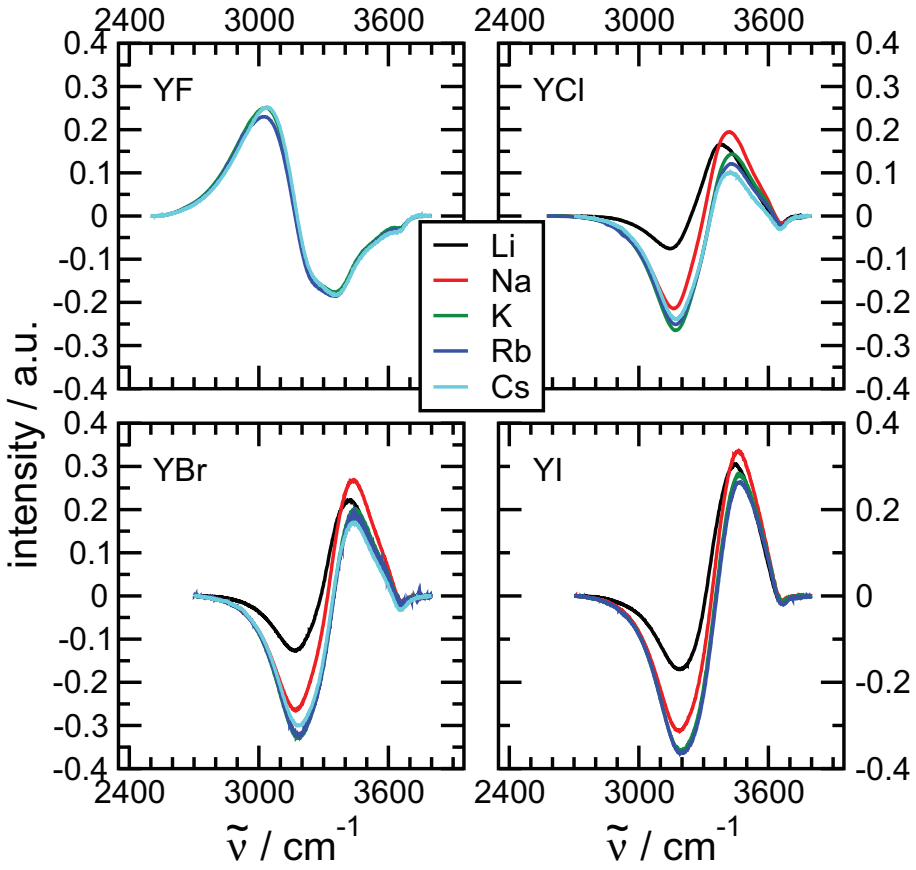

Figure 4.25: Cation dependent difference spectra of 4 M solutions of Li, Na, K, Rb and Cs halides at 303 K.

	Li^+-Na^+	Na^+-K^+	K^+-Rb^+	Rb^+-Cs^+
F^-	-	-	−3	+13
Cl^-	+39	+13	−6	−5
Br^-	+17	+6	+2	−5
I^-	+16	+3	+1	-
avg.	**+24**	**+7**	**−2**	**+1**

Table 4.10: Cation dependent shifts of the maxima of the positive peak of 4 M alkali halide solutions at 303 K. The shift of the positive peak from NaCl to KCl is found at the intersection of column Na^+-K^+ and row Cl^-.

	Li^+-Na^+	Na^+-K^+	K^+-Rb^+	Rb^+-Cs^+
1 M	+12	+2	−2	+1
2 M	+15	+7	−3	+2
4 M	+24	+7	−2	+1

Table 4.11: Cation dependent average shifts of the maxima of the positive peak of 4 M alkali halide solutions at 303 K. The average shift of any anion in combination with Na^+ to the combination with K^+ at 2 M is found at the intersection of the row 2 M with the row Na^+-K^+.

Similar to the observations made with the anion dependencies is the influence of the concentration on both peaks. No shifting of the peaks positions could be shown to be related to the concentration of the salt (see tables 4.11 and 4.13). No great changes can be expected here with one exception. That is the lithium ion, which has a greater effect because of higher charge density. Also due to its size it does not alter the water structure as much as the others as it fits smoothly into it (compare table 4.14 and figure 4.28).

	Li^+-Na^+	Na^+-K^+	K^+-Rb^+	Rb^+-Cs^+
F^-	-	-	+3	+6
Cl^-	+16	+9	+1	0
Br^-	+5	+13	−1	−1
I^-	−3	+8	+4	-
avg.	**+6**	**+10**	**+2**	**+2**

Table 4.12: Cation dependent shifts of the minima of the network peak of 4 M alkali halide solutions. The shift of the network peak from NaCl to KCl is found at the intersection of column Na^+-K^+ and row Cl^-.

	Li^+-Na^+	Na^+-K^+	K^+-Rb^+	Rb^+-Cs^+
1 M	−5	+1	+1	+8
2 M	+6	+10	+2	+2
4 M	−2	+4	+3	+4

Table 4.13: Cation dependent average shifts of the minima of the network peak of 4 M alkali halide solutions at 303 K. The average shift of any anion in combination with Na^+ to the combination with K^+ at 2 M is found at the intersection of the row 2 M with the row Na^+-K^+.

The hydrogen bonded water network is less reduced by the lithium salts. This becomes clear when looking at figure 4.25 where the network peak of the Li halides is a lot smaller compared to the Na, K, Rb and Cs halides. At the same time the intensity of the positive peak attributed to the anion interaction via the hydrogen remains very much at the same magnitude for all alkaline halides. This is another very strong indication that this peak must be due to anionic interaction, since the anion stays the same in each of the four diagrams in figure 4.25 and the intensity of the peak remains fairly constant.

4.5.2 Shifts in the difference spectra of bivalent cation solutions

Additionally investigating the salts $MgCl_2$, $MgBr_2$ MgI_2 and the equivalents for calcium adds some very interesting features to the picture, which shall be discussed here and in the section regarding the Hofmeister series (see section 4.6.1). The data obtained for these additional six salts fit nicely into the conclusions on monovalent ions drawn above but a separate interpretation for the bivalent ions keeps things clearer.

cation	r (nm)	anion	r (nm)
Li^+	0.71	F^-	1.24
Na^+	0.97	Cl^-	1.80
K^+	1.41	Br^-	1.98
Rb^+	1.50	I^-	2.25
Cs^+	1.73	NO_3^-	1.77
		ClO_4^-	2.41
		SCN^-	2.20
Mg^{2+}	0.70	SO_4^{2-}	2.42
Ca^{2+}	1.03	PO_4^{3-}	2.38

Table 4.14: Ionic radii of several HOFMEISTER ions in solution. All data from [137] except SCN^- from [138] and PO_4^{3-} from [139].

Figure 4.26 shows the difference spectra of the six salts at 303 K. Three main features can be observed in each graph. There is the very dominant positive peak at around 3400 cm^{-1}, the small negative quasi free OH group contribution at 3655 cm^{-1} and another positive peak which forms around 3000 cm^{-1} for the calcium salts and around 3100 cm^{-1} for the magnesium salts. The question is, can the large positive peak at 3400 cm^{-1} still be attributed to the anionic influence on the OH stretch band. The peak at 3655 cm^{-1} has been extensively discussed. The new positive peak at 3000 and 3100 cm^{-1} needs clarification and will be focused on in this section.

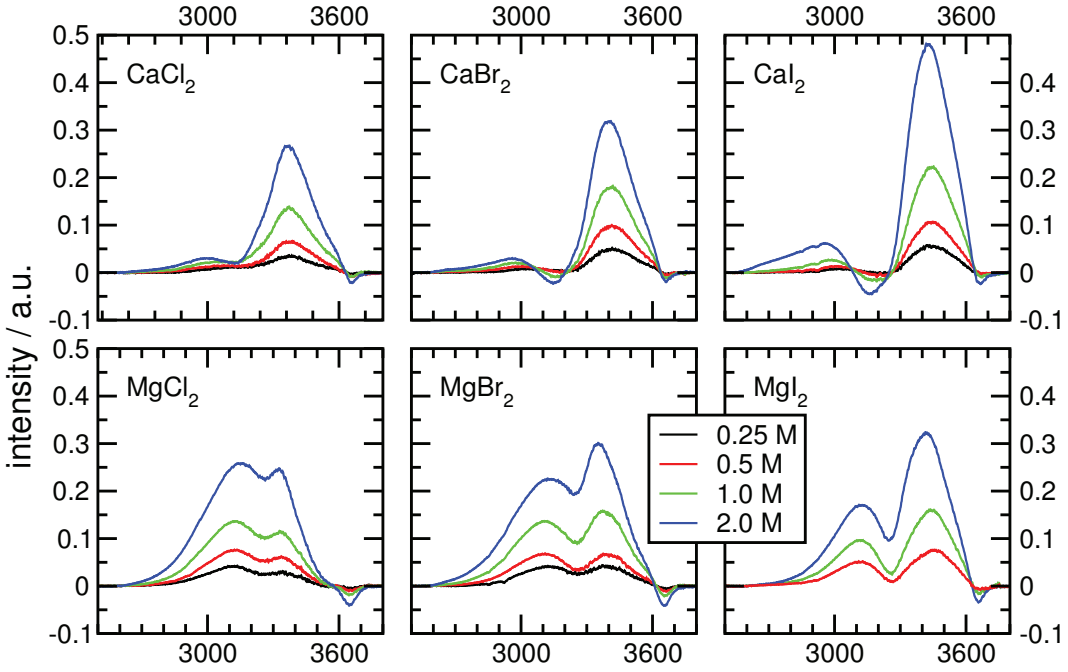

Figure 4.26: Anion dependent difference spectra of Mg and Ca halides salts as function of concentration at 303 K.

Unfortunately MgF_2 and CaF_2 are of very low solubility and cannot be examined in this respect. The peak positions for the magnesium and calcium salts are given in table 4.15 and 4.16. To connect with table 4.4 lithium values are also noted.

	Li^+	Ca^{2+}	Mg^{2+}
Cl^-	3381	3367	3327
Br^-	3422	3398	3355
I^-	3447	3428	3418

Table 4.15: Maxima of the positive peak at $\sim$3400 cm^{-1} of 4 M solutions of Li halides and 2 M solutions of Ca and Mg halides.

	Li^+	Ca^{2+}	Mg^{2+}
Cl^-	3146	2995	3148
Br^-	3169	2965	3131
I^-	3191	2959	3125

Table 4.16: Maxima and minima of the network peak of 4 M solutions of Li halides and 2 M solutions of Ca and Mg halides.

For the monovalent salts the peak positions were relatively constant across the table (cation dependent) and constantly changing down the table (anion dependent). For the bivalent salts this is not the case any longer. The peaks are also shifting cation dependent, the anion dependency is observed like for the monovalent salts.

Anion dependency

In figure 4.27 2 M anionic dependent solutions of the six salts are presented at 303 K. The maximum concentration of 2 M was chosen to retain comparability with the monovalent ions at 4 M concentrations by keeping the amount of anions equivalent[5].

The large positive peak at $\sim$3400 cm^{-1} and its shifts from Cl^- over Br^- to I^- (see table 4.17) show very similar but larger shifts compared to those which have already been observed for the monovalent ions in table 4.7. The peak which has already been assigned to the anionic interaction for the monovalent salts can be attributed to anionic interaction also for the bivalent salts.

[5]The difference spectra for the 0.5 and 1 M solutions can be found in appendix 4.4

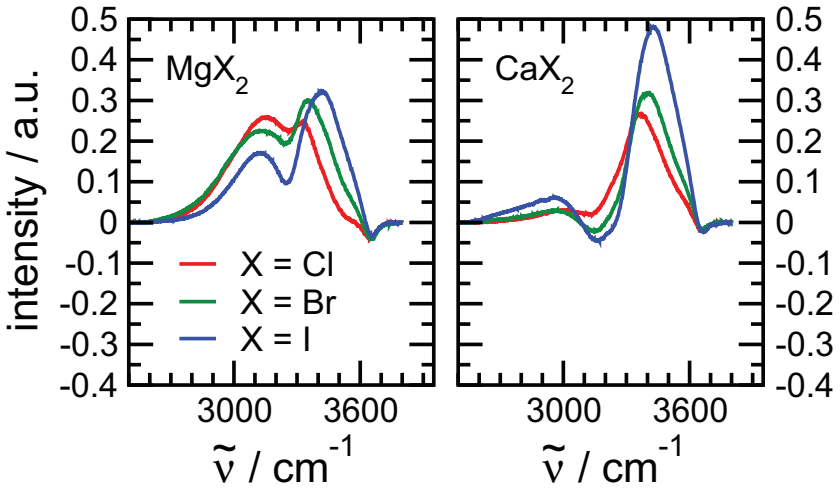

Figure 4.27: Anion dependent difference spectra of 2 M Mg and Ca halide solutions at 303 K.

The peak positions in table 4.15 lead to the anion dependent shifts presented in table 4.17. Like for the monovalent ions they demonstrate the strong anionic dependency. The values are higher than those for the monovalent alkaline halide solutions (see table 4.6).

	Li^+	Ca^{2+}	Mg^{2+}
Cl^--Br^-	+41	+31	+28
Br^--I^-	+25	+30	+63

Table 4.17: Anion dependent shifts of the maxima of the positive peak of 4 M solutions of Li halides and 2 M solutions of Ca and Mg halides. The shift of the positive peak from $CaCl_2$ to $CaBr_2$ is found at the intersection of column Ca^{2+} and row Cl^--Br^-.

Cation dependency

The chosen bivalent salts show a more complex cation dependent behaviour than the monovalent salts. The shifts of both, the network and the anionic peak for the monovalent ions with a constant anion from Na^+ to Cs^+ are rather small. The already mentioned deviational behaviour is expressed by a big shift from Li^+ to Na^+ see table 4.10.

For the bivalent salts this shift is even more pronounced for the step from Ca^{2+} to Mg^{2+}. Ca^{2+} and Mg^{2+} are of similar proportions as the Li^+ (see figure 4.28) but at the same time have twice the charge.

This is why these three cations are able to influence the anionic peak as well. One anion and one cation interact with the same OH group: The anion directly with the hydrogen, the cation via the oxygen. Cooperative effects lead to the cation supporting the anion effect because of its high charge density and further reaching influence and cause a significant shift of the anionic peak to lower wavenumbers see figure 4.29 and table 4.18.

	Li^+-Ca^{2+}	Ca^{2+}-Mg^{2+}
Cl^-	−14	−40
Br^-	−24	−43
I^-	−19	−10

Table 4.18: Cation dependent shifts of the maxima of the positive peak of 4 M Li halide and 2 M Ca and Mg halide solutions.

A closer look at the peak between 3000 and 3100 cm^{-1} reveals that it is found precisely in the same region in which the reduction of the pure water network was observed as a negative contribution with the monovalent ions. This positive peak has the same origin and also represents the network peak for the bivalent salts. This shall also be discussed in more detail in the HOFMEISTER section 4.6.1. Just like Li^+, the cations Ca^{2+} and Mg^{2+} as kosmotropes support the formation of water network and cause a further increase of the pure water hydrogen bonded network peak. A picture of the cationic dependency including monovalent and bivalent cations is found in the next section see figure 4.29.

Especially for calcium a peculiar behaviour is observed which makes interpretation rather difficult. For $CaBr_2$ and CaI_2 a dip into the negative area is formed (see figure 4.26). This dip disappears with $CaCl_2$ and is not observed for the magnesium salts at all. This phenomenon can be explained with the interaction of anions with the OH group: Ions of lower charge density such as I^- interact at higher wavenumbers. Charge density is higher for Cl^-, therefore the positive anionic peak moves downwards to lower wavenumbers and the two contributions fuse, making the negative dip disappear for $CaCl_2$.

This also shows that a decomposition of a difference spectra into distinct contributions is highly controversial in this area. One cannot presume, like for the quasi free OH contribution at higher wavenumbers, that only one contribution is to be found at this point.

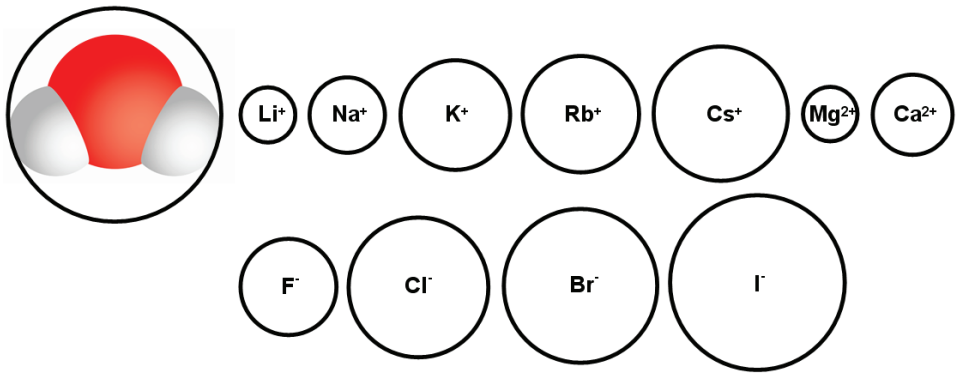

Figure 4.28: Ions in solution in exact proportion to the water diameter which is 275 nm.

4.6 The Hofmeister series

A few terms have to be defined before going into detail with the Hofmeister series. For the terms structure maker and structure breaker the interaction between two water molecules is the reference. If an ion interacts stronger with a water molecule than a water molecule would with its own kind it is called a structure maker or kosmotrope. If the water-ion interaction is weaker than between two water molecules it is a structure breaker or chaotrope. [63]

Changes observed in the OH stretch band are always the result of the interaction between ions and water molecules and changes of the pure H_2O structure caused by long range effects discussed in section 2.2.4. [70] This interaction influences the intensity in particular areas of the OH stretch band. The structure that is made or broken is therefore a structure which is imposed on the water by ion-dipole forces of different strength for different ions. [77] The structure made or broken has very little to do with the general accepted picture of tetrahedrally arranged water molecules. Around a kosmotrope more and stronger hydrogen bonds can be found per water molecule, while around a chaotrope less and weaker hydrogen bonds are present. [70]

One major problem occurring with the interpretation of infrared spectra of aqueous solutions is the fact that all effects are additive and observed at the same time. Only relative changes can be studied by leaving the anion or the cation constant as done and described in section 4.5. A cation dependent effect, e.g. chloride ions in combination with several cations may be observed and interpreted. The predicament occurs when another effect is observed with the changing anion and a constant cation. One may not be able to explain the latter effect on the same grounds as the cation dependent effect, because different premises are given due to the additive nature of the ion effect on the structure of water.

4.6.1 Cation dependent behaviour of the alkaline halides

All salts of the alkaline metals from lithium to caesium as well as the earth alkaline metals magnesium and calcium where investigated in combination with all halogens from fluorine to iodine in solution. The solubilities of the fluoride salts were mostly to low as to be of much use for the experiments. LiF, CaF_2, MgF_2 were not examined at all.

NaF only up to 1 M concentrations and beyond that up to 4 M concentrations only KF, RbF and CsF were available. This is unfortunate, because the fluoride salts show very interesting features which would be interesting to study in more detail.

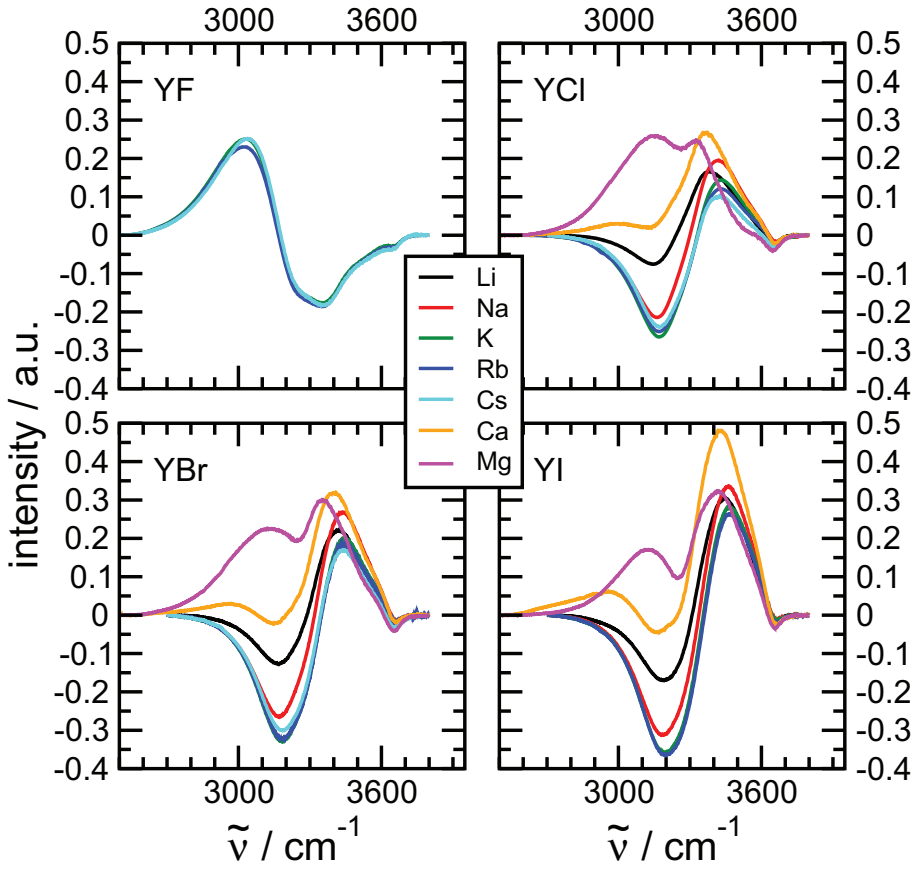

Figure 4.29: Cation dependent difference spectra of 4 M solutions for the monovalent and 2 M solutions for the bivalent cations to ensure the anion dependency at 303 K.

The low solubilities below 0.1 M for LiF, CaF_2 and MgF_2 are too low to observe any effects with the employed method. In figure 4.29 4 M solutions of the four halides in combination with the listed cations are presented. Again the 4 M solutions are chosen, as the shapes of the spectra do not change significantly upon changing concentration, and the 4 M spectra are very well structured. The other concentrations can be seen in the appendix 5.

The HOFMEISTER series for cations has been accounted for only scarcely in literature [72, 140], as focus is mainly put on the anionic series. [15, 65, 67–69, 94] The HOFMEISTER series for cations is therefore very little developed and no standard exists. [3, 72, 141] General trends can be observed though and two groups of ionic compounds tend to be arranged together on the one or the other side of the series. As kosmotropes are generally defined: Mg^{2+}, Ca^{2+}, Li^+, Na^+ and NH_4^+. Chaotropes are the larger cations such as K^+, Rb^+ and Cs^+. The arrangements within each group may alter and some ions may even be borderline ions which on some occasions are regarded as chaotropes and on other occasions as kosmotropes.

	F^-	Cl^-	Br^-	I^-	
K^+	−0.1763	−0.2641	−0.3285	−0.3634	chaotropes
Rb^+	−0.1843	−0.2517	−0.3229	−0.3598	
Cs^+	−0.1835	−0.2378	−0.3006	-	
Na^+	-	−0.2140	−0.2652	−0.3143	kosmotropes
Li^+	-	−0.0745	−0.1272	−0.1693	
Ca^{2+}	-	0.2604	0.0677	0.0992	
Mg^{2+}	-	0.4978	0.2247	0.1519	

Table 4.19: Peak heights of the network peak for 2 and 4 M solutions of bivalent and monovalent ions respectively.

This order can be found in figure 4.29 from the behaviour of the network peak. For all investigated halide salts, except the fluorides for reasons stated above, the outlook of the difference spectra is very similar. Focus is put on the peak between 3200 and 3300 cm^{-1} for Cl^-, Br^- and I^-. This peak has been attributed to the influence of the ion on the hydrogen bonded network of water in section 4.4.1. The behaviour of this peak can be divided into two groups. First of all there are the Cs^+, Rb^+ and K^+ peaks which are found at very similar peak heights for each halide combination, even with fluoride. For the fluoride salts the minima around 3400 cm^{-1} is attributed to the influence on the hydrogen bonded network and they also show very similar behaviour.

These cations which are traditionally assigned to be chaotropes form a triplet in these spectra. Going from K^+ to Na^+ there is a first and very obvious cut in the peak heights. From there on following the series over Li^+ and Ca^{2+} to Mg^{2+} there is a steady increase. These four salts form the second group and are generally assigned to the kosmotropes.[6] The increase of this peak for $MgCl_2$ has been observed and described by Rossi et al. in 1996. They also attributed it to the increase of the hydrogen bonded network. [17]

In figure 4.30 the peak heights of the network peaks are depicted against the cations in the order of their Jones Dole viscosity B coefficient. The order found in this work differs slightly from the classical view of the Hofmeister series related to the Jones Dole viscosity B coefficient. That is why there is a small dip from Cs^+ to K^+. If Cs^+ and K^+ would swap places, this would lead to a straight line overall for all salts and a perfect match with the series. All other ions are in agreement with the literature. [66]

In table 4.19 the peak heights of the network peaks are noted with this slightly different arrangement which is also known from Marcus and his classification using his ΔG_{HB}[7] parameter presented in table 4.20. [3] Despite this uncertainty regarding the sequence

[6] The established and most cited series put up by Collins has the Ca^{2+} in front of Mg^{2+}, there are also reports in which Mg^{2+} and Ca^{2+} change places. [72]

[7] ΔG_{HB} is a factor introduced by Marcus and defines water structure in terms of the extent of hydrogen bonding, not its strength or dynamics

cation	ΔG_{HB}
K^+, Rb^+, Cs^+	−0.9 to −0.7
Na^+	−0.1 to 0.1
Li^+	0.1 to 0.4
Ca^{2+}	0.4 to 0.7
Mg^{2+}	0.9 to 1.1

Table 4.20: Ions arranged according to their effects on the structure of water represented by the parameter ΔG_{HB}. [3]

of the cations K^+, Rb^+ and Cs^+ show very similar behaviour in their influence on the OH stretch band and to regard them as triplet in that respect seems appropriate. The differences in heights between the K, Rb and Cs halides are very small and may even be due to experimental error. This behaviour determined for the 4 M solutions can also be found with the 2 and 1 M solutions. The jump from the chaotropic triplet to the first kosmotropes, in this case Na^+, is also very distinct for the 1 M fluoride solutions (see figure 4) where the network peak is located at 3400 cm^{-1}. The other fluoride salts are experimentally not accessible because of very low molar solubilities (see table 2.4).

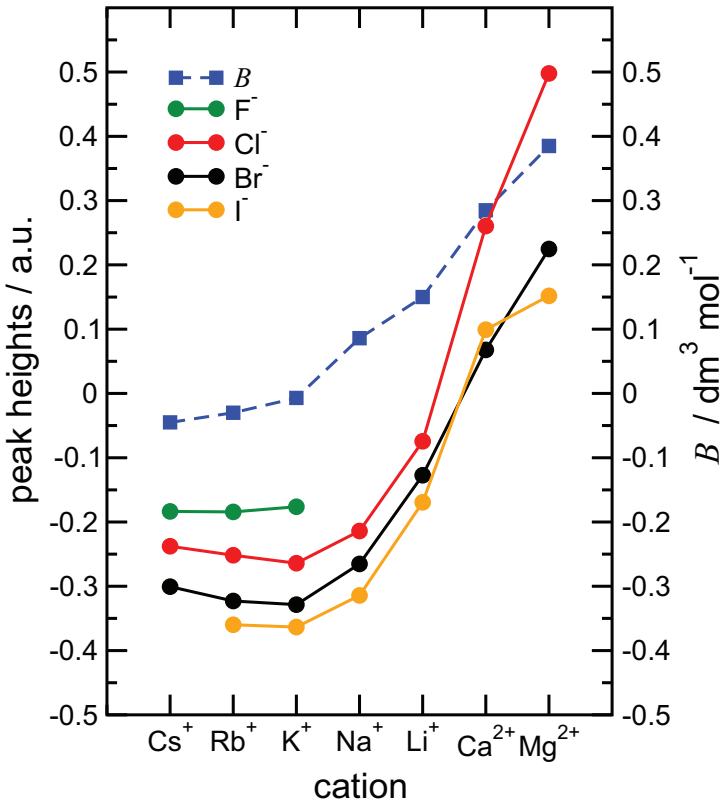

Figure 4.30: The JONES DOLE viscosity B coefficient of selected cations in comparison to the height ot the network peak in the difference spectra taken from table 4.19. The right y-axis shows the B coefficient (blue dashed line), the left y-axis represents the peak heights (straight lines).

So besides the JONES DOLE viscosity B coefficient this, or a very similar, order can also be found for ΔG_{HB}. [3, 63] Both parameters are indicators of the structuredness of water. In this classification the chaotropes K^+, Rb^+ and Cs^+ are also arranged as a triplet in the same category (see table 4.20). [3, 142] The JONES DOLE viscosity B coefficient is an expression for the viscosity of a salt solution. These tendencies and correlations demonstrate that it is safe to presume this peak to be an indicator for the influence of ions on the structure of water.

4.6.2 The sodium series and hydrophobicity

Talking about the HOFMEISTER series goes hand in hand with hydrophobic effects. Generally speaking hydrophobicity occurs when water is repelled from a substance or a molecule. To speak of water being repelled from a charged ion seems peculiar but the idea behind this effect can be observed even for charged ions. A set of several sodium salts is analysed in this section. Mainly monovalent anions are examined, but also bivalent and even a trivalent anion is investigated. For those solutions it was inevitable to choose the concentration levels in such a way as to keep the amount of the sodium ions equivalent. To ensure the qualitative comparability in terms of the anion the amount of the cation has to be constant.

In the previous section it was outlined that quasi free OH groups can be drawn up by charged ions. Their concentration decreases as the concentration of the salt increases. These quasi free OH groups have been identified at $3655\,cm^{-1}$. This behaviour is detected for all ions from Na_2SO_4 to NaI, in figure 4.31 recognisable by the small negative peak at $3655\,cm^{-1}$. Solutions containing sodium and a polyatomic only weakly charged ion, such as ClO_4^-, SCN^- and NO_3^- do not show this distinctive behaviour of free OH group reduction.

The anions SO_4^{2-} or PO_4^{3-} [8] are of similar ionic radii but carry twice and thrice the charge. This makes them a far better reducer of quasi free OH groups even though the anionic concentration is only a half or a third compared to the monovalent ions.

For the bottom row salts in figure 4.31 no negative contribution can be seen at all at $3655\,cm^{-1}$ indicated by the grey dashed line. One reason as already noted is the low charge density. A second reason being sterical ones. Br^- and I^- which have a similar ionic radius as NO_3^- or ClO_4^-/SCN^- respectively draw up the free OH groups while NO_3^-, ClO_4^- and SCN^- do not.

[8] Na_3PO_4 acts basic in aqueous surrounding leading to the formation of HPO_4^{2-} and OH^-. [143] An extra category of anions which can draw up free OH groups is hence present. A very clear cut peak can again be found at $3655\,cm^{-1}$.

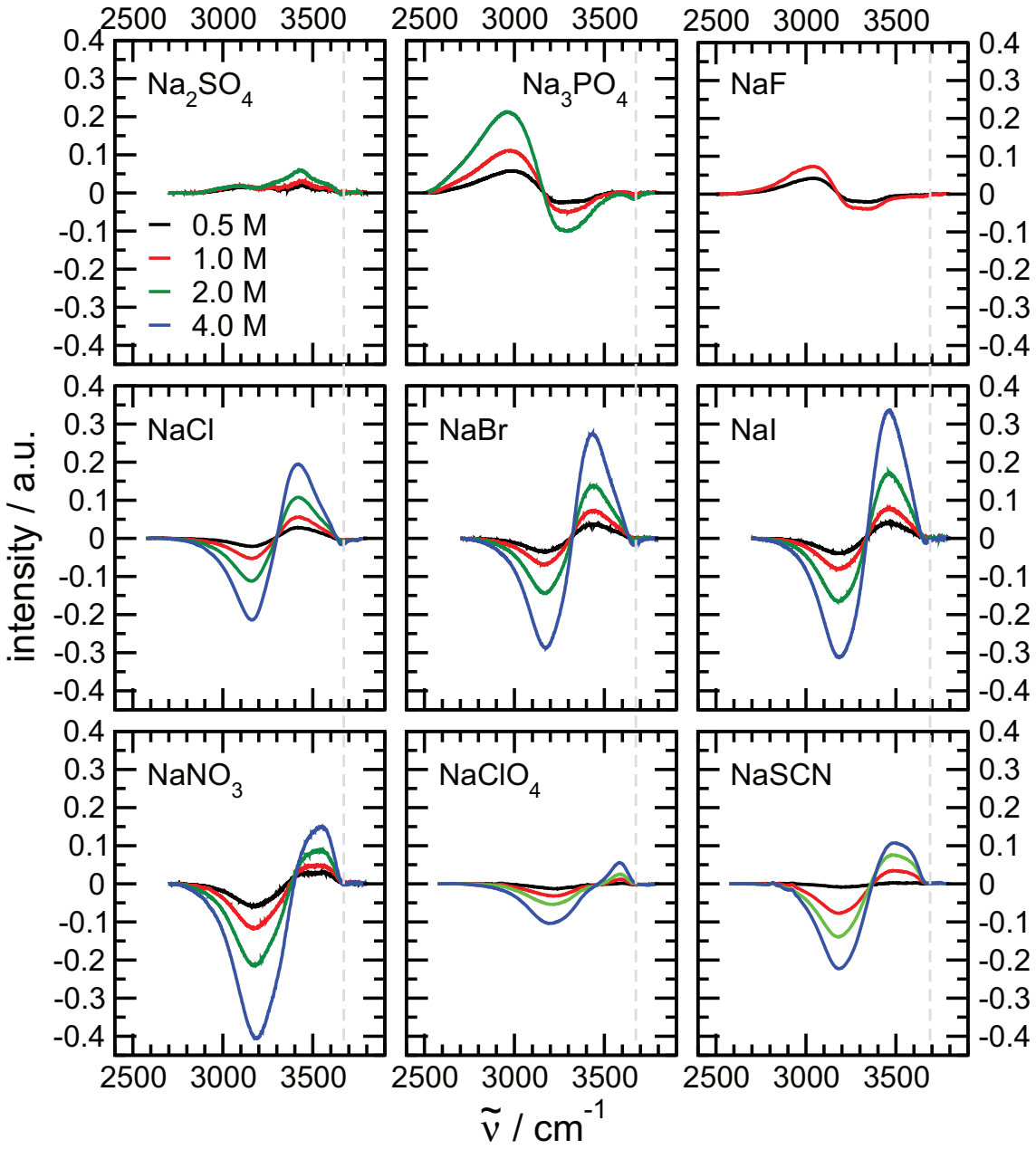

Figure 4.31: Anion dependent difference spectra of selected sodium salts in order of the HOFMEISTER series as function of concentration. The amount of Na^+ is ensured to be constant. Concentrations in the legend refer to the amount of Na^+ in the solution. I.e., 0.5; 1.0 and 2.0 M are 0.25, 0.5 and 1.0 M for Na_2SO_4 respectively. With Na_3PO_4 the same concentrations refer to 0.166; 0.33 and 0.66 M. The position of the quasi free OH group is indicated by the grey dashed line. The original spectra are found in appendix 10

Hydrogen bonds are formed more readily with the easily accessible charge of the spherical iodide or bromide than with the planar, tetrahedral or linear anions. For these three ions the effect is very obvious. No reduction of quasi free OH groups is observed which leads to the conclusion that the concentration of the quasi free OH group is left unchanged.

$$SO_4^{2-} > HPO_4^{2-} \simeq F^- > Cl^- > Br^- > NO_3^- > I^- > \simeq ClO_4 > SCN^- \ [9]$$

This reduction of the quasi free OH groups can be related to the original HOFMEISTER series. FRANZ HOFMEISTER put up a series of ions according to their ability to decrease or increase the solubility of proteins, that is to support precipitation or inhibit it, maybe even increasing solubility. [64]

He came up with an explanation in terms of water being engaged with the hydrated ions leaving less water to keep the protein hydrated and thus causing precipitation or vice versa. [67, 144] Features found in the spectra in this work can be correlated to HOFMEISTER'S theory as follows. The weakly charged polyatomic anions are all found on the less precipitating side of the series. The fact that those ions do not reduce the quasi free OH groups fits into the explanation which HOFMEISTER came up with to explain the hydrophobic effect of salts on proteins.

A highly charged ion such as SO_4^{2-}, kosmotrope by definition, interacts stronger with water than water with itself, thus reducing the concentration of quasi free OH groups and leaving less to interact with, with any given biomolecule: the chance of precipitation increases. The bigger and less charged SCN^- has little to offer to water. It is chaotropic and water molecules in its vicinity would rather enjoy a stronger bond to its own kind and leave the anion unattended. [5, 145] The amount of quasi free OH groups is almost unchanged and the hydrogen bonded network almost remains in its state: Precipitation is less likely to occur. It is also known for apolar or hydrophobic solutes that water can arrange itself around such a particle in a tangential manner.

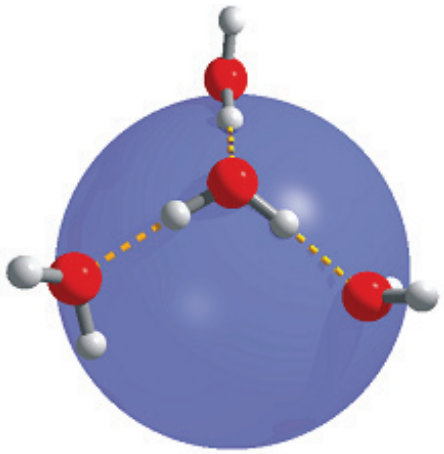

Figure 4.32: Apolar particle surrounded by hydrating water. [51]

[9] This series is based on [63] and [65]. In some other publications some ions may swap places. [3]

This means that a cage like structure is formed around it similar to what can be observed for clathrate hydrates. A maximum number of hydrogen bonds is thus preserved [51], which in turn would imply less quasi free OH groups to be present.

A recent publication by BONDARENKO et al. mentions that for $NaClO_4$ in solution no evidence could be found for strong hydrogen bonds between the nearest water molecule and the anion, ClO_4^- can therefore be considered as hydrophobic. [146] This finding supports the sophisticated RAMAN studies of WALRAFEN on the same topic. [147] On the other hand BONDARENKO et al. observe a strong decrease of the infinite hydrogen bonded network, which naturally must occur, caused by the mere presence of solutes causing local disorder. [145, 146]

The SCN^- ion is a strong hydrogen bond acceptor in crystals. The charge of the thiocyanate ion is delocalised and in solution a hydrogen bond can be formed from virtually all directions. [148] However, in solvation studies with methanol it was found that a substantial part of the SCN^- anions are not hydrogen bonded and can be considered "free". [149] The fact that the hydration number of SCN^- is reported to be around one, supports this notion. [150]

The hydrogen phosphate and the sulfate anion show very similar behaviour when it comes down to hydrogen bonding. PYE et al. identify the hydrogen phosphate coordinated with three water molecules to be the most stable form. They also identify the possibility of a dangling OH group in the presence of phosphate but rule this out as anomalous behaviour. [151] The nitrate ion, similar to thiosulfate, is described in literature as showing hydrophobic characteristics. [152] These data from literature support the classification and the results presented in this work regarding the behaviour of larger anions being either chao- or kosmotropes and reducing the concentration of quasi free OH groups.

Discussions were also driven in the direction whether or not precipitation could also be caused by direct ion-biomolecule interaction, i.e. ions electrostatically binding to the biomolecule. [153] Traditionally in the Hofmeister series I^- is placed above NO_3^-. Iodide therefore being a stronger stabiliser than nitrate. From the above drawn conclusions regarding the reduction of quasi free OH groups to be equivalent to the stabilising behaviour this ordering could not be verified. Iodide clearly reduces quasi free OH groups. Therefore other effects, such as direct interaction, can play a vital part in this mechanism. Nevertheless, a tendency can be observed that ions which do not reduce the amount of quasi free OH groups are found in the region of the HOFMEISTER series which is regarded as stabilising proteins.

This interpretation of the data adds additional information for finally answering the questions regarding protein stabilising or destabilising in the context of the HOFMEISTER

series. Whether or not salts in protein solution beside the effect of reducing quasi free OH groups also interact with proteins directly, increasing or decreasing their solubility cannot be determined from experiments dealing with aqueous salt solutions alone.

4.7 Hydrate formation

In figures 4.1 and 4.2 the spectra of frozen H_2O and D_2O are presented. D_2O freezes at a slightly higher temperature around 277 K. Upon the addition of any salt the freezing point is depressed. This physical effect is due to the decreasing chemical potential of the solution compared to that of pure water. [87] A very similar effect, the elevation of the boiling point, is also caused by the addition of a non-volatile substance, e.g. salt, to water. [154]

Frozen water forms the well described tetrahedral network, where each water molecule is surrounded by four adjacent water molecules. [126] Even though an aqueous solution containing any salt has a lower freezing point than pure water, eventually the solution will freeze. The freezing point being dependent on the concentration and the kind of salt. Salts are almost insoluble in ice, with a solubility in the micromolar range. [16] During the freezing process this insolubility of salts in ice leads to the rejection of the dissolved salt into the still liquid phase. Ending up with the formation of highly concentrated brine in so called brine pockets [10] or the expulsion onto the surface of the ice lattice. [88, 156] A mixture of pure ice, high concentrated brine, salt hydrates and the crystalline salt have been described to form during the freezing process. [90, 156] Although frozen water is devoid of salts, there have been reports from molecular dynamics simulations of single ions being incorporated into the ice lattice. [16]

This physical process is not only interesting for the marine chemists or oceanographer who are interested in the formation of sea ice but also for freezing processes which take place in the atmosphere in the formation of clouds. [157] The expulsion of salt from freezing salt water is an alternative to reverse osmosis for the desalination of water.

In this work experiments on the freezing behaviour of simple monovalent salts have been carried out. Focus was put on the alkali chlorides and the sodium halides, both series sharing sodium chloride, at a concentration level of 0.5 M and lowering the temperature beginning at 293 K in 10 K steps. Both series (LiCl, NaCl, KCl, RbCl, CsCl and NaF, NaCl, NaBr, NaI) were investigated in order to detect any anionic or cationic dependent behaviour. Several mono- or dihydrates are known for the simple salts. In this works'

[10] In real sea ice these brine pockets would slowly be washed out through a system of channels and spill out from the bottom of the ice. The resulting highly saline and more dense water beneath the ice is an important influence on the ocean overturning circulation caused by convection. [155]

case, they are: $LiCl{\cdot}H_2O$, $NaCl{\cdot}2H_2O$, $NaBr{\cdot}2H_2O$, $NaI{\cdot}H_2O$. [90] For KCl solutions for example no other solids apart from KCl and ice are present in the phase diagram when the solution is frozen. [158]

The chosen concentration of 0.5 M is very similar to that of real sea water. The concentration of sea water is usually given as 35 g/L. Approximately 85% of the dissolved salt is sodium and chloride. Additionally there is sulfate, calcium, magnesium and potassium making up most of the remaining percentage. Presuming only sodium chloride is present, 35 g/L would give a molarity of 0.6 M.

4.7.1 The freezing process

The behaviour of the OH stretch band of a 0.5 M NaCl solution is depicted in figure 4.33a. It is presented exemplarily for all other salts presented in figures 4.34 and 4.35. A general trend can be observed for almost all salts. The system investigated here is in its physical constitution comparable with sea water. Sea water freezes at around 271 K. For all solutions a significant change of the spectrum can be seen just below 273 K.

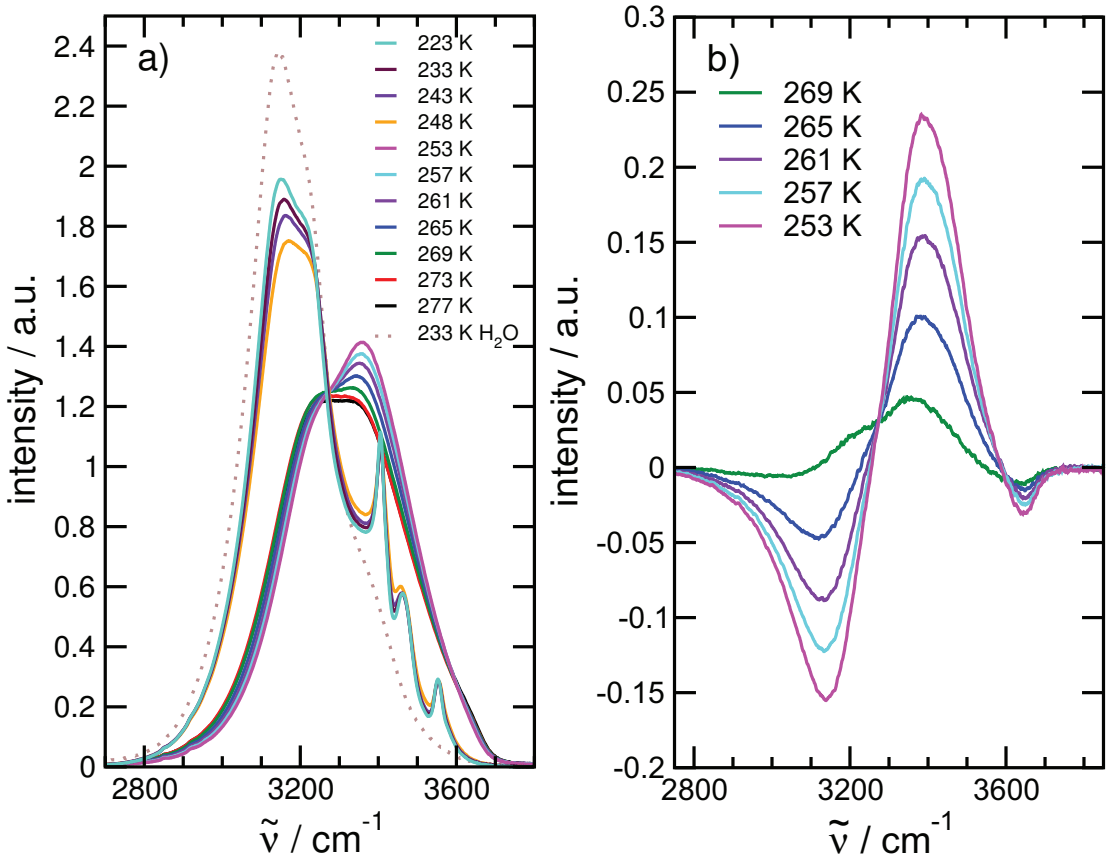

Figure 4.33: a) 0.5 M NaCl solution from 277 K to 223 K, b) difference spectra of 0.5 M NaCl solution from 269 K to 253 K, pure water just above the freezing point taken as reference.

The freezing process has begun and an increase of intensity can be observed around 3400 cm^{-1}. Depicted in 4.33b are the difference spectra of the freezing salt solution below 273 K until complete freezing has occurred. These difference spectra of a freezing solution show a very strong resemblance with the difference spectra and with their distinct increase and decrease of intensity of a set of salt solutions at ambient conditions at various concentrations (see figure 4.20).

From NaF a somewhat different concentration dependent behaviour is known for the course of the intensities at ambient conditions. An increase is observed at the lower end of the OH stretch band upon increasing the concentration. The same feature can be seen in figure 4.34 during the freezing process of a NaF solution.

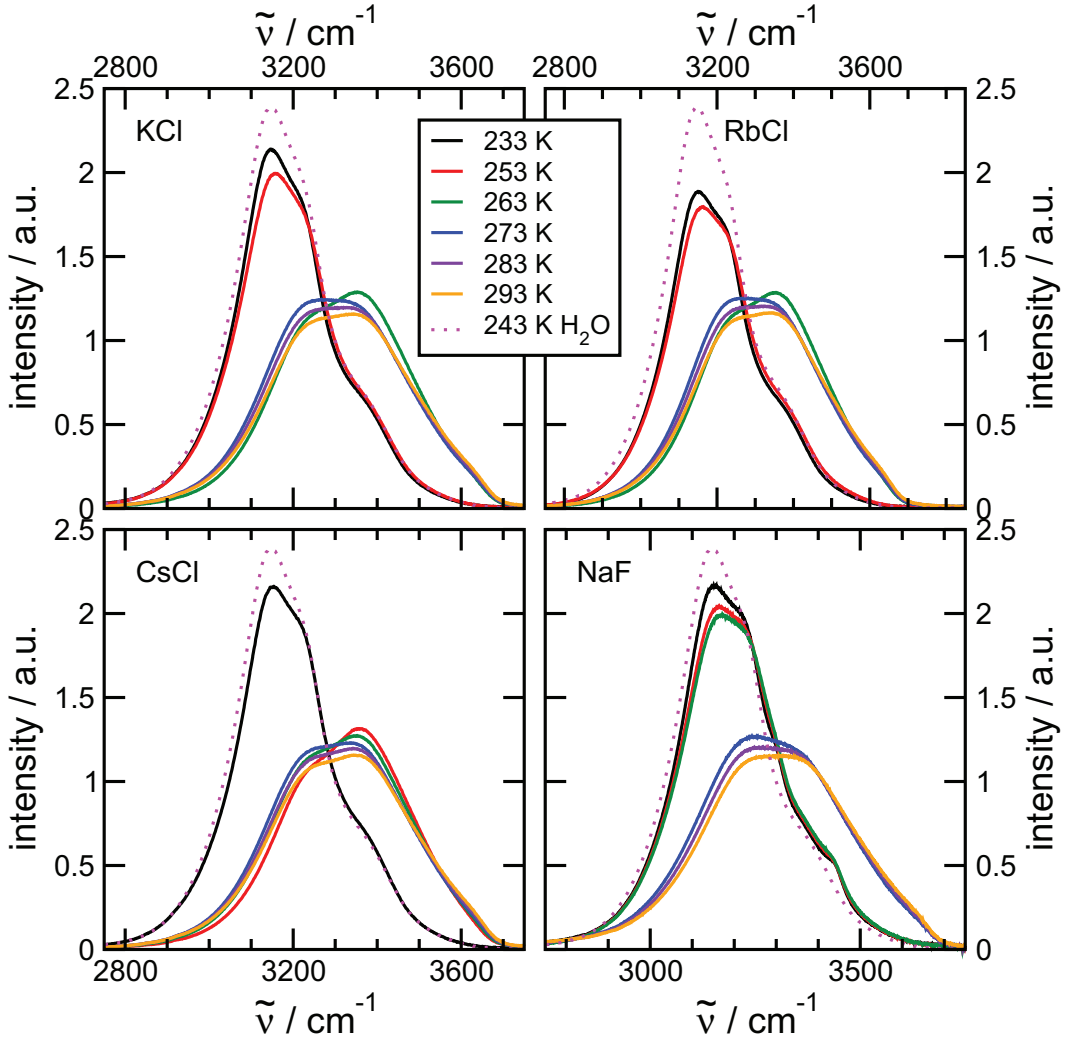

Figure 4.34: Spectra of freezing 0.5 M KCl, RbCl, CsCl and NaF solutions. The dotted spectrum is pure water in its solid state.

It can be deduced from these pictures that the phenomenon of brine rejection can be

observed with these spectra. The cooling mechanism of the Golden Gate Unit is achieved by heating the crystal electrically from below against the liquid nitrogen cooling from above. The drop of the salt solution begins to freeze from the top forming standard hexagonal ice while the dissolved salt remains in the liquid phase and the still liquid solution becomes more and more concentrated. This is why the spectra obtained, resemble such a strong similarity with spectra of increasing higher concentration at ambient conditions. Then at some point the ice lattice reaches the bottom of the drop, i.e. the crystal-probe interface where detection takes place, and the whole drop is frozen. This point is the step from the still liquid spectra with the increasing intensity at higher wavenumbers to the ice like spectra known from figure 4.1 where the centre of gravity is found at much lower wavenumbers.

What remains visible is the standard ice spectra for all solutions in figure 4.34 and 4.35 with the prominent peak at the low wavenumber end of the OH stretch band but also the formation of hydrates for NaCl, NaBr and NaI, which can be apprehended by the clear cut peaks in figure 4.35.

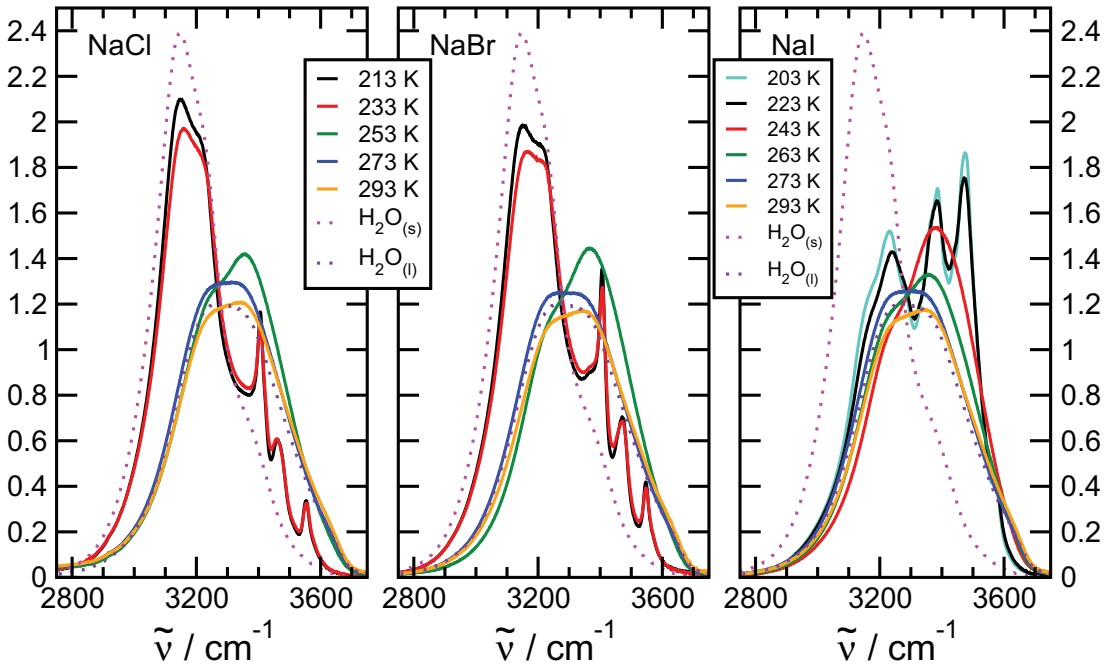

Figure 4.35: Spectra of freezing 0.5 M NaCl, NaBr and NaI solutions. The dotted lines depict pure water in its solid and liquid state.

4.7.2 Frozen sodium halide solutions

In figure 4.36 the spectra of all sodium halides are presented in their frozen state for H_2O and D_2O solution. For all salts apart NaF the formation of clear cut peaks can be observed. These peaks can, with the aid of similar D_2O experiments and values from literature, be attributed to the water molecules in sodium salt hydrates. The different physical properties of D_2O make spectra of the D_2O solution much more distinguished than the H_2O spectra.

Ford and Falk produced NaCl·2D_2O with 0.3 mol% NaCl·2HDO from a saturated solution and they identify two peaks in the OH stretch at 3423 and 3531 cm^{-1}. [159] In figure 4.37 two peaks can readily be identified at 3429 and 3540 cm^{-1} and can unambiguously be attributed to the two water molecules in NaCl·2HDO. The third peak at 3300 cm^{-1} is attributed to the unaffected and uncoupled OH group of the HDO molecule. This peak can also be seen at the exact same position in the pure 95% D_2O/ 5% H_2O spectrum in the same figure (dotted brown line).

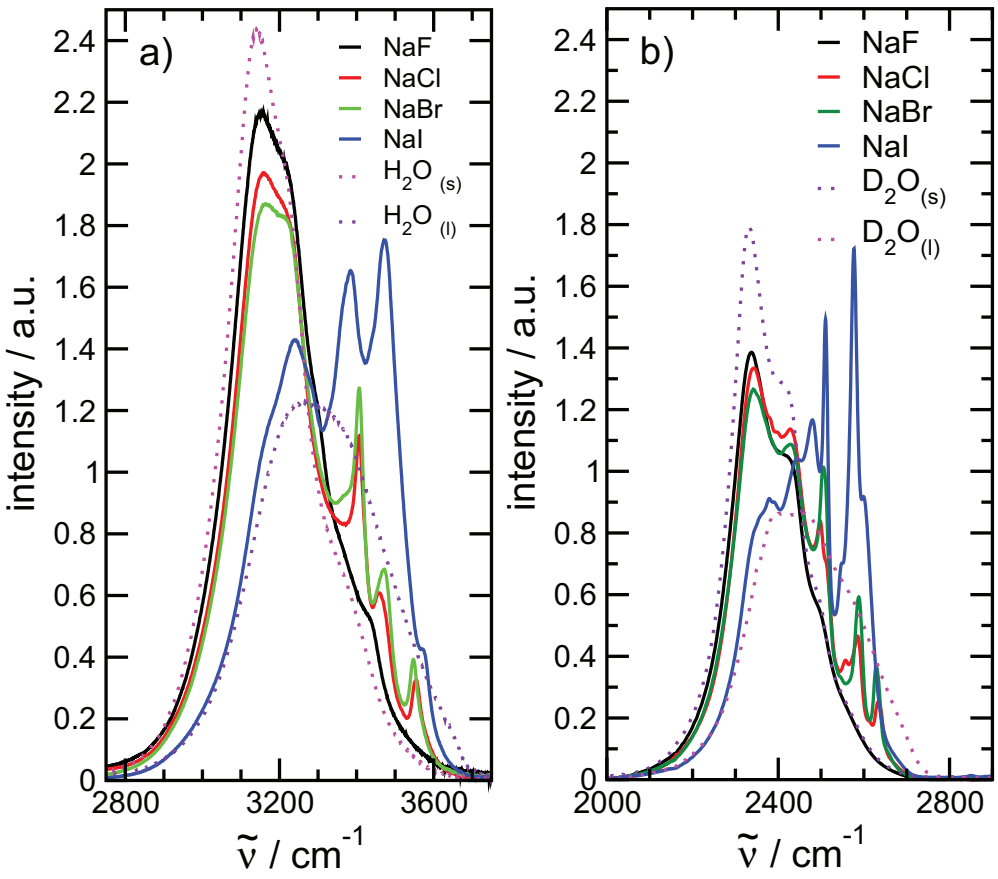

Figure 4.36: Frozen sodium halide solutions at 233 K (223 K for NaI) with a concentration of 0.5 M in a) H_2O and b) D_2O. Hydrate formation can be observed. The dotted lines depict pure water in its solid and liquid state.

In pure water three peaks are attributed to the $NaCl{\cdot}2H_2O$. The one at $3557\,cm^{-1}$ is in good agreement with the peak at $3542\,cm^{-1}$ in NaCl·HDO, the difference being due to the different physical nature of the two solutions. Two more peaks are seen at 3403 and $3464\,cm^{-1}$. The second peak in the HDO experiment positioned at $3429\,cm^{-1}$ marks exactly the middle of the two peaks found with pure water. This leads up to the conclusion that these are coupled in H_2O and decoupled in D_2O forming one single contribution only.

In figure 4.33a the formation of $NaCl{\cdot}2H_2O$ occurs between 253 K and 248 K. Again, this is proof for the formation of hydrates. For a solution of 0.5 M NaCl the formation of hydrates occurs at the eutectic temperature of 250.8 K. [160] Isomorphism has been reported for $NaCl{\cdot}2H_2O$ and $NaBr{\cdot}2H_2O$. [159,161] Comparing the NaCl and NaBr spectra in figure 4.36 the similarity of the spectra due to this isomorphism is striking. This analogy leads to the conclusion that hydrate formation is also observed for the NaI solution. The peaks of $NaI{\cdot}D_2O$ spectra coincide with data in ref. [161].

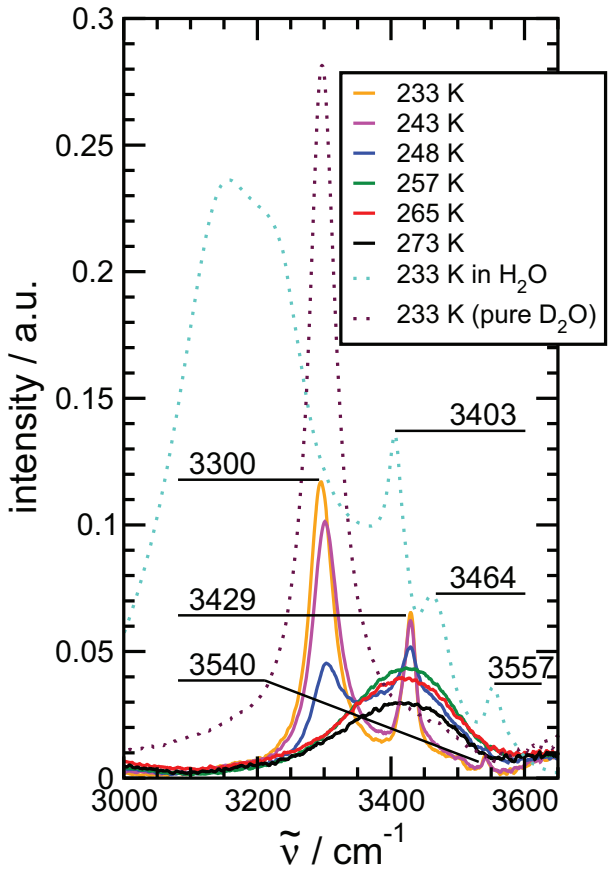

Figure 4.37: OH stretch region of a freezing 0.5 M NaCl solutions in 95mol% D_2O with 5mol% H_2O (straight line) and in pure H_2O at 233 K (blue dotted line). Pure D_2O containing atmospheric H_2O is also presented (brown dotted line). The values indicate the peak positions in wavenumbers.

The large peak at 3100 cm^{-1} seen in figure 4.36 is attributed to the tetrahedral hydrogen bonded network, the ice structure. Its intensity drops significantly from F^- over Cl^-, Br^- to I^-. This can be interpreted in terms of where the hydrates are located and where solidified salts remain. NaF does not form hydrates and therefore must recrystallise at the bottom of the sample drop, because it freezes from top to bottom. Some crystals are presumably expelled at the outer rim too, but some parts will also take up space at the bottom of the drop thus decreasing the volume of the probed sample, leading to a decrease of intensity. The larger the ions get the more space is taken up, NaCl and NaBr hydrates behave very similar, NaI is very large consuming a lot of space and reducing the ice like structure in proximity to the surface significantly.

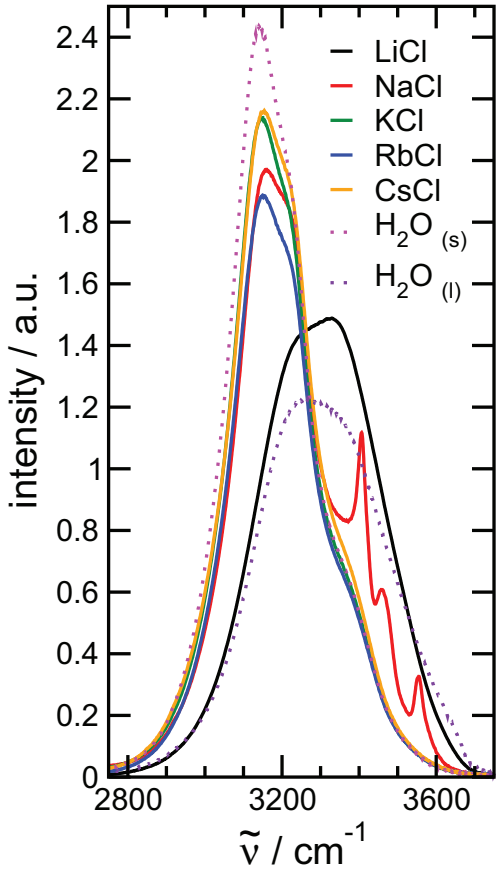

Figure 4.38: OH stretch region of frozen 0.5 M alkali chloride solutions in H_2O. The dotted lines depict pure water in its solid and liquid state.

4.7.3 Frozen alkali chloride solutions

The spectra of the 0.5 M alkali chloride solutions are presented in figure 4.38. For NaCl the above discussed hydrate formation is observed, which makes it unique in that respect in this series. For KCl, RbCl and CsCl solutions no hydrate formation was observed nor

expected. But the freezing process takes places just as described in section 4.7.1. In this series LiCl displays an interesting behaviour too, unlike the other salts it seems not to be frozen at 233 K.

Supercooled lithium chloride solution

LiCl is a special case, it seems that it does not freeze completely until about 183 K. From phase diagrams of the LiCl-H_2O system a eutectic temperature at around 200 K has been reported. [162] The classic formation of the peak attributed to the ice structure at 3100 cm^{-1} cannot be observed.

It is a well established fact that LiCl solutions are easily supercooled and that glassy states are formed. [162] In figure 4.39a the OH stretch band of a 0.5 M solution of LiCl is depicted from 277 to 183 K. The structure of the band only alters its intensity recognisably while the shape basically stays the same.

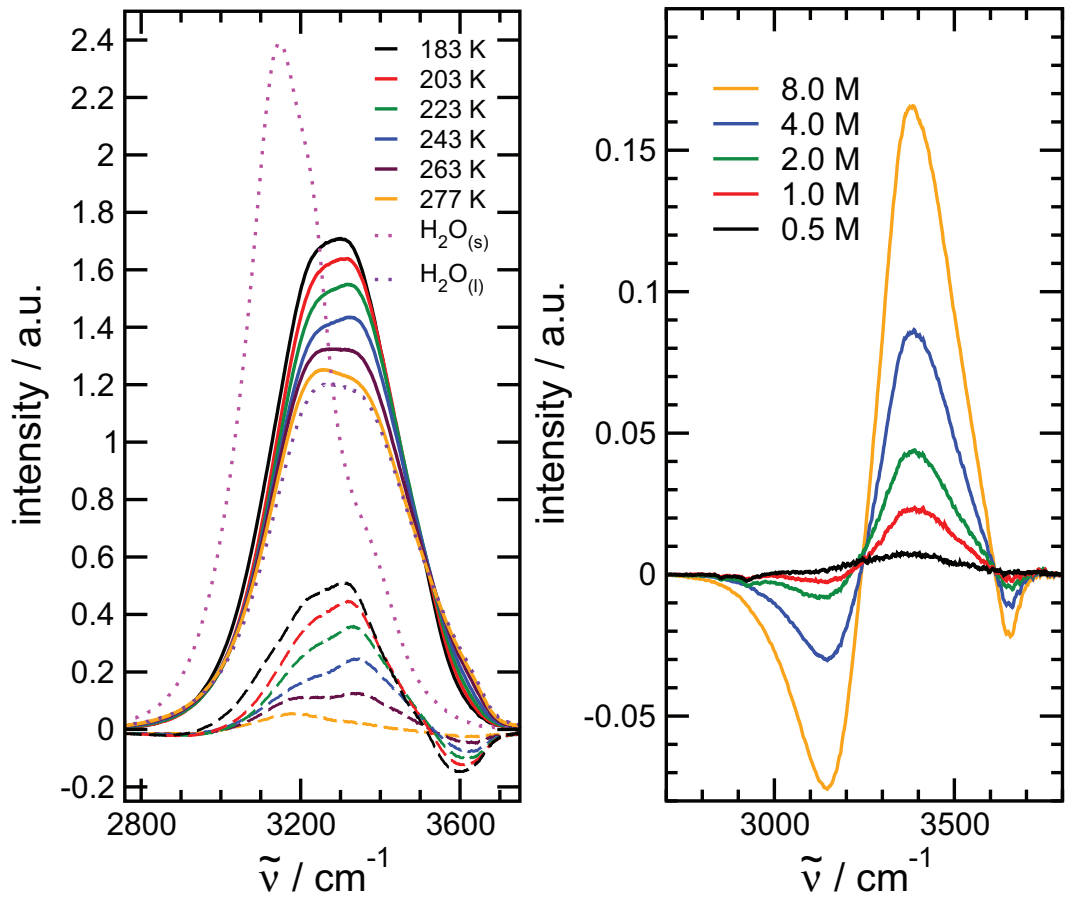

Figure 4.39: OH stretch region of a) a frozen 0.5 M lithium chloride solution in H_2O. The dashed lines represent the difference spectra. The dotted lines depict pure water in its solid and liquid state. And b) LiCl solutions at several concentrations at ambient conditions.

This behaviour goes along with findings from neutron diffraction experiments carried out by Winkel et al. in lithium chloride solutions [163]: The strength of the hydrogen bond increases as the average hydration number increases with decreasing temperature. The increasing strength must lead to the increase of intensity and the increasing hydration number to a reduction of non bonded OH groups. As outlined in section 4.4.2 the free OH groups are found at around $3655\,\mathrm{cm}^{-1}$.

It is unlikely that free OH groups are not reduced upon cooling an aqueous solution of lithium chloride. Extreme caution has to be exercised nevertheless when interpreting the high wavenumber end of the supercooled LiCl difference spectra. These spectra are temperature dependent and unlike the free OH group contribution from the concentration dependent spectra at ambient temperature (see appendix 4), a clear shift of the contribution can be observed to lower wavenumbers upon decreasing the temperature. Slowly increasing the concentration of LiCl as shown in figure 4.39b does not cause this shift. This shift results purely from the temperature effect which also causes a pure water spectrum to shift to lower wavenumbers as described in section 4.1. So it is safe to presume that although the peak is not exactly positioned at $3655\,\mathrm{cm}^{-1}$ it still represents the reduction of free OH groups.

5 Conclusion

The effects of ions on water regarding the HOFMEISTER series were the main focus of this work. A couple of other very interesting topics and essential questions regarding the structure and fundamental vibrations of liquid water and the influence of ions on water had inevitably to be explored and developed in more detail in order to explain HOFMEISTER effects. A short summary shall outline the main theories which were established during the course of this work. A following outlook shall present some promising prospective ideas.

5.1 Summary

A general outlook of the temperature dependent behaviour of the OH and OD stretch band of pure H_2O and D_2O is given in **section 4.1**. The temperature range from 233 K to 353 K is covered and it is described why and how intensities of stretching or bending vibrations decrease or increase respectively with rising temperatures. Similarities and differences are discussed as well as the different physical nature due to the different isotopes.

In **section 4.2** positions of the symmetric and the asymmetric stretching vibration in the IR spectrum were suggested. With the help of pure H_2O and D_2O measurements in combination with isotopic substitution experiments a new interpretation was developed. The spectra in the temperature range from 303 K to 333 K were simultaneously decomposed into six contributions. The experiments dealing with isotopic substitution delivered a single band shaped OH peak at $3410\,\mathrm{cm}^{-1}$ for a small amount of H_2O in D_2O and a single band shaped OD peak for a small amount of D_2O in H_2O at $2504\,\mathrm{cm}^{-1}$. In the pure liquid symmetric and asymmetric stretch are coupled while they are not in an isotopic mixture containing HDO. This leads to the conclusion that contributions four and five at $3362\,\mathrm{cm}^{-1}$ and $3495\,\mathrm{cm}^{-1}$ for H_2O and $2473\,\mathrm{cm}^{-1}$ and $2594\,\mathrm{cm}^{-1}$ for D_2O embrace the peaks at $3410\,\mathrm{cm}^{-1}$ and $2504\,\mathrm{cm}^{-1}$ and can be assigned to the symmetric and asymmetric stretch vibrations of the water molecule.

This was supported by the size of the gaps which can be found between contributions four and five. They are significantly larger for D_2O as one would expect from studies of water dissolved in ionic liquids.

In **section 4.3** again with the help of several isotopic mixtures of H_2O and D_2O, a new approach was made to identify the position of the first overtone of the bending vibration of H_2O. In a 50:50 mixture of H_2O and D_2O a feature is identified on the lower edge of the OH stretch band in that region where you would expect the first overtone to be positioned. It is decomposed to determine intensity and the exact wavenumber position.

The relation between bending motion and first overtone in the mixture is consequently applied to the spectral features of the spectrum of pure H_2O. While for the mixture the position was $2959\,\mathrm{cm}^{-1}$, applying the ratios onto the pure H_2O spectrum leads to a position of the first overtone at $3364\,\mathrm{cm}^{-1}$ making up roughly 2.4 % of the overall intensity of the OH stretch band.

The existence of quasi free OH groups was thoroughly examined in **section 4.4**. Difference spectra were calculated by subtracting a pure water spectrum from a spectrum of any salt solutions at similar experimental conditions. In these difference spectra a single negative contribution at $3654\,\mathrm{cm}^{-1}$ was found for all solutions of alkaline halide salts and attributed to quasi free OH groups in the bulk phase. Quasi free, because they are still influenced by the surrounding water although they are not hydrogen bonded to another water molecule. It may not be mistaken with the dangling OH groups which are observed in interfacial studies at $3700\,\mathrm{cm}^{-1}$. The experimental setup used in this work is not sensitive to interfacial phenomena.

It is a negative contribution and therefore represents a contribution which is being reduced due to the presence of the dissolved salt, i.e. it is less concentrated in a salt solution than in pure water. The very high wavenumber allows no other conclusion but attributing it to quasi free OH groups. Doubts whether or not the isosbestic point separating the positive and negative contribution may not be a real one could be erased since it is a constant non shifting contribution. In the case of all alkali salts in combination with chloride, bromide and iodide there is a positive contribution next to the negative quasi free OH group contribution. Intermingling of positive and negative contributions can be a problem. Fortunately with the fluorine salts there is a negative contribution next to the quasi free OH group contribution, which remains clearly visible as a distinct feature. Any intermingling of positive and negative bands can be ruled out in this case.

Further support comes from molecular dynamics simulations. The water-water site-site radial distribution function $g_{OO}(r)$ is calculated and an outward shift of the second peak can be observed from NaCl to CsCl. The second peak is generally regarded as the signature of the tetrahedral bonding in water. The hydrogen bonded network is strengthened with increasing size and lower charge density of the cation. This can only lead to the one explanation that quasi free OH groups are reduced in favour of more water molecules

bonded in a tetrahedral fashion.

The ionic dependencies and differences between anionic and cationic behaviour are described in **section 4.5**. Besides the quasi free OH group two additional features can be observed in the difference spectra. A large negative and a large positive peak, again for all alkali halides but also for magnesium and calcium in combination with halides. The large positive contribution is attributed to the interaction between anion and OH group directly via the hydrogen. The negative peak represents the reduction of the strength of the pure hydrogen bonded network. The wavenumber of the anionic peak shows a distinct behaviour when the cation remains the same and the anion is changed. The peak moves from lower to higher wavenumbers in order of F^-, Cl^-, Br^- and I^-. So does the hydrogen bonded network peak, but the change is less pronounced.

Looking at the peaks when the cation changes and the anion remains the same, reveals that in fact the influence of the cation is minor, but only for the position of the peaks and the intensity of the positive peak attributed to the anion-water interaction. What is affected significantly is the reduction of hydrogen bonded water network. The reduction is biggest for Cs^+, Rb^+, K^+ and then becomes less and less going to Na^+, Li^+ and then becoming even positive for Ca^{2+} and Mg^{2+}, meaning an enforcement not a reduction of the hydrogen bonded network.

The results in **section 4.6** are divided in two parts. Firstly HOFMEISTER effects are discussed cationic dependent with chloride as constant anion and secondly anionic dependent with the sodium series.

The cationic dependency is mainly found in the above described behaviour of the hydrogen bonded network peak and its intensity. A similarity can be observed to the order of the cationic HOFMEISTER series. The network peak of the Cs^+, Rb^+ and K^+ solutions show very similar behaviour, all having an equally strong reduction of the intensity of the network, these cations are by definition chaotropes. Following the series the reduction becomes less and less with Na^+ and Li^+ solutions until it even becomes positive for Ca^{2+} and Mg^{2+} solutions. These are the kosmotropes, i.e. the structure maker.

Originally the HOFMEISTER series put ions in the order of their ability to increase or decrease the solubility of proteins. HOFMEISTER put up a theory that ions which cause precipitation of proteins interact a lot stronger with the dissolved salts than with the protein. Less water is hence available for the solution of the protein. Salts which do not change or may even increase the solubility interact a lot weaker with water. The spectra recorded for the sodium series and especially the changing concentration of the quasi free OH group support this explanation.

A strong interaction with water would mean a reduction of quasi free OH groups, weak

interactions would not change the concentrations of quasi free OH groups. Ions like SO_4^{2-}, PO_4^{3-} and F^- are known to cause precipitation and a reduction of quasi free OH groups can be observed spectroscopical with these ions. On the other hand ions like SCN^-, NO_3^- or ClO_4^- are known to interact very weakly with water, almost showing hydrophobic characteristics. For these ions no reduction of the quasi free OH groups could be observed. Around these ions, water molecules can even arrange in a tangential manner keeping the water network largely intact causing no change in the concentration of quasi free OH groups.

While carrying out experiments on the aqueous salt solution below 273 K some interesting features were observed and are described in **section 4.7**. The interesting observations were made possible by the single reflection ATR set up used. While the salt solution freezes from the top it was possible to spectroscopical observe the increase of the concentration in the remaining liquid phase, a process called brine rejection, until the moment where the whole drop would be frozen. This increase of concentration very much resembled the outlook of the alkaline halide solution spectra at varying concentrations at ambient conditions. Even the somewhat different behaviour of the fluoride salts compared at different concentrations could be reproduced during the freezing process. An exception is the supercooling of the lithium salt solution. In this case the behaviour at ambient conditions was not observed but a massive reduction of quasi free OH groups is clearly visible in the spectrum. For the NaCl, NaBr and NaI solution the formation of hydrates could be observed.

This freezing process is very similar to what can be observed during the formation of sea ice. In places where ice is formed brine rejection is a major player in causing convection in the oceans. By means of ATR spectroscopy a very good method is available to spectroscopical analyse processes related to the formation of sea ice. This may prove to be useful and practical for marine chemists who are doing research in that area.

5.2 Outlook

A well founded and broad range of experimental data and theories has been established in this work. But the nature of a scientific paper is that it is never a closed file. Questions, aspects and problems still remain regarding this work, which would have surpassed its extent and remain for studies in progress and studies to come.

For both, the pure water and aqueous salt solution experiments, it would be very fruitful to examine the terahertz region to find out more about the hydrogen bonds themselves. The OH stretch is only sensitive to changes in the network of hydrogen bonds, but does not represent the actual hydrogen bond. Experiments can be carried out with THz spec-

troscopy to investigate water network dynamics in aqueous salt solutions. The vibration of the hydrogen bond can be observed directly in the THz region. [6] Additional experiments at similar experimental conditions as used in this work, but in the THz region would be a great benefit for the overall picture.

Regarding the aqueous salt solutions, closing gaps is a very promising plan to obtain a broader understanding and to figure out if the theories developed are applicable on a broader range. Not all combinations of alkaline and earth alkaline cations with the halides have been tested. Salts of some elements may not be feasible to investigate, for example francium as it is radioactive or beryllium which reacts vigorously with water. Salts of barium or even strontium would complete the set of experiments nicely. To use strontium halogens an isotope separation would have to be carried out, as only a few isotopes of strontium are stable and not radioactive. This makes it rather unsuitable for experiments, although experiments on strontium chloride in aqueous solution are known from literature. [17]

Experimental conditions are another aspect of this work which leave a lot of room for more experiments. The maximum concentration used in this work was 4 M, but some salts show tremendously high values of molar concentration. LiCl for example, has a molar solubility of 20 mol/l and it would not be uninteresting to see how the concentration of the quasi free OH groups behaves or how peak positions shift at that concentration level.

Taking a look at differently charged cations of the same element, e.g. Fe, in combination with any halide (e.g. $FeCl_2$/$FeCl_3$), would certainly be worth an investigation. To carry out experiments on mixtures of salts would also be an interesting task. Especially the fluoride salts in combination with another halide should be focused on in that respect. The fluoride and chloride ions interact at different wavenumbers with the OH stretch. The question is whether or not an annihilation of opposing effects could be observed.

It should be noted that the anion dependent Hofmeister series was only investigated for the sodium salts. A more complete examination with potassium and rubidium is mandatory to further test and hopefully support the results obtained in this work.

It also may not be forgotten that the Hofmeister series originally dealt with the solubility of proteins. From simple aqueous salt solutions only an understanding of the influence of ions on water can be achieved. Small organic compounds, e.g. acetamides, need to be added to the solutions in future studies to advance in this field of the behaviour of biomolecules in the presence of ions in an aqueous solution.

For the hydrate formation experiments only solutions of sodium halides and alkaline chloride salts were examined by ATR spectroscopy. As mentioned above, a more extensive approach with more variations would provide a better foundation and more possibilities

for comparison. It would certainly be worthwhile to analyse the freezing behaviour of potassium halides and alkaline or earth alkaline bromides for example.

Bibliography

[1] P. Ball. Water as an Active Constituent in Cell Biology. *Chem. Rev.*, 108:74–108, 2008.

[2] H. J. Bakker. Structural Dynamics of Aqueous Salt Solutions. *Chem. Rev.*, 109:1456–1473, 2008.

[3] Y. Marcus. Effect of Ions on the Structure of Water: Structure Making and Breaking. *Chem. Rev.*, 109:1346–1370, 2009.

[4] H. J. Bakker and J. L. Skinner. Vibrational Spectroscopy as a Probe of Structure and Dynamics in Liquid Water. *Chem. Rev.*, 110:1498–1517, 2010.

[5] R. Ludwig and D. Paschek. Wasser: Anomalien und Rätsel. *Chem. Unserer Zeit*, 39:164–175, 2005.

[6] D. A. Schmidt, Ö. Birer, S. Funkner, B. P. Born, R. Gnanasekaran, G. S. Schwaab, D. M. Leitner, and M. A. Havenith. Rattling in the Cage: Ions as Probes of Sub-picosecond Water Network Dynamics. *J. Am. Chem. Soc.*, 131:18512–18517, 2009.

[7] J. Skinner. Following the Motions of Water Molecules in Aqueous Solutions. *Science*, 328:985–986, 2010.

[8] B. Auer and J. L. Skinner. Dynamical effects in line shapes for coupled chromophores: Time-averaging approximation. *J. Chem. Phys.*, 127:104105, 2007.

[9] A. W. Omta, M. F. Kropman, S. Woutersen, and H. J. Bakker. Negligible Effect of Ions on the Hydrogen-Bond Structure in Liquid Water. *Science*, 301:347–349, 2003.

[10] K. J. Tielrooij, R. L. A. Timmer, H. J. Bakker, and M. Bonn. Structure Dynamics of the Proton in Liquid Water Probed with Terahertz Time-Domain Spectroscopy. *Phys. Rev. Lett.*, 102:198303, 2009.

[11] M. Heyden, J. Sun, S. Funkner, G. Mathias, H. Forbert, M. Havenith, and D. Marx. Dissecting the THz spectrum of liquid water from first principles via correlations in time and space. *Proc. Natl. Acad. Sci. USA*, 107:12068–12073, 2010.

[12] A. K. Soper. The quest for the structure of water and aqueous solutions. *J. Phys.: Condens. Matter*, 9:2717–2730, 1997.

[13] D. A. Schmidt and K. Miki. Structural Correlations in Liquid Water: A New Interpretation of IR Spectroscopy. *J. Phys. Chem. A*, 111:10119–10122, 2007.

[14] K. D. Collins, G.W. Neilson, and J. E. Enderby. Ions in water: Characterizing the forces that control chemical processes and biological structure. *Biophys. Chem.*, 128:95–104, 2007.

[15] M. C. Gurau, S-M. Lim, E. T. Castellana, F. Albertorio, S. Kataoka, and P. S. Cremer. On the Mechanism of the Hofmeister Effect. *J. Am. Chem. Soc.*, 126:10522–10523, 2004.

[16] L. Vrbka and P. Jungwirth. Brine Rejection from Freezing Salt Solutions: A Molecular Dynamics Study. *Phys. Rev. Lett.*, 95:148501, 2005.

[17] A. V. Rossi, C. U. Davanzo, and M. Tubino. The Structure of Liquid Water in Aqueous Solutions: A Proposed Model From Near and Mid Infrared Spectroscopy. *J. Braz. Chem. Soc.*, 7:403–410, 1996.

[18] J. Riemenschneider, J. Holzmann, and R. Ludwig. Salt Effects on the Structure of Water Probed by Attenuated Total Reflection Infrared Spectroscopy and Molecular Dynamics Simulations. *ChemPhysChem*, 9:2731–2736, 2008.

[19] B. M. Auer and J. L. Skinner. Water: Hydrogen bonding and vibrational spectroscopy, in the bulk liquid and at the liquid/vapor interface. *Chem. Phys. Lett*, 470:13–20, 2009.

[20] Martin Chaplin. Water absorption spectrum. http://www.lsbu.ac.uk/water/vibrat.html, 20.06.2011. 15.25h.

[21] D. Eisenberg and W. Kauzmann. *The structure and properties of water*. Oxford University Press, London, 1969.

[22] J. Grdadolnik. ATR-FTIR SPECTROSCOPY: ITS ADVANTAGES AND LIMITATIONS. *Acta Chim. Slov.*, 49:631–642, 2002.

[23] J.-J. Max and C. Chapados. Isotope effects in liquid water by infrared spectroscopy. IV. No free OH groups in liquid water. *J. Chem. Phys.*, 133:164509, 2010.

[24] S. Gopalakrishnan, D. Liu, H.C. Allen, M. Kuo, and M. J. Shultz. Vibrational Spectroscopic Studies of Aqueous Interfaces: Salts, Acids, Bases and Nanodrops. *Chem. Rev.*, 106:1155–1175, 2006.

[25] S. M. Pershin, A. F. Bunkin, V. A. Lukyanchenko, and R. R. Nigmatullin. Detection of the OH band fine structure in liquid water by means of new treatment procedure based on the statistics of the fractional moments. *Laser Phys. Lett.*, 4:809–813, 2007.

[26] S. Gopalakrishnan, P. Jungwirth, D. J. Tobias, and H.C. Allen. Air-Liquid Interfaces of Aqueous Solutions Containing Ammonium and Sulfate: Spectroscopic and Molecular Dynamics Studies. *J. Phys. Chem. B*, 109:8861–8872, 2005.

[27] J. D. Smith, C. D. Cappa, K. R. Wilson, R. C. Cohen, P. L. Geissler, and R. J. Saykally. Energetics Of Hydrogen Bond Network Rearrangements in Liquid Water. *Science*, 306:851–853, 2004.

[28] F. H. Stillinger. Water Revisited. *Science*, 209:451–457, 1980.

[29] J. D. Smith, C. D. Cappa, K. R. Wilson, R. C. Cohen, P. L. Geissler, and R. J. Saykally. Unified description of temperature-dependent hydrogen-bond rearrangements in liquid water. *Proc. Natl. Acad. Sci. USA*, 102:14171–14174, 2005.

[30] A. Luzar. Resolving the hydrogen bond dynamics conundrum. *J. Chem. Phys.*, 113:10663–10675, 2000.

[31] J.-B. Brubach, A. Mermet, A. Filabozzi, A. Gerschel, and P. Roy. Signatures of the hydrogen bonding in the infrared bands of water. *J. Chem. Phys.*, 122:184509, 2005.

[32] R. Ludwig. The Importance of Tetrahedrally Coordinated Molecules for the Explanation of Liquid Water Properties. *ChemPhysChem*, 8:938–943, 2007.

[33] J. Schiffer and D. F. Hornig. Vibrational Dynamics in Liquid Water: A New Interpretation of the Infrared Spectrum of the Liquid. *J. Chem. Phys.*, 49:4150–4160, 1968.

[34] S. Y. Venyaminov and F. G. Prendergast. Water (H_2O and D_2O) Molar Absorbtivity in the $1000 - 4000 cm^{-1}$ Range and Quantitative Infrared Spectroscopy of Aqueous Solutions. *Analytical Biochemistry*, 248:234–245, 1997.

[35] G. E. Walrafen. Raman Spectral Studies of the Effects of Temperature on Water Structure. *J. Chem. Phys.*, 47:114–126, 1967.

[36] Z-F. Wei, Y-H. Zhang, L-J. Zhao, J-H. Liu, and X-H. Li. Observation of the First Hydration Layer of Isolated Cations and Anions through the FTIR-ATR Difference Spectra. *J. Phys. Chem. A*, 109:1337–1342, 2005.

[37] A. Millo, Y. Raichlin, and A. Katzir. Mid-infrared Fiber-optic Attenuated Total Reflection Spectroscopy of the Solid-Liquid Phase Transition of Water. *Appl. Spec.*, 59:460–466, 2005.

[38] W. B. Fischer, A. Fedorowicz, and A. Koll. Structured water around ions-FTIR difference spectroscopy and quantum-mechanical calculations. *Phys. Chem. Chem. Phys.*, 3:4228–4234, 2001.

[39] J. Riemenschneider, A. Wulf, and R. Ludwig. The Effects of Temperature and H/D Isotopic Dilution on the Transmission and Attenuated Total Reflection FTIR Spectra of Water. *Z. Phys. Chem.*, 223:1011–1022, 2009.

[40] K. Ohno, M. Okimura, N. Akai, and Y. Katsumoto. The effect of cooperative hydrogen bonding on the OH stretching-band shift for water clusters studied by matrix-isolation infrared spectroscopy and density functional theory. *Phys. Chem. Chem. Phys.*, 7:3005–3014, 2005.

[41] Y. Raichlin, A. Millo, and A. Katzir. Investigations of the Structure of Water Using Mid-IR Fiberoptic Evanescent Wave Spectroscopy. *Phys. Rev. Lett.*, 93:185703, 2004.

[42] T. Köddermann, F. Schulte, M. Huelsekopf, and R. Ludwig. Formation of Water Clusters in a Hydrophobic Solvent. *Angew. Chem. Int. Ed.*, 42:4904–4908, 2003.

[43] A. Wulf and R. Ludwig. Structure and Dynamics of Water Confined in Dimethyl Sulfoxide. *ChemPhysChem*, 7:226–272, 2006.

[44] INTERNATIONAL UNION OF PURE and APPLIED CHEMISTRY. GLOSSARY OF TERMS USED IN PHOTOCHEMISTRY 3rd EDITION. *Pure Appl. Chem.*, 79:p. 359, 2007.

[45] P. L. Geissler. Temperature Dependence of Inhomogeneous Broadening: On the Meaning of Isosbestic Points. *J. Am. Chem. Soc.*, 127:14930–14935, 2005.

[46] R. C. Dougherty and L. N. Howard. Equilibrium structural model of liquid water: Evidence from heat capacity, spectra, density, and other properties. *J. Chem. Phys.*, 109:7379–7393, 1998.

[47] Y. Maréchal. Infrared spectra of water.I. Effect of temperature and of H/D isotopic dilution. *J. Chem. Phys.*, 95:5565–5573, 1991.

[48] W. C. Röntgen. Ueber die Constitution des flüssigen Wassers. *Ann. Phys.*, 281:91–97, 1892.

[49] F. Rull. Structural investigation of water and aqueous solutions by Raman spectroscopy. *Pure Appl. Chem.*, 74:1859–1870, 2002.

[50] H. E. Stanley and J. Teixeira. Interpretation of the unusual behavior of H_2O and D_2O at low temperatures: Tests of a percolation model. *J. Chem. Phys.*, 73:3404–3422, 1980.

[51] R. Ludwig. Water: From Clusters to the Bulk. *Angew. Chem. Int. Ed.*, 40:1808–1827, 2001.

[52] G. E. Walrafen, M. S. Hokmabadi, and W.-H. Yang. Raman isosbestic points from liquid water. *J. Chem. Phys.*, 85:6964–6969, 1986.

[53] N. A. Chumaevskii and M. N. Rodnikova. Some peculiarities of liquid water structure. *J. Mol. Liq.*, 106:167–177, 2003.

[54] M. Klose and J. I. Naberuchin. *Wasser - Struktur und Dynamik.* Akademie-Verlag Berlin, GDR, 1986.

[55] B. M. Auer and J. L. Skinner. IR and Raman spectra of liquid water: Theory and interpretation. *J. Chem. Phys.*, 128:224511, 2008.

[56] P. Larouche, J.-J. Max, and C. Chapados. Isotope effects in liquid water by infrared spectroscopy. II. Factor analysis of the temperature effect on H_2O and D_2O. *J. Chem. Phys.*, 129:064503, 2008.

[57] B. Hribar, N. T. Southall, V. Vlachy, and K. A. Dill. How Ions Affect the Structure of Water. *J. Am. Chem. Soc.*, 124:12302–12311, 2002.

[58] W. Mikenda. Stretching frequency versus bond distance correlation of O-D(H)...Y (Y = N, O, S, Se, Cl, Br, I) hydrogen bonds in solid hydrates. *J. Mol. Structure*, 147:1–15, 1986.

[59] R. C. Weast (ed.). *Handbook of Chemistry and Physics.* CRC Press, Inc., 1982.

[60] C. D. Cappa, J. D. Smith, K. R. Wilson, B. M. Messer, M. K. Gilles, R. C. Cohen, and R. J. Saykally. Effects of Alkali Metal Halide Salts on the Hydrogen Bond Network of Liquid Water. *J. Phys. Chem. B*, 109:7046–7052, 2005.

[61] A. K. Soper, G. W. Neilson, J. E. Enderby, and R. A. Howe. A neutron diffraction study of hydration effects in aqueous solutions. *J. Phys. C.: Solid State Phys.*, 10:1793–1801, 1977.

[62] J. Holzmann, R. Ludwig, A. Geiger, and D. Paschek. Pressure and Salt Effects: Two Sides of the Same Coin? *Angew. Chem. Int. Ed.*, 46:8907–8911, 2007.

[63] K. D. Collins. Charge Density-Dependent Strength of Hydration and Biological Structure. *Biophys J.*, 72:65–76, 1997.

[64] F. Hofmeister. Zur Lehre von der Wirkung der Salze. Zweite Mittheilung. Ueber Regelmässigkeiten in der eiweissfällenden Wirkung der Salze und ihre Beziehung zum physiologischen Verhalten derselben. *Arch. Exp. Pathol. Pharmakol.*, 24:247–260, 1888.

[65] R. L. Baldwin. How Hofmeister Ion Interactions Affect Protein Stability. *Biophys. J.*, 71:2056–2063, 1996.

[66] K. D. Collins. Ions from the Hofmeister series and osmolytes: effects on proteins in solution and in crystallization process. *Methods*, 34:300–311, 2004.

[67] K. D. Collins and M. W. Washabaugh. The Hofmeister effect and the behaviour of water at interfaces. *Q. Rev. Biophys.*, 18:323–422, 1985.

[68] W. Kunz, P. L. Nostro, and B. W. Ninham. The present state of affairs with Hofmeister effects. *Curr. Opin. Colloid Interface Sci.*, 9:1–18, 2004.

[69] Y. Zhang and P. S. Cremer. Interactions between macromolecules and ions: the Hofmeister series. *Curr. Opp. in Chem. Biol.*, 10:658663, 2006.

[70] J. Holzmann. *Molekulardynamische Simulationen von Wasser und wäßrigen Salzlösungen*. Dissertation, Universität Rostock, 2010.

[71] Wright M. R. *An introduction to aqueous electrolyte solutions*. Wiley, England, 2007.

[72] M. G. Cacace, E. M. Landau, and J. J. Ramsden. The Hofmeister series: salt and solvent effects on interfacial phenomena. *Q. Rev. Biophys.*, 30:241–277, 1997.

[73] G. Jones and M. Dole. The viscosity of aqueous solutions of strong electrolytes with special reference to barium chloride. *J. Am. Chem. Soc.*, 51:2950–2964, 1929.

[74] G. Kelbg. Hans Falkenhagen und die Entwicklung der Elektrolyttheorie. *Wissenschaftliche Zeitschrift der Universität Rostock*, 35:319–323, 1965.

[75] R. A. Robinson and R. H. Stokes. *Electrolyte Solutions.* Butterworth Scientific Publications: London, 1959.

[76] K. Hamaguchi and E. P. Geiduschek. The Effect of Electrolytes on the Stability of the Deoxyribonucleate Helix. *J. Am. Chem. Soc.*, 84:1329–1338, 1962.

[77] F. Franks. *Water.* Royal Society of Chemistry, London, 1983.

[78] R. Mancinelli, A. Botti, F. Bruni, M. A. Ricci, and A. K. Soper. Hydration of Sodium, Potassium, and Chloride Ions in Solution and the Concept of Structure Maker/Breaker. *J. Phys. Chem. B*, 111:13570–13577, 2007.

[79] R. Mancinelli, A. Botti, F. Bruni, M. A. Ricci, and A. K. Soper. Perturbation of water structure due to monovalent ions in solution. *Phys. Chem. Chem. Phys.*, 9:2959–2967, 2007.

[80] A. W. Omta, M. F. Kropman, S. Woutersen, and H. J. Bakker. Influence of ions on the hydrogen-bond structure in liquid water. *J. Chem. Phys.*, 119:12457–12461, 2003.

[81] R. Leberman and A. K. Soper. Effect of high salt concentrations on water structure. *Nature*, 378:364–366, 1995.

[82] J. D. Smith, R. J. Saykally, and P. L. Geissler. The Effects of Dissolved Halide Anions on Hydrogen Bonding in Liquid Water. *J. Am. Chem. Soc.*, 129:13847–13856, 2007.

[83] M. F. Kropman and H. J. Bakker. Dynamics of Water Molecules in Aqueous Solvation Shells. *Science*, 291:2118–2120, 2001.

[84] S. R. Dillon and R. C. Dougherty. Raman Studies of the Solution Structure of Univalent Electrolytes in Water. *J. Phys. Chem.A.*, 106:7647–7650, 2002.

[85] R. C. Dougherty. Density of Salt Solutions: Effect of Ions on the Apparent Density of Water. *J. Phys. Chem. B.*, 105:4514–4519, 2001.

[86] J. D. Lee. *Concise Inorganic Chemistry, 5th Edition.* Chapmann and Hall, 1996.

[87] P. W. Atkins and J. A. Beran. *Chemie: einfach alles*. VCH Weinheim, 1996.

[88] G. Birnbaum. *Reports on Polar Research - Numerical modelling of the interaction between atmosphere and sea ice in the Arctic marginal ice zone*. Alfred Wegener Institute for Polar and Marine Research, 1998.

[89] F. Cottier, H. Eicken, and P. Wadhams. Linkages between salinity and brine channel distribution in young sea ice. *J. Geophys. Res.*, 104:15859–15871, 1999.

[90] S. Klotz, L. E. Bove, T. Strässle, T. C. Hansen, and A. M. Saitta. The preparation and structure of salty ice VII under pressure. *Nature Materials*, 8:405–409, 2009.

[91] G. N. I. Clark, G. L. Hura, J. Teixeira, A. K. Soper, and T. Head-Gordon. Small-angle scattering and th structure of ambient liquid water. *Proc. Natl. Acad. Sci. USA.*, 107:14003–14007, 2010.

[92] A. Musinu, G. Paschina, and G. Piccaluga. On the structure of the NH_4^+ ion in aqueous solution. *Chem. Phys. Lett.*, 80:163–167, 1981.

[93] C. Rønne, P.-O. Åstrand, and S. R. Keiding. THz Spectroscopy of Liquid H_2O and D_2O. *Phys. Rev. Lett.*, 82:2888–2891, 1999.

[94] W. Wachter, W. Kunz, R. Buchner, and G. Hefter. Is There an Anionic Hofmeister Effect on Water Dynamics? Dielectric Spectroscopy of Aqueous Solutions of NaBr, NaI, $NaNO_3$, $NaClO_4$ and NaSCN. *J. Phys. Chem. A*, 109:8675–8683, 2005.

[95] E. H. Hardy, A. Zygar, M. D. Zeidler, M. Holz, and F. D. Sacher. Isotope effect on the translational and rotational motion in liquid water and ammonia. *J. Chem. Phys.*, 114:3174–3181, 2001.

[96] H. Ohtaki and T Radnai. Structure and Dynamics of Hydrated Ions. *Chem. Rev.*, 93:1157–1204, 1993.

[97] P. Wernet, D. Nordlund, U. Bergmann, M. Cavalleri, M. Odelius, H. Ogasawara, L. Å. Näslund, T. K. Hirsch, L. Ojamäe, P. Glatzel, L. G. M. Petterson, and A. Nilsson. The Structure of the First Coordination Shell in Liquid Water. *Science*, 304:995–999, 2004.

[98] A. P. Lyubartsev, K. Lassonen, and A. Laaksonen. Hydration of Li^+ ion. An ab initio molecular dynamics simulation. *J. Chem. Phys.*, 114:3120–3126, 2001.

[99] H. Günzler and H.-U. Gremlich. *IR Spectroscopy - An Introduction*. Wiley-VCH Verlag GmbH, Weinheim, 2002.

[100] P. R. Griffiths and J. A. de Hasseth. *Fourier Transform Infrared Spectroscopy*. Wiley-Interscience, Hoboken New Jersey, 2007.

[101] T. Butz. *Fouriertransformation für Fußgänger*. B.G. Teubner Stuttgart Leipzig, 1998.

[102] J. Fahrenfort. Attentuated total reflection: a new principle for the production of useful infra-red reflection spectra of organic compounds. *Spectrochim. Acta*, 17:698–709, 1961.

[103] T. Wizenmann. Ein tiefer Blick ins Glas. *Nachr. Chem.*, 7/8:792–793, 2010.

[104] Specac. MKII Golden Gate^{TM} Single Reflection ATR System. *User Manual*, Issue 10, 2001.

[105] TeraView. TPS spectra 3000 User's Guide. 001-0005, Rev 2, D, 2009.

[106] J.-J. Max and C. Chapados. IR spectroscopy of aqueous alkali halide solutions: Pure salt-solvated water spectra and hydration numbers. *J. Chem. Phys.*, 115:2664–2675, 2001.

[107] M. Hancer, R. P. Sperline, and J. D. Miller. Anomalous Dispersion Effects in the IR-ATR Spectroscopy of Water. *Appl. Spec.*, 54:138–143, 2000.

[108] D. A. Schmidt and K. Miki. Defective Continuous Hydrogen-Bond Networks: An Alternative Interpretation of IR Spectroscopy. *ChemPhysChem*, 9:1914–1919, 2008.

[109] F. Al-Sagheer and M. J. Hey. Hofmeister anion effects on aqueous solutions of poly(ethylene oxide) studied by attenuated total reflectance FT-IR spectroscopy. *Colloids and Surfaces A: Physicochem. Eng. Aspects*, 245:99–103, 2004.

[110] Bruker. *OPUS Referenzhandbuch, Version 6*. Bruker Optik GmbH, 2006.

[111] N. J. Harrick. *Internal Reflection Spectroscopy*. Wiley, New York, 1967.

[112] J.-J. Max, V. Gessinger, C. van Driessche, P. Larouche, and C. Chapados. Infrared spectroscopy of aqueous ionic salt solutions at low concentrations. *J. Chem. Phys.*, 126:184507, 2007.

[113] M. Sovago, R. K. Campen, G. W. H. Wurpel, M. Müller, H. J. Bakker, and M. Bonn. Vibrational Response of Hydrogen-Bonded Interfacial Water is Dominated by Intramolecular Coupling. *Phys. Rev. Lett.*, 100:173901, 2008.

[114] M. Huelsekopf. *Experimentelle und theoretische Untersuchungen der Flüssigkeitsstruktur verzweigeter Alkohole.* Dissertation, Universität Dortmund, 2002.

[115] W. H. Press, S. A. Teukolsky, W. T. Vetterling, and B. P. Flannery. *Numerical Recipes in FORTRAN: the art of scientific computing.* Cambridge University Press, 1994.

[116] W. H. Press, S. A. Teukolsky, W. T. Vetterling, and B. P. Flannery. *Numerical Recipes in C.* Cambridge University Press, 1992.

[117] D. W. Marquardt. An Algorithm for Least Squares Estimation of Nonlinear Parameters. *J. Soc. Ind. App. Math.*, 11:431–441, 1968.

[118] F. Schulte. *Theoretische und Experimentelle Untersuchungen zur Struktur von Wasser in unterschiedlichen Lösungsmitteln.* Dissertation, Universität Dortmund, 2006.

[119] M. J. D. Low and R. T. Yang. Infrared Spectra of Water in Aqueous Solutions Using Internal Reflection Spectroscopy. *Spec. Lett.*, 6:299–303, 1973.

[120] P. A. Giguère and M. Pigeon-Gosselin. The Nature of the 'Free' OH Groups in Water. *J. Ram. Spec.*, 17:341–344, 1986.

[121] F. O. Libnau, O. M. Kvalheim, A. A. Christy, and J. Toft. Spectra of Water in the near- and mid-infrared region. *Vib. Spec.*, 7:243–254, 1994.

[122] J. J. Loparo, S. T. Roberts, R. A. Nicodemus, and A. Tokmakoff. Variation of the transition dipole moment across the OH stretching band of water. *Chem. Phys.*, 341:218–229, 2007.

[123] S. McQueen-Mason and D. J. Cosgrove. Disruption of hydrogen bonding between plant cell wall polymers by proteins that induce wall extension. *Proc. Nati. Acad. Sci. USA*, 91:6574–6578, 1994.

[124] A. Wulf, T. Köddermann, C. Wertz, A. Heintz, and R. Ludwig. Water vibrational bands as a polarity parameter in ionic liquid. *Z. Phys. Chem.*, 220:1361–1376, 2006.

[125] G. E. Walrafen. Raman Spectral Studies of the Effects of Temperature on Water and Electrolyte Solutions. *J. Chem. Phys.*, 44:1546–1558, 1966.

[126] V. Buch and J. P. Devlin. A new interpretation of the OH-stretch spectrum of ice. *J. Chem. Phys.*, 110:3437–3443, 1999.

[127] J.-J. Max and C. Chapados. Isotope effects in liquid water by infrared spectroscopy. *J. Chem. Phys.*, 116:4626–4642, 2002.

[128] J.-J. Max and C. Chapados. Isotope effects in liquid water by infrared spectroscopy. III. H_2O and D_2O spectra from 6000 to 0 cm^{-1}. *J. Chem. Phys.*, 131:184505, 2009.

[129] W. A. P. Luck and W. Ditter. Band overlapping and water structure. *J. Mol. Structure*, 1:339–348, 1967-1968.

[130] G. W. Robinson, C. H. Cho, and J. Urquidi. Isosbestic points in liquid water: Further strong evidence for the two-state mixture model. *J. Chem. Phys.*, 111:698–702, 1999.

[131] J. D. Eaves, J. J. Loparo, C. J. Fecko, S. T. Roberts, A. Tokmakoff, and P. L. Geissler. Hydrogen bonds in liquid water are broken only fleetingly. *Proc. Natl. Acad. Sci. USA*, 102:13019–13022, 2005.

[132] P. A. Giguère. Bifurcated hydrogen bonds in water. *J. Ram. Spec.*, 15:354–359, 1984.

[133] F. Sciortino, A. Geiger, and H. E. Stanley. Effect of defects on molecular mobility in liquid water. *Nature*, 354:218–221, 1991.

[134] Y. Chen, Y.-H. Zhang, and L.-J. Zhao. ATR-FTIR spectroscopic studies in aqueous $LiClO_4$, $NaClO_4$ and $Mg(ClO_4)_2$. *Phys. Chem. Chem. Phys.*, 6:537–542, 2004.

[135] J.-J. Max and C. Chapados. Infrared spectroscopy of methanol-hexane liquid mixtures. I. Free OH present in minute quantities. *J. Chem. Phys.*, 128:224512, 2008.

[136] J. Riemenschneider and R. Ludwig. Comment on "Isotope effects in liquid water by infrared spectroscopy. IV. No free OH groups in liquid water". *J. Chem. Phys.*, accepted, 2011.

[137] Y. Marcus. Ionic Radii in Aqueous Solutions. *Chem. Rev.*, 88:1475–1498, 1988.

[138] Y. Iwadate, K. Kawamura, K. Igarashi, and J. Mochinaga. Effective Ionic Radii of NO_2^- and SCN^- Estimated in Terms of the Böttcher Equation and the Lorentz-Lorenz Equation. *J. Phys. Chem.*, 86:5205–5208, 1982.

[139] T. Muto, S. Takeshita, T. Isobe, T. Sawayama, and S. Niikura. Photobleaching properties of YVO_4:Eu^{3+} Nanophosphors Synthesized by Hydrothermal Treatment. *ECS Transactions*, 16:135–140, 2009.

[140] Y. Koga, H. Katayanagi, J. V. Davies, and H. Kato. The Effects of Chloride Salts of Some Cations on the Molecular Organization of H_2O. Towards Understanding the Hofmeister Series. II. *Bull. Chem. Soc. Jpn.*, 79:1347–1354, 2006.

[141] C. D. Cappa, J. D. Smith, B. M. Messer, R. C. Cohen, and R. J. Saykally. Effects of Cations on the Hydrogen Bond Network of Liquid Water: New Results from X-ray Absorption Spectroscopy of Liquid Microjets. *J. Phys. Chem. B*, 110:5301–5309, 2006.

[142] Y. Marcus. Viscosity B-Coefficients, Structural Entropies and Heat Capacities, and the Effects of Ions on the Structure of Water. *J. Sol. Chem.*, 23:831–848, 1994.

[143] E. Riedel. *Anorganische Chemie.* de Gruyter Berlin, 2004.

[144] R. Zangi, M. Hagen, and B. J. Berne. Effect of Ions on the Hydrophobic Interaction between Two Plates. *J. Am. Chem. Soc.*, 129:4678–4686, 2007.

[145] A. Geiger, A. Rahman, and F. H. Stillinger. Molecular dynamics study of the hydration of Lennard-Jones solutes. *J. Chem. Phys.*, 70:263–276, 1979.

[146] G. V. Bondarenko and Y. E. Gorbaty. Hydrogen bonding in aqueous solutions of $NaClO_4^-$. *Molecular Physics*, 109:783–788, 2011.

[147] G. E. Walrafen. Raman Spectral Studies of the Effects of Perchlorate Ion on Water Structure. *J. Chem. Phys.*, 52:4176–4198, 1970.

[148] G. R. Desiraju and T. Steiner. *The weak hydrogen bond: in structural chemistry and biology.* Oxford University Press, 2001.

[149] P. W. Schultz, G. E. Leroi, and A. I. Popov. Solvation of SCN^- and $SeCN^-$ Anions in Hydrogen-Bonding Solvents. *J. Am. Chem. Soc.*, 118:10617–10625, 1996.

[150] P. E. Mason, G. W. Neilson, C. E. Dempsey, A. C. Barnes, and J. M. Cruickshank. The hydration structure of guanidinium and thiocyanate ions: Implications for protein stability in aqueous solution. *Proc. Natl. Acad. Sci. USA*, 100:4557–4561, 2003.

[151] C. C. Pye and M. R. Michels. An ab Initio Investigation of Hydrogen Phosphate Ion Hydration. *Can. J. Anal. Sci. Spec.*, 49:175–184, 2004.

[152] V. N. Afanas'ev and E. Y. Tyunina. Structural Features of Ion Hydration in Sodium Nitrate and Thiosulfate. *Russ. J. Gen. Chem.*, 74:673–678, 2004.

[153] E. Sedlák, L. Stagg, and P. Wittung-Stafshede. Effect of Hofmeister ions on protein thermal stability: Roles of ion hydration and peptide groups? *Archives of Biochemistry and Biophysics*, 479:69–73, 2008.

[154] G. Wedler. *Lehrbuch der Physikalischen Chemie*. Wiley-VCH, 2004.

[155] A. Conti. Floating Ice. *Water Encyclopedia*, pages 69–70, 2005.

[156] S. Bauerecker, P. Ulbig, V. Buch, L. Vrbka, and P. Jungwirth. Monitoring Ice Nucleation in Pure and Salty Water via High-Speed Imaging and Computer Simulations. *J. Phys. Chem. C*, 112:76317636, 2008.

[157] T. Koop, B. Luo, A. Tsias, and T. Peter. Water activity as the determinant for homogeneous ice nucleation in aqueous solutions. *Nature*, 406:611–614, 2000.

[158] Wiley VCH. *Ullmann's Agrochemicals, Volume 1*. Wiley VCH, 2007.

[159] T. A. Ford and M. Falk. IR Study of Hydrogen Bonding in Sodium Chloride Dihydrate. *J. Mol. Structure*, 3:445–452, 1969.

[160] J. Schiffer and D. F. Hornig. On a Reported New Form of Ice. *J. Chem. Phys.*, 35:1136–1137, 1961.

[161] G. Brink and L. Glasser. Studies in Hydrogen Bonding: Modeling of Water in Crystalline Hydrates. *J. Phys. Chem.*, 94:981–984, 1990.

[162] J. Pátek and J. Klomfar. Solid-liquid phase equilibrium in the systems of LiBr-H_2O and LiCl-H_2O. *Fluid Phase Equilib.*, 250:138–149, 2006.

[163] K. Winkel, M. Seidl, T. Loerting, L. E. Bove, S. Imberti, V. Molinero, F. Bruni, R. Mancinelli, and M. A. Ricci. Structural study of low concentration LiCl aqueous solutions in the liquid, supercooled, and hyperquenched glassy states. *J. Chem. Phys.*, 134:024515, 2011.

[164] Institut für Arbeitssicherheit der Deutschen Gesetzlichen Unfallversicherung. GESTIS-Stoffdatenbank. http://biade.itrust.de, 22.06.2011. 10.30h.

[165] INTERNATIONAL UNION OF PURE and APPLIED CHEMISTRY. Iupac periodic table of the elements. http://old.iupac.org/reports/periodic_table/IUPAC_Periodic_Table21Jan11.pdf, 20.06.2011. 15.07h.

Appendix

1 Spectroscopical setup

Advanced	Resolution	$1\,\mathrm{cm}^{-1}$
	Scan time	50 scans
	Data	4200 to $600\,\mathrm{cm}^{-1}$
Optics	Source	Globar MIR
	Aperture setting	3 mm
	Detector	DTGS
	Scanner velocity	6;10.0 KHz
Acquisition	Laser wavenumber	15798
	Interferogram size	31990 points
	Low pass filter	1;10 KHz
	Acquisition mode	Single Sided Fast Return
FT	Phase correction mode	Mertz
	Apodization function	Triangular
	Zero filling factor	2

Table 1: Functional settings of the Vector 22 spectrometer.

2 Physical data of salts

Salt	molar mass	solubility	Salt	molar mass	solubility
	g/mol	g/l		g/mol	g/l
LiF	25.9394	1.3[1,2]	RbF	104.4662	1310
LiCl	42.3940	830	RbCl	120.9208	910
LiBr	86.8450	1770	RbBr	165.3718	1100
LiI	133.8455	1650	RbI	212.3723	1520
NaF	41.9882	40	CsF	151.9039	3700
NaCl	58.4428	360	CsCl	168.3585	1860
NaBr	102.8938	910	CsBr	212.8095	1080
NaI	149.8942	1790	CsI	259.8099	790
NaSCN	81.0722	139			
$NaNO_3$	84.9947	874[2]	MgF_2	62.3018	0.08
$NaClO_4$	122.4404	916[2]	$MgCl_2$	95.2110	542
Na_2SO_4	142.0421	170[2]	$MgBr_2$	184.1130	1020
Na_3PO_4	163.9407	88[2]	MgI_2	278.1139	1480
KF	58.0967	950	CaF_2	78.0748	0.016
KCl	74.5513	347	$CaCl_2$	110.9840	745
KBr	119.0023	670	$CaBr_2$	199.8860	1420
KI	166.0028	1440	CaI_2	293.8869	2090

[1] 25 °C
[2] taken from ref [164]

Table 2: Physical data of investigated salts. Molar Mass from IUPAC [165], density from Handbook of Chemistry and Physics [59], solubilities from Lee [86], unless indicated otherwise.

3 The overtone of the bending vibration of the H_2O molecule

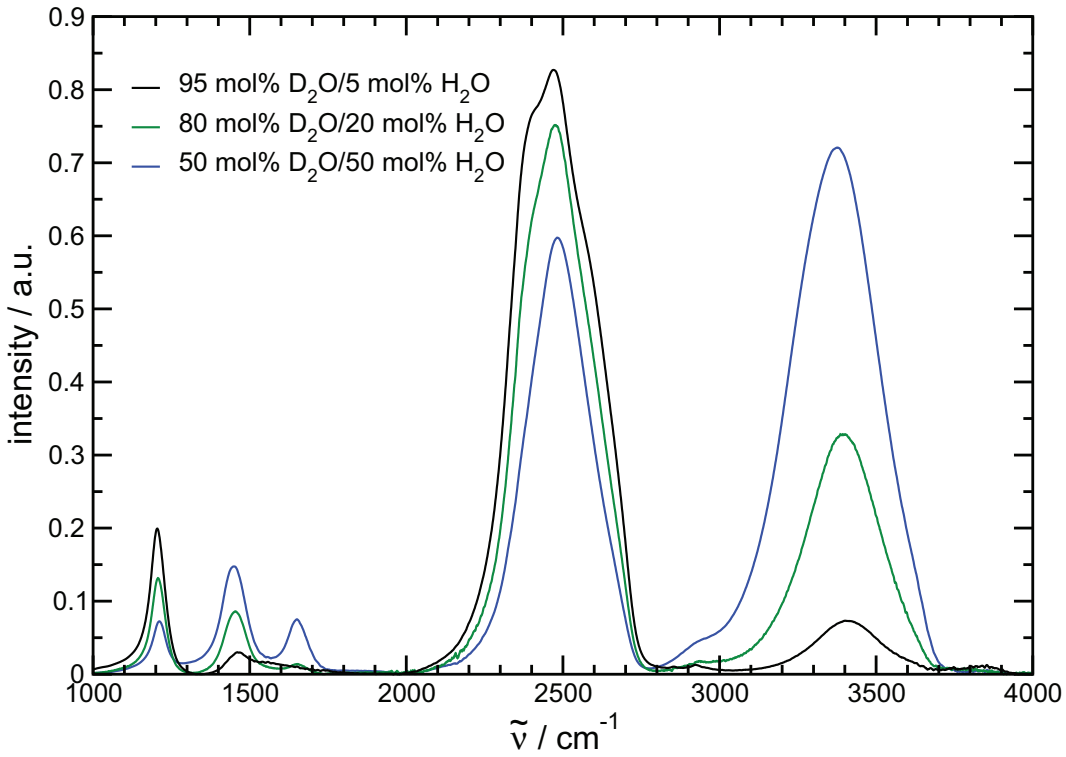

Figure 1: Development of the overtone $2\nu_2$ at several mol% ratios of H_2O and D_2O at 303 K.

4 Ionic Dependencies

4.1 Peak positions

One molar solutions

	Li^+	Na^+	K^+	Rb^+	Cs^+
F^-	-	3043	3036	3031	3043
Cl^-	3386	3420	3423	3419	3417
Br^-	3432	3431	3444	3436	3442
I^-	3461	3463	3460	3470	3461

Table 3: Maxima of the positive peak of 1 M alkali halide solutions at 303 K.

	Li^+	Na^+	K	Rb^+	Cs^+
F^-	-	3339	3331	3327	3348
Cl^-	3137	3161	3165	3162	3170
Br^-	3179	3168	3178	3178	3181
I^-	3207	3183	3182	3193	3192

Table 4: Minima of the negative peak of 1 M alkali halide solutions at 303 K.

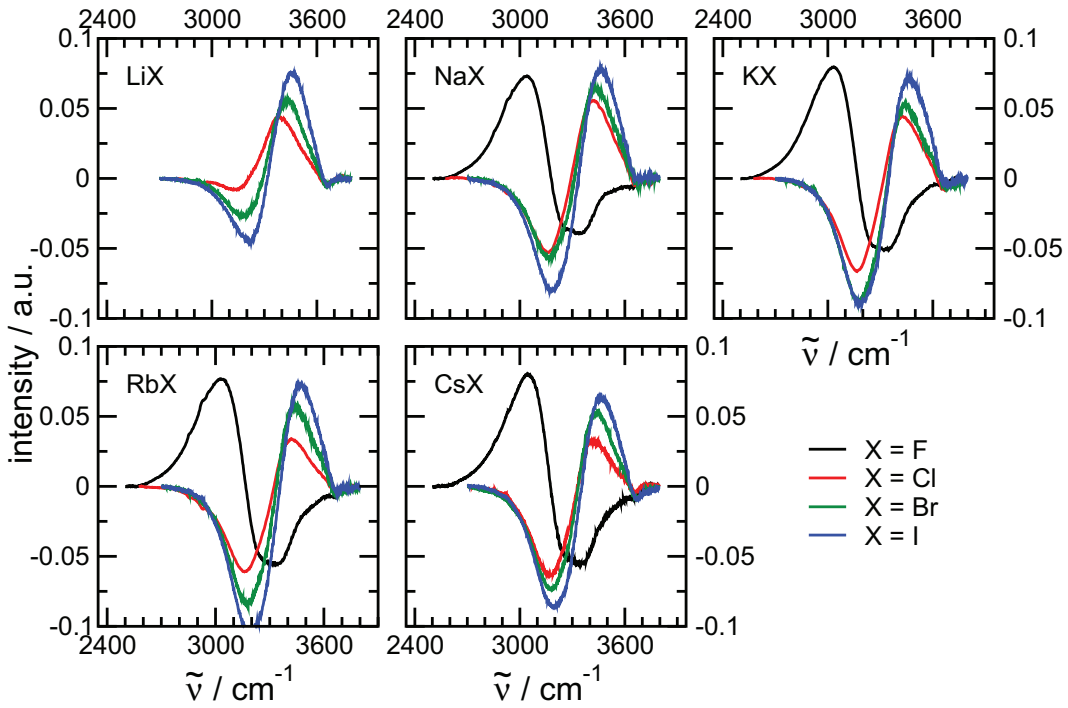

Figure 2: Anion dependent difference spectra of 1 M solutions of Li, Na, K, Rb and Cs halides at 303 K.

Two molar solutions

	Li^+	Na^+	K^+	Rb^+	Cs^+
F^-	-	-	3036	3032	3045
Cl^-	3387	3419	3429	3423	3416
Br^-	3430	3436	3444	3441	3442
I^-	3457	3463	3465	3466	3468

Table 5: Maxima of the positive peak of 2 M alkali halide solutions at 303 K.

	Li^+	Na^+	K^+	Rb^+	Cs^+
F^-	-	-	3338	3340	3346
Cl^-	3147	3160	3168	3164	3170
Br^-	3174	3171	3176	3179	3180
I^-	3198	3182	3180	3190	3196

Table 6: Minima of the negative peak of 2 M alkali halide solutions at 303 K.

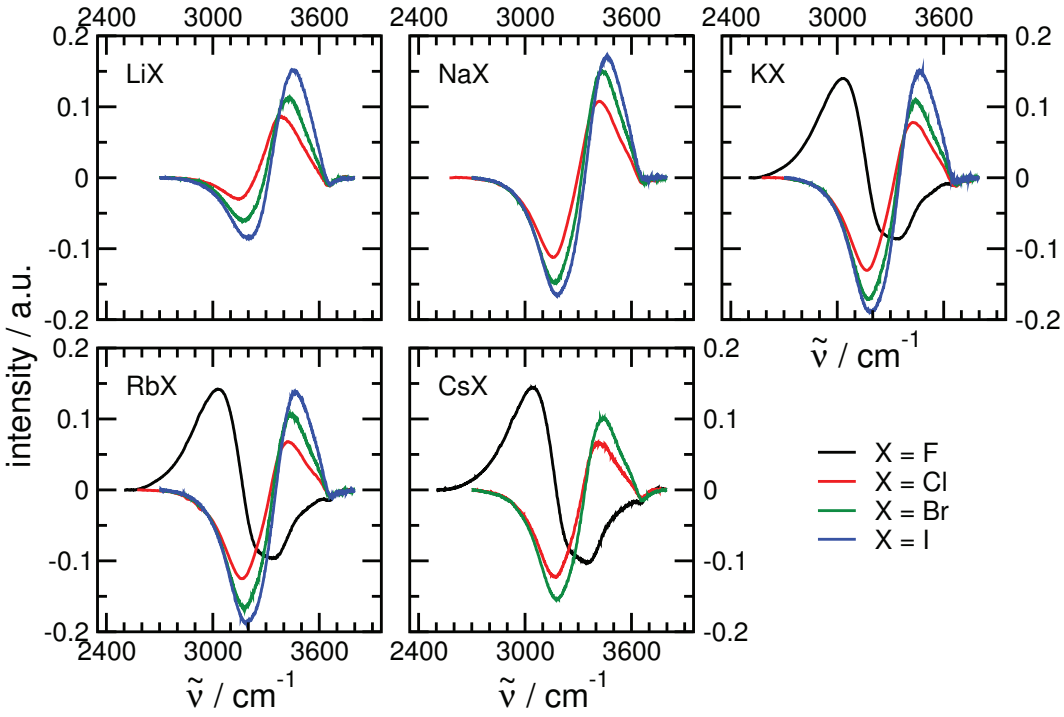

Figure 3: Anion dependent difference spectra of 2 M solutions of Li, Na, K, Rb and Cs halides at 303 K.

4.2 Anionic dependency

One molar solutions

	Li^+	Na^+	K^+	Rb^+	Cs^+	**avg.**
F^--Cl^-	-	+377	+387	+388	+374	**+382**
Cl^--Br^-	+46	+11	+21	+17	+25	**+24**
Br^--I^-	+29	+32	+16	+24	+19	**+24**

Table 7: Anion dependent shifts of the maxima of the positive peak of 1 M alkali halide solutions at 303 K. The shift of the positive peak from RbCl to RbBr is found at the intersection of column Rb^+ and row Cl^--Br^-.

	Li^+	Na^+	K^+	Rb^+	Cs^+	**avg.**
F^--Cl^-	-	−178	−166	−165	−178	**−172**
Cl^--Br^-	+42	+7	+13	+4	+11	**+15**
Br^--I^-	+28	+15	+4	+15	+11	**+15**

Table 8: Anion dependent shifts of the minima of the negative peak of 1 M alkali halide solutions at 303 K. The shift of the negative peak from RbCl to RbBr is found at the intersection of column Rb^+ and row Cl^--Br^-.

Two molar solutions

	Li^+	Na^+	K^+	Rb^+	Cs^+	**avg.**
F^--Cl^-	-	-	+393	+391	+371	**+385**
Cl^--Br^-	+43	+17	+15	+18	+26	**+24**
Br^--I^-	+27	+27	+21	+25	+26	**+25**

Table 9: Anion dependent shifts of the maxima of the positive peak of 2 M alkali halide solutions at 303 K. The shift of the positive peak from RbCl to RbBr is found at the intersection of column Rb^+ and row Cl^--Br^-.

	Li^+	Na^+	K^+	Rb^+	Cs^+	**avg.**
F^--Cl^-	-	-	−170	−176	−176	**−174**
Cl^--Br^-	+27	+11	+8	+15	+10	**+14**
Br^--I^-	+24	+11	+4	+11	+16	**+13**

Table 10: Anion dependent shifts of the minima of the negative peak of 2 M alkali halide solutions at 303 K. The shift of the negative peak from RbCl to RbBr is found at the intersection of column Rb^+ and row Cl^--Br^-.

4.3 Cationic dependency

One molar solutions

	Li^+-Na^+	Na^+-K^+	K^+-Rb^+	Rb^+-Cs^+
F^-	-	-7	-5	$+10$
Cl^-	$+34$	$+3$	-4	-2
Br^-	-1	$+13$	-8	$+6$
I^-	$+2$	-3	$+10$	-9
avg.	**+12**	**+2**	**−2**	**+1**

Table 11: Cation dependent shifts of the maxima of the positive peak of 1 M alkali halide solutions at 303 K. The shift of the positive peak from NaCl to KCl is found at the intersection of column Na^+-K^+ and row Cl^-.

	Li^+-Na^+	Na^+-K^+	K^+-Rb^+	Rb^+-Cs^+
F^-	-	-8	-4	$+21$
Cl^-	$+24$	$+4$	-3	$+8$
Br^-	-11	$+10$	0	$+3$
I^-	-24	-1	$+11$	-1
avg.	**−5**	**+1**	**+1**	**+8**

Table 12: Cation dependent shifts of the minima of the negative peak of 1 M alkali halide solutions at 303 K. The shift of the negative peak from NaCl to KCl is found at the intersection of column Na^+-K^+ and row Cl^-.

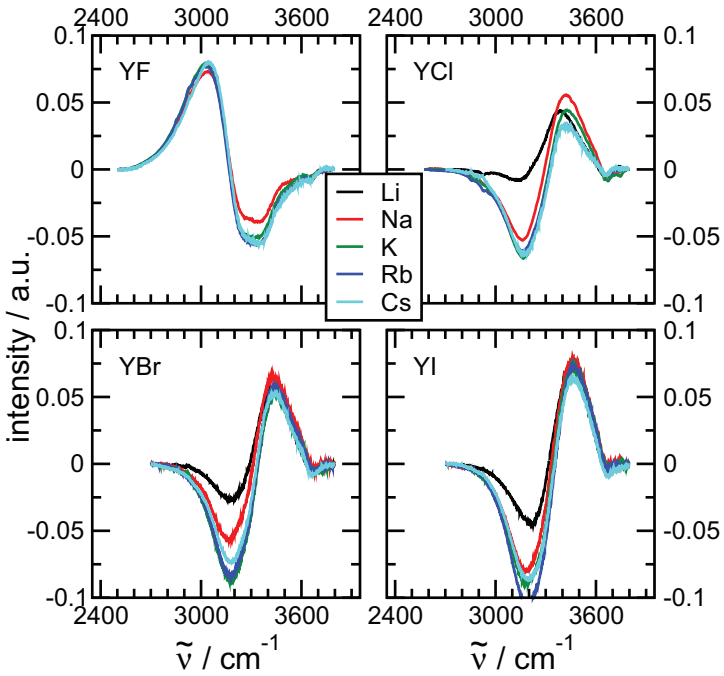

Figure 4: Cation dependent difference spectra of 1 M solutions of Li, Na, K, Rb and Cs halides at 303 K.

Two molar solutions

	Li^+-Na^+	Na^+-K^+	K^+-Rb^+	Rb^+-Cs^+
F^-	-	-	−4	+13
Cl^-	+32	+10	−6	−7
Br^-	+6	+8	−3	+1
I^-	+6	+2	+1	+2
avg.	**+15**	**+7**	**-3**	**+2**

Table 13: Cation dependent shifts of the maxima of the positive peak of 2 M alkali halide solutions at 303 K. The shift of the positive peak from NaCl to KCl is found at the intersection of column Na^+-K^+ and row Cl^-.

	Li^+-Na^+	Na^+-K^+	K^+-Rb^+	Rb^+-Cs^+
F^-	-	-	+2	+6
Cl^-	+13	+8	−4	+6
Br^-	−3	+5	+3	+1
I^-	−16	−2	+10	+6
avg.	**−2**	**+4**	**+3**	**+5**

Table 14: Cation dependent shifts of the minima of the negative peak of 2 M alkali halide solutions at 303 K. The shift of the negative peak from NaCl to KCl is found at the intersection of column Na^--K^+ and row Cl^-.

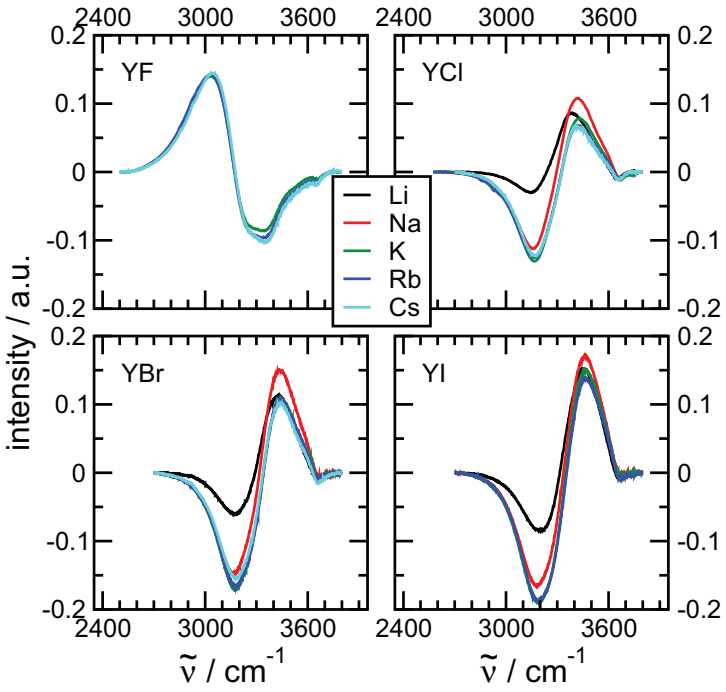

Figure 5: Cation dependent difference spectra of 2 M solutions of Li, Na, K, Rb and Cs halides at 303 K.

4.4 Anionic dependent behaviour of Ca and Mg halides

One molar solutions

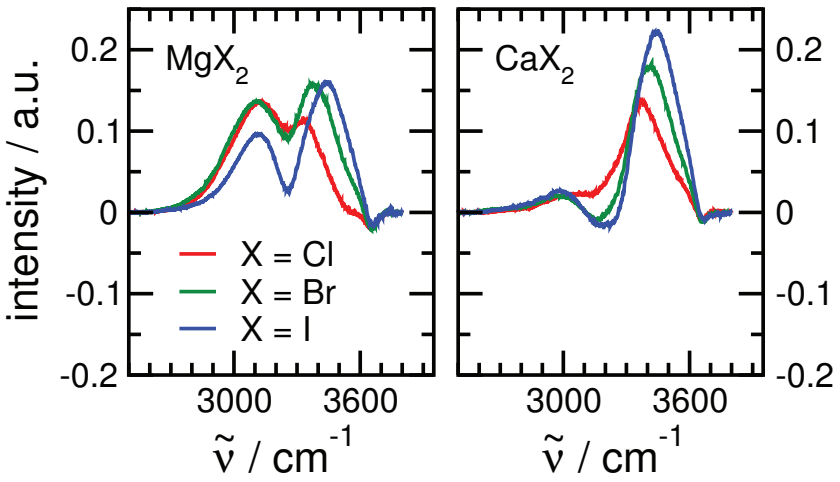

Figure 6: Anion dependent difference spectra of 1 M Mg and Ca halide solutions at 303 K.

Half molar solutions

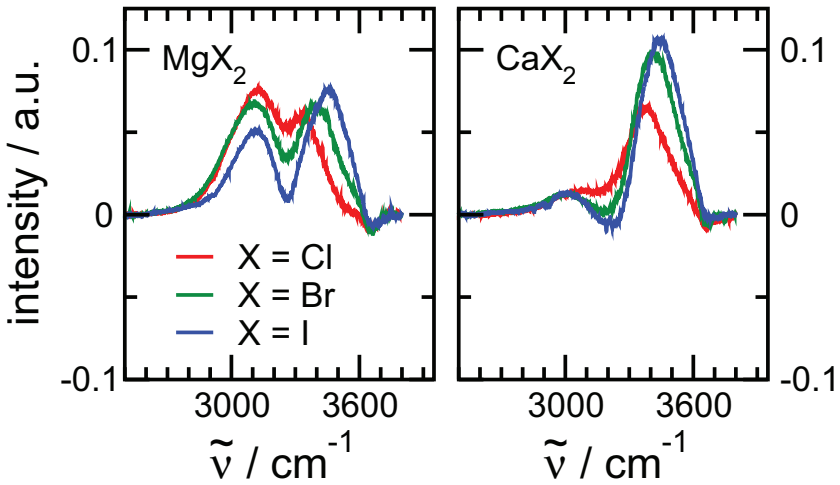

Figure 7: Anion dependent difference spectra of 0.5 M Mg and Ca halide solutions at 303 K.

5 Hofmeister series

5.1 Cation dependent peak heights of the hydrogen bonded network peak

One molar solutions

	F^-	Cl^-	Br^-	I^-
K^+	−0.0509	−0.0663	−0.0892	−0.0887
Rb^+	−0.0556	−0.0612	−0.0838	−0.1040
Cs^+	−0.0548	−0.0420	−0.0737	−0.0865
Na^+	−0.0394	−0.0531	−0.0568	−0.0800
Li^+	-	−0.0085	−0.0270	−0.0453
Ca^{2+}	-	0.0145	0.0123	−0.0132
Mg^{2+}	-	0.0756	0.0672	−0.0449

Table 15: Peak heights of the hydrogen bonded network peak for 1 M solutions for the alkaline metals and 0.5 M for the earth alkaline metals in order to ensure anion dependency at 303 K.

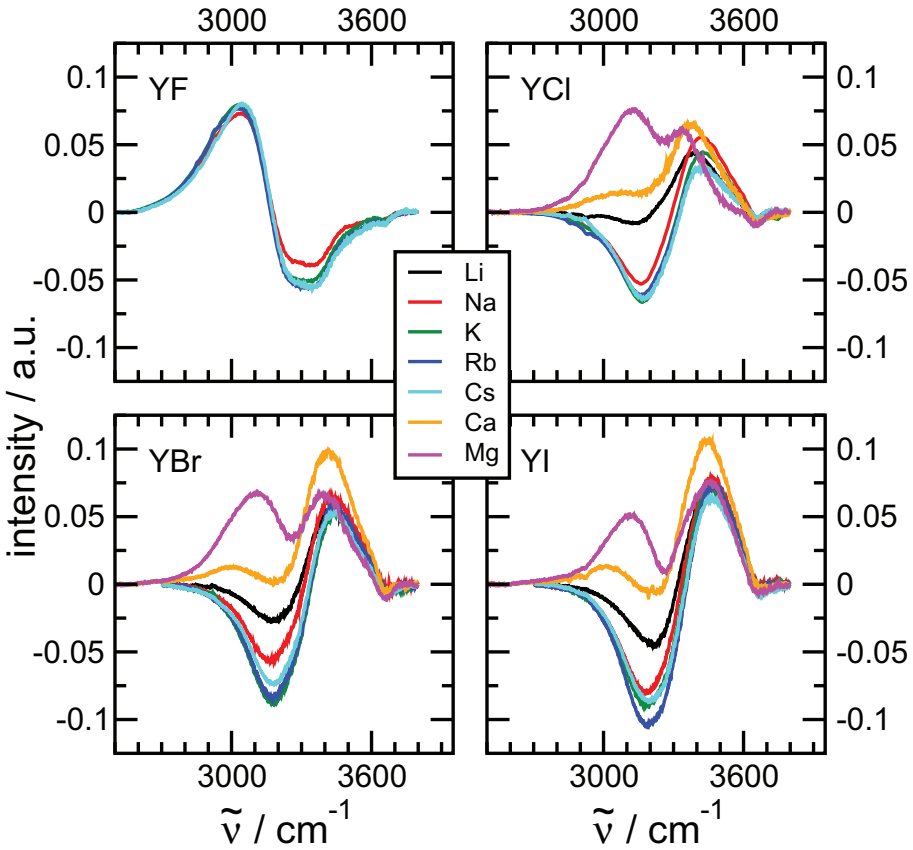

Figure 8: Cation dependent difference spectra of 1 M solutions for the monovalent and 0.5 M solutions for the bivalent cations to ensure the anion dependency at 303 K.

Two molar solutions

	F^-	Cl^-	Br^-	I^-
K^+	−0.0869	−0.1300	−0.1711	−0.1881
Rb^+	−0.0956	−0.1252	−0.1651	−0.1869
Cs^+	−0.1028	−0.1195	−0.1545	−0.1830
Na^+	-	−0.1126	−0.1474	−0.1650
Li^+	-	−0.0298	−0.0605	−0.0858
Ca^{2+}	-	0.0223	0.0195	0.0264
Mg^{2+}	-	0.1366	0.1368	0.0865

Table 16: Peak heights of the hydrogen bonded network peak for 2 M solutions for the alkaline metals and 1 M for the earth alkaline metals in order to ensure anion dependency at 303 K.

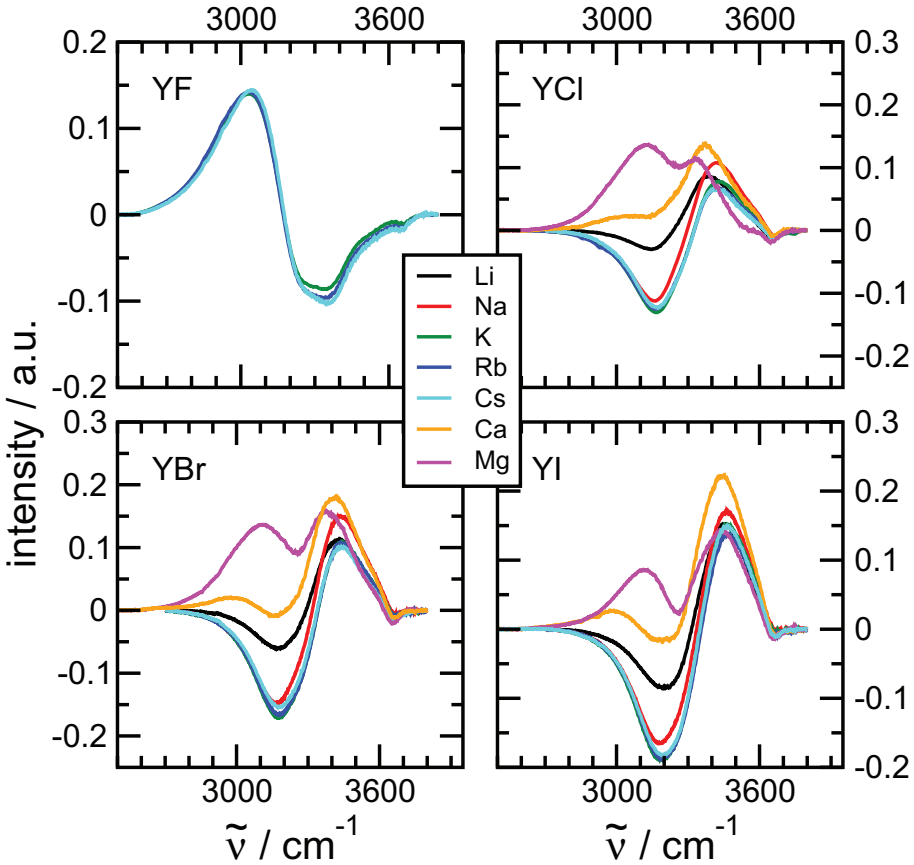

Figure 9: Cation dependent difference spectra of 2 M solutions for the monovalent and 1 M solutions for the bivalent cations to ensure the anion dependency at 303 K.

5.2 The sodium series

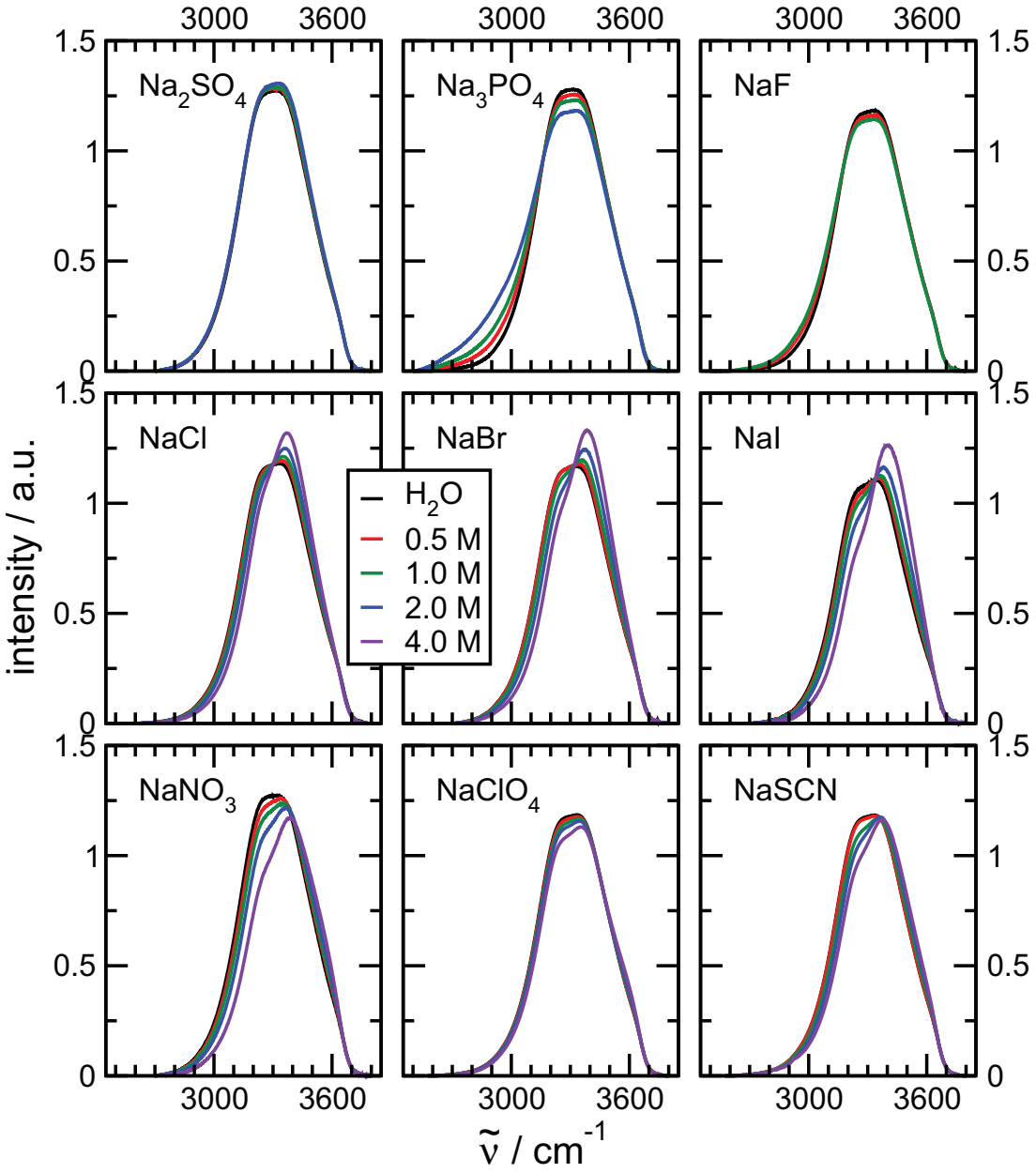

Figure 10: Anion dependent original spectra of selected sodium salts in order of the HOFMEISTER series. The amount of Na^+ is ensured to be equal. The concentration refers to the amount of Na^+ in the solution. That is, 0.5; 1.0 and 2.0 M for Na_2SO_4 are 0.25, 0.5 and 1.0 respectively. Similar with the Na_3PO_4 the same concentrations refer to 0.166; 0.33 and 0.66 M

Acknowledgements

First and foremost I would like to express my appreciation and gratitude to Prof. Ralf Ludwig for giving me the opportunity to work as a PhD student in his group. He always had a very open ear for scientific problems and discussions but was also very cooperative and understanding when it came down to family planning. His support and advice made the time during my PhD a great experience which I will cherish, for sure. Many thanks also go to Kira Ludwig for the regular and friendly invitations to dinner and always trying to bring the group together. Her advice regarding rhetorical and presentational matters has also been of great benefit.

For scientific and technical support a big "Thank you!" goes to each former and present member of the research group and all laboratory assistants and colleagues from the container in Dr.-Lorenz-Weg, with which I had the honour to work with over the course of more than four eventful years. Without their help regarding all the small and not so small details, be it computers, software, lab equipment or leaking roofs, this work would not have been possible.

My appreciation also goes to Prof. Alfred Flint as well as Dr. Dietmar Paschek who participated in financially supporting me.

Last but not least very special thanks go to my friends, my entire family and especially to Kristina who supported me along the way, wherever they could.